4-1-2010

Seismic Performance of Sprayed Fire Resistive Material (SFRM) on Steel Moment Frame Buildings

Nicole Leo Braxtan

Stephen Pessiki

Follow this and additional works at: http://preserve.lehigh.edu/engr-civil-environmental-atlss-reports

Seismic Performance of Sprayed Fire Resistive Material (SFRM) on Steel Moment Frame Buildings

by

Nicole Leo Braxtan

Stephen Pessiki

ATLSS Report No. 10-03

April 2010

Seismic Performance of Sprayed Fire Resistive Material (SFRM) on Steel Moment Frame Buildings

by

Nicole Leo Braxtan
Post-doctoral Research Associate
Department of Civil and Environmental Engineering

Stephen Pessiki
Professor and Chairperson
Department of Civil and Environmental Engineering

ACKNOWLEDGEMENTS

TABLE OF CONTENTS

LIST OF TABLES

LIST OF FIGURES

ix

ABSTRACT

Sprayed fire resistive material (SFRM) is an integral part of structural fire protection for multistory steel building construction. SFRM is intended to thermally protect structural steel elements during a fire. Damage to the SFRM can compromise the efficacy of the SFRM and lead to elevated temperatures in the steel substrate and thus a reduction in strength and stiffness of the steel.

The work presented in this report is part of a broader research program to evaluate the efficacy of sprayed fire resistive material in steel moment frame building structures in the event of a post-earthquake fire. The focus of this report is cyclic loading tests of beam-column assemblages with SFRM to determine earthquake induced damage to the SFRM.

Large-scale tests were performed to evaluate damage patterns in the SFRM in a beam column connection under the action of seismic loading. Details are provided on member selection, connection details, steel fabrication, and SFRM application.

Damage occurred to the SFRM in the beam column assemblage specimens at story drift levels of 1% to 3.9%. The degree of damage to the SFRM depends upon the earthquake intensity. Damage to the SFRM begins with debonding of the SFRM from the steel as the steel yields. This occurs at drifts as low as 1%; the steel moment frame considered in this research is expected to develop 3% story drift under the action of a design earthquake and have a life safety performance level (BSSC, 2003). However, even though the SFRM is debonded from the yielded portions of the connection at this drift level, the three dimensional geometry of the SFRM in the beam-column connection prevents the SFRM from falling off the connection region.

Under a design earthquake causing story drifts of 3% to 4%, anticipated inelastic buckling (in the beam flanges in this study) creates tears in the SFRM at the locations of the buckling. The tears separate the SFRM in to sections that can then fall away from the connection, exposing the steel at those locations. The steel moment frame considered in this research is in the latter stages of the life safety performance level when this damage occurs.

CHAPTER 1
INTRODUCTION

1.1 INTRODUCTION

Current U.S. practice uses a combination of active and passive fire protection systems to provide structural fire protection in multistory building construction. Active fire protection systems include sprinklers, firefighters, automatic door closers, fire extinguishers, and fans or other devices used to control smoke. Passive fire protection systems are those built into the building system that do no require specific activation, such as sprayed fire-resistive materials (SFRMs). Sprinklers and other active systems are intended to extinguish a fire or to limit its spread, and SFRM is intended to thermally protect structural steel elements during a fire.

Past events have demonstrated that earthquakes can cause fires in buildings, damage active fire protection systems such as sprinklers, and reduce the effectiveness of fire-fighting capabilities. In such an event where the active fire protection systems are compromised by an earthquake, passive systems such as SFRM may be the only available means to mitigate the effects of the fire on the structural system in a building. However, during an earthquake, the integrity of the SFRM may become compromised because of damage to the underlying steel structure to which the SFRM is bonded. For example, for traditional strong-column weak-beam designs, large deformation demands are place on the beams in the vicinity of the columns, which in turn place large demands on the ability of the SFRM to remain attached to the beams. Lesser demands from the earthquake are placed on the column; thus the column SFRM may remain intact during the earthquake. Damage to the SFRM in the plastic hinge region in the beam adjacent to the column provides a means to conduct heat directly into the column in the event of a post-earthquake fire. Thus damaged SFRM may reduce the structural performance of the building columns at elevated temperature during a post-earthquake fire.

1.1.1 Research Objective

The work presented is this report is part of a broader research program to evaluate the efficacy of sprayed fire resistive material in steel moment frame building structures in the event of a post-earthquake fire. The focus of the work performed to date has been on the axial load behavior of the steel column in a fire as influenced by damage to the SFRM in the beams adjacent to the columns.

1.1.2 Summary of Approach

The scope of this work includes four tasks.

> Task 1 – tensile plate tests to investigate the bond of SFRM to steel plates at various levels of post-yield strain in the plates.
> Task 2 – cyclic loading tests of beam-column assemblages with SFRM to determine earthquake induced patterns in the SFRM.
> Task 3 – nonlinear finite element heat transfer analyses to determine the fire-induced temperature distribution in the beam-column connection region due to damaged SFRM on the beam.

Task 4 – nonlinear finite element structural analyses of the strength of the columns, at the elevated temperatures determined in Task 3, due to fire and damaged SFRM.

A previous report presented the results of Task 1 (Braxtan and Pessiki, 2010). This report addresses the results of Task 2. Task 2 consists of the beam-column assemblage tests to examine the bond of SFRM to steel in the 3-D configuration of the beam-column connection region. Beam-column assemblages with SFRM applied are subject to quasi-static cyclic loading at the beam tip to cause large deformations in the beam. Damage to the SFRM at locations where there are large deformations in the steel is then investigated.

1.2 ORGANIZATION OF REPORT
The remainder of this report is organized into four chapters (Chapters 2 through 5) that each discuss an important aspect of this research.

Chapter 2 presents the background information relevant to this research. The sprayed fire resistive materials studied in this research are described, and the existing ASTM methods for testing these materials are discussed. Typical moment resistant frames (MRFs) are discussed, and details of the prototype frame used in this research are presented.

Chapter 3 presents the beam column assemblage used for the large scale testing in this research. The assemblage was used to evaluate damage patterns in the SFRM in a beam column connection under the action of seismic loading. Details are provided on member selection, connection details, steel fabrication, and SFRM application.

Chapter 4 presents the results and discussion of the beam-column assemblage tests. The results from the DM assemblage test are presented in Section 4.2, and the results from the WM assemblage test are presented in Section 4.3. The presentation of results includes a description of the overall behavior of the specimen, beam behavior, panel zone behavior, and SFRM response.

Chapter 5 presents the conclusions of this research.

1.3 SUMMARY OF FINDINGS
Damage occurs to the SFRM in the beam column assemblage specimens at story drift levels of 1% to 3.9%. The degree of damage to the SFRM depends upon the earthquake intensity. Damage to the SFRM begins with debonding of the SFRM from the steel as the steel yields. This occurs at drifts as low as 1%; the steel moment frame considered in this research is expected to develop 3% story drift under the action of a design earthquake and have a life safety performance level (BSSC, 2003). However, even though the SFRM is debonded from the yielded portions of the connection at this drift level, the three dimensional geometry of the SFRM in the beam-column connection prevents the SFRM from falling off the connection region.

Under a design earthquake causing story drifts of 3% to 4%, anticipated inelastic buckling (in the beam flanges in this study) creates tears in the SFRM at the locations of the buckling. The tears separate the SFRM in to sections that can then fall away from the connection, exposing the steel at those locations. The steel moment frame considered in this research is in the latter stages of the life safety performance level when this damage occurs.

For the strong-column, weak beam assemblages treated in this research, damage to the SFRM was concentrated in the beam flanges where inelastic damage to the underlying steel occurred. For the wet-mix SFRM, damage extended in to the beam web.

1.4 NOTATION
The following notation is used throughout this report.

A	= area of the cap
A_g	= gross area of the column
A_{tab}	= area of the shear tab
A_w	= area of the beam web
CA	= cohesive/adhesive force
C_d	= double curvature factor
C_{pr}	= factor to account for overstrength including strain hardening
C_v	= web shear coefficient
C_1, C_2	= material constants defined in UL fire resistance ratings
D	= heated perimeter of steel column
DL	= factored dead load, equal to the self weight of the beam
F	= recorded force
F_{yb}	= yield strength of the beam
F_{yc}	= yield strength of the column
F_{yf}	= minimum yield stress of the loaded flange
F_{ytab}	= yield strength of the tab
F_{yw}	= minimum yield stress of the beam web
H	= height of the column
L_b	= maximum unbraced length of the beam
L_{beam}	= length of the beam
M	= mass of the SFRM sample
M_{pb}	= plastic moment in beam
M_{pc}	= plastic moment in column
M_{pr}	= probably plastic moment in beam
M_r	= the required flexural strength of the beam
N	= length of the bearing
P_{brb}	= required brace strength for the beam
P_{brc}	= required brace strength for the column
P_{uc}	= required compressive strength of the column per LRFD load combinations
R	= required fire rating

R_n = strength of the beam
R_y = ratio of the expected yield stress to the specified minimum yield stress
R_{yb} = ratio of the expected yield strength to the minimum required yield strength of the beam
R_{yc} = ratio of the expected yield strength to the minimum required yield strength of the column
W = weight of the steel column
W_1/D_1 = weight to heated perimeter of approved beam
W_2/D_2 = weight to heated perimeter of substitute beam
V = volume of the SFRM sample
V_f = shear force at the face of the column
V_n = nominal shear strength
Z_b = plastic section modulus for the beam
Z_c = plastic section modulus of the column
a_i = amplitude of each loading step
a_n = final amplitude of loading
b = one half the full flange width, b_{fb} of the beam
b_{fb} = width of the beam flange
d_b = depth of the beam
d_c = depth of the column
d_z = panel zone depth between continuity plates
h = clear distance between flanges less the fillet at each flange
h_{DM} = required thickness of the DM
h_{WM} = required thickness of the WM
h_o = distance between flange centroids
h_{SFRM} = required thickness of the SFRM
h_1 = thickness of the SFRM in the approved beam
h_2 = required thickness of SFRM in the substitute beam
k = distance from the outer face of the flange to the web toe of the fillet
r_{yb} = radius of gyration about the y axis of the beam
t = thickness of the flange
t_f = thickness of the beam flange being loaded
t_{fb} = thickness of the beam flange
t_{cf} = thickness of column flange
t_p = thickness of the panel zone, column web thickness plus doubler plates
t_{wb} = thickness of the web of the beam
t_{wc} = thickness of the column web
w_z = panel zone width between column flanges
Δ = beam tip displacement
Δ_m = maximum deformation
Δt = time interval
Δ_o = smallest deformation amplitude
β_{br} = required brace stiffness
δ = displacement at the top of the column
ε_y = yield strain

5

ϕ = strength reduction factor
θ = storey drift ratio
ρ = density of the SFRM

1.5 UNIT CONVERSIONS

Metric units are used consistently throughout this report. The following unit conversions can be used to convert to U.S. customary units.

$1 \text{ kg/m}^3 = 6.24\text{x}10^{-2} \text{ lb/ft}^3$
$1 \text{ mm} = 25.4 \text{ in.}$
$1 \text{ N} = 2.25\text{x}10^{-1} \text{ lbf}$
$1 \text{ Pa} = 1.45\text{x}10^{-4} \text{ psi}$

CHAPTER 2
BACKGROUND

2.1 INTRODUCTION
This chapter presents the background information relevant to this research. The sprayed fire resistive materials (SFRMs) studied in this research are described, and the existing ASTM methods for testing these materials are discussed. Typical moment resistant frames (MRFs) are discussed, and details of the prototype frame used in this research are presented.

2.2 SPRAYED FIRE RESISTIVE MATERIAL
SFRM is used as a method of passive fire protection to thermally insulate structural steel elements during a fire. Figure 2.1 is a photograph of SFRM applied to typical beams and columns in a building under construction. Two commonly used SFRM materials are treated in this research: a dry-mix material and a wet-mix material.

2.2.1 Sprayed Fire Resistive Material Description
The dry-mix material is a portland cement and mineral wool fiber mixture. The product is conveyed in the dry state under low air pressure and water is added at the spray nozzle as the product is being applied. This dry-mix material is referred to as DM in this paper.

The wet-mix material is a mixture of vermiculite and gypsum. It is combined with water in a large mixer before being pumped in a wet-slurry state to a spray nozzle where compressed air creates a spray pattern as the product is applied. It is predominantly sprayed but can be applied using a trowel. This wet-mix material is referred to as WM in this paper.

2.2.2 Test Methods for Sprayed Fire Resistive Material
Several test methods exist to evaluate the properties of SFRM. Of interest to this research are methods to evaluate the bond strength of SFRM to structural members, and the thickness and density of SFRM. This section of the report reviews ASTM E736: Standard Test Method for Cohesion/Adhesion of Sprayed Fire-Resistive Material (SFRM) Applied to Structural Members, and ASTM E605: Standard Test Methods for Thickness and Density of Sprayed Fire-Resistive Material (SFRM) applied to Structural Members.

2.2.2.1 ASTM E736: Standard Test Method for Cohesion/Adhesion of Sprayed Fire-Resistive Material (SFRM) Applied to Structural Members
This test method is used to evaluate the cohesive or adhesive strength of SFRM applied to structural members. A brief summary of the method is as follows. Specimens are prepared by applying 12 to 25 mm of SFRM to a 300 mm by 300 mm galvanized steel plate or field testing is performed on structural members with existing SFRM. A bottle cap with a hook inserted into it, similar to that shown in Figure 2.3, is filled with a two-component glue and placed on the SFRM surface. After the glue has cured, a spring type scale is attached to the hook and force is applied, pulling on the cap until the SFRM fails.

7

Failure within the SFRM is classified as a cohesive failure and failure between the SFRM and the steel surface is classified as an adhesive failure. The maximum force is recorded from the scale and the bond strength is determined based on the force and the area of the cap.

$$CA = \frac{F}{A} \qquad (2.1)$$

where

        CA = cohesive/adhesive force, Pa
        F = recorded force, N
        A = area of the cap, m^2

2.2.2.2 ASTM E605: Standard Test Methods for Thickness and Density of Sprayed Fire-Resistive Material (SFRM) Applied to Structural Members
As the name suggests, this test method is used to determine the thickness and density of SFRM on structural members. Test specimens are prepared by applying SFRM to a 1.5 mm thick, bare or galvanized steel plate that is 400 mm by 400 mm in area, or field testing is performed on structural members with existing SFRM. Thickness measurements are taken at 12 locations on the plate, or member, and an average thickness is found based on these results. The thickness is found by inserting a pin through the SFRM until it reaches the steel substrate. The pin includes a scale that measures the depth of penetration from the surface of the SFRM to the steel substrate.

The density of the SFRM is then determined as follows. A 5800 mm^2 sample of SFRM is cut from the plate, or member, and the mass determined using a scale. The volume of the SFRM is then found using the displacement method described in the standard. The density is calculated as

$$\rho = \frac{m \cdot 1000}{V} \qquad (2.2)$$

where

        ρ = density of the SFRM, kg/m^3
        M = mass of the sample, g
        V = volume of the sample, cm^3

2.3 STEEL MOMENT RESISTANT FRAMES
Moment resistant frames (MRFs) resist lateral forces in buildings. They are commonly used in areas of high seismicity as they provide the necessary ductility to accommodate the large deformations associated with earthquakes. The major components of MRFs are beams, columns, and beam-column panel zones.

This section introduces the details of moment resistant frames designed using design recommendations in use both before and after the Northridge Earthquake of 1994.

2.3.1 Typical Moment Resistant Frames

Figure 2.4 shows a typical MRF prior to the Northridge Earthquake in 1994. The main components of the connection are welded beam flanges and a shear tab. The full penetration welds were achieved using weld access holes and backing bars.

Following the 1994 Northridge earthquake, inspections revealed brittle fractures in the connection regions commonly propagating from the weld between the beam bottom flange and the column flange. This prompted evaluation of the existing moment resistant and recommendations for improved design methods for new moment resistant frames.

Figure 2.5 shows details for a typical post-Northridge MRF with welded unreinforced flanges and welded webs (WUF-W) as recommended by FEMA 350 (2000). The backing bar on the beam bottom flange is to be removed to help prevent the brittle fractures experienced in the Pre-Northridge connections and doubler plates are often used to strengthen the column web in the connection region. FEMA 350 also outlines other types of moment connections typically used in design.

A study by Ricles et al. (2001) described the design and analysis of typical welded MRFs based on the prototype frame shown in Figure 2.6. This figure shows a general six story, six bay office building located in the Los Angeles area. The frame was designed based on 1994 NEHRP provisions for special moment-resisting frames and was based on seismic hazard exposure Group III, soil type D, and an effective peak velocity-related coefficient of 0.4. The member sizes and overall geometry of this frame will be used in the assemblage tests presented in Chapter 5 and Chapter 6 and the finite element analyses in Chapter 7 and Chapter 8.

Figure 2.1 – Photograph of sprayed fire resistive material in building

(a)   (b)
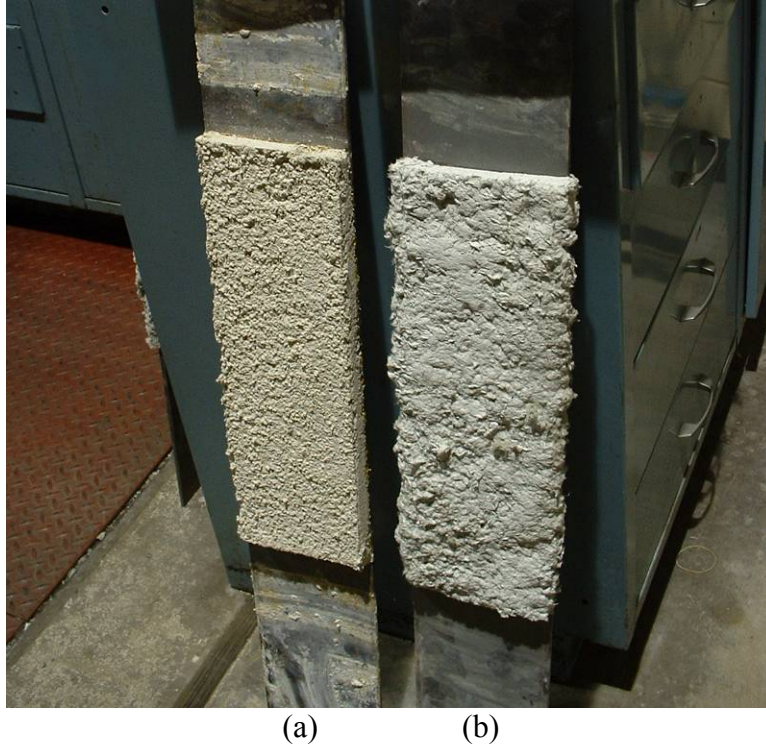
Figure 2.2 – Photograph of wet-mix and dry-mix materials: (a) cementitious wet-mix material; and (b) fibrous dry-mix material
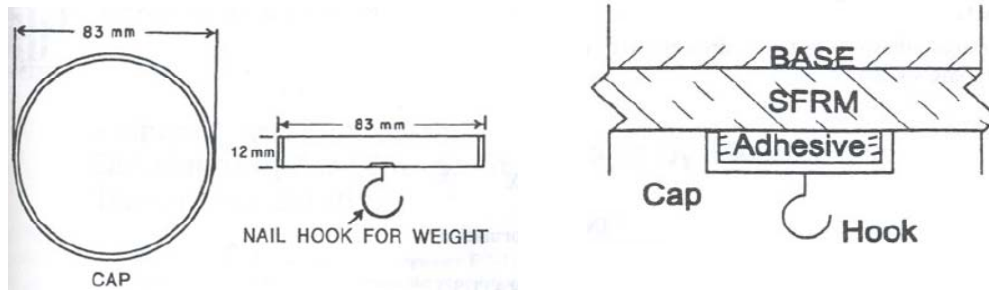
Figure 2.3 – Cap used in ASTM E736 for bond testing (ASTM E736, 2000)
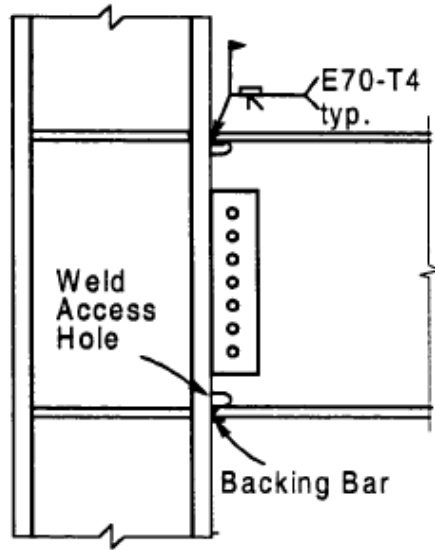
Figure 2.4 – Typical moment resistant frame prior to 1994 Northridge Earthquake (Bruneau et al., 1998)
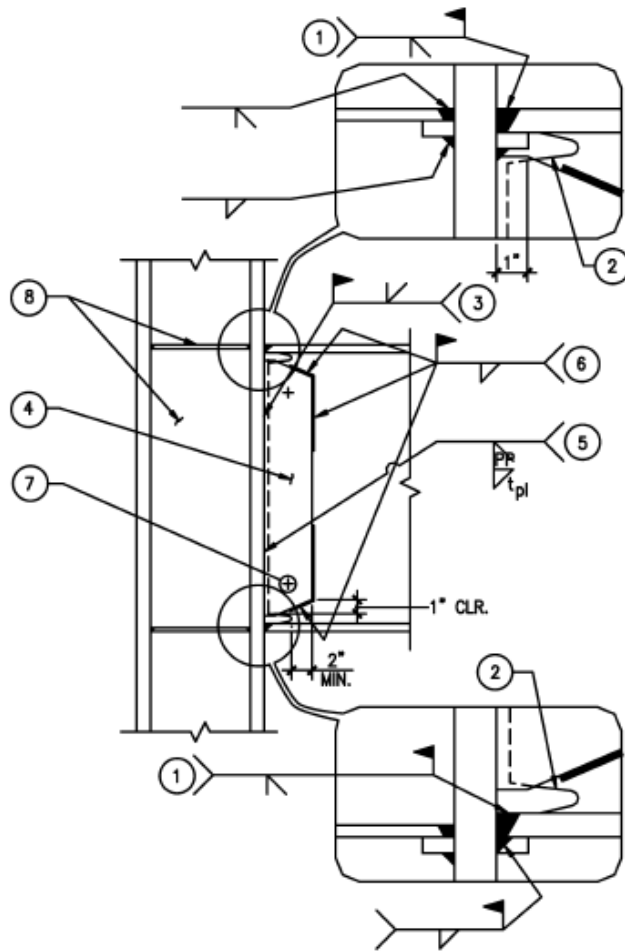
Notes
1. CJP groove weld at top and bottom flanges. At top flange, either (1) remove weld backing, backgouge, and add 5/16" minimum fillet weld, or (2) leave backing in place and add 5/16" fillet under backing. At bottom flange, remove weld backing, backgouge, and add 5/16" minimum fillet weld. Weld: QC/QA Category AH/T.
2. Weld access hole, see Figure 3-5.
3. CJP groove weld full length of web between weld access holes. Provide non-fusible weld tabs. Remove weld tabs after welding and grind end of weld smooth at weld access hole. Weld: QC/QA Category BH/T.
4. Shear tab of thickness equal to that of beam web. Shear tab length shall be so as to allow 1/8" overlap with the weld access hole at top and bottom, and the width shall extend 2" minimum back along the beam, beyond the end of the weld access hole.
5. Full-depth partial penetration from far side. Weld: QC/QA Category BM/T.
6. Fillet weld shear tab to beam web. Weld size shall be equal to the thickness of the shear tab minus 1/16". Weld shall extend over the top and bottom one-third of the shear tab height and across the top and bottom. Weld: QC/QA Category BL/L.
7. Erection bolts: number, type, and size selected for erection loads.
8. For continuity plates and web doubler plates see Figure 3-6.

Figure 2.5 – Recommended MRF detailing for welded unreinforced flanges – welded web (FEMA 350, 2000)

13
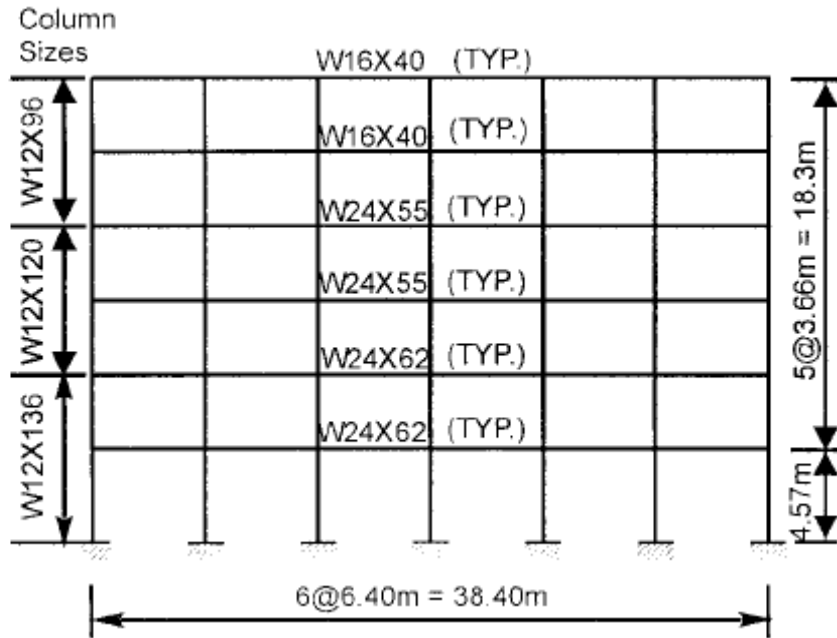
Figure 2.6 – Elevation of prototype moment resistant frame used by Ricles et al. (2001)

CHAPTER 3
ASSEMBLAGE TEST SET-UP

3.1 INTRODUCTION
This chapter presents the beam column assemblage used for the large scale testing in this research. This assemblage was used to evaluate damage patterns in the SFRM in a beam column connection under the action of seismic loading. Details are provided on member selection, connection details, steel fabrication, and SFRM application.

3.2 STEEL BEAM-COLUMN ASSEMBLAGE
The beam-column assemblage member sizes were based on a typical moment-resisting frame (MRF) used in previous research by Ricles et al. (2001) and discussed more in detail in Section 2.3.1. Detailing for the assemblage connection is specific to this research and presented in this chapter. The SFRM details were based on code required fire resistance ratings.

The overall geometry and member sizes for the beam-column assemblage were selected based on an exterior column at midheight of the typical MRF, on the fourth floor. Member properties are shown in Table 3.1 and the overall specimen geometry is shown in Figure 3.1. Under the action of lateral load on the frame, inflection points would typically form at midheight of the columns and midspan of the beam. As an alternative to lateral loading on a full frame, a beam column assemblage including half of the height of the column above and below the connection and half of the span of the beam was constructed. Pin supports attached the specimen to the reaction wall at the top and bottom of the column, and vertical load was applied at the beam tip. Deformations experienced in this setup are similar to those experienced in a lateral load frame and simpler in geometry to test, namely double curvature in the column, and large deformations in the beam adjacent to the column.

The column was a W12x120 and the beam was a W24x55. For this research all members were A992 Grade 50 steel.

3.2.1 Specimen Design
FEMA 350 (2000), the AISC Seismic Provisions (2005), and the AISC Specification (2005) were used to design the specimen.

3.2.1.1 Member Requirements
To ensure that plastic deformations occur in the beam before local buckling, the AISC Seismic Provisions (2005) limit the beam flange slenderness ratio for seismic compactness

$$\frac{b}{t_{fb}} < 0.30\sqrt{\frac{E}{F_{yb}}} \tag{3.1}$$

where
b = one half the full flange width, b_{fb} of the beam
t_{fb} = thickness of the beam flange, referred to as "t" in the Provisions

F_{yb} = yield strength of the beam, referred to as F_y in Provisions

Also, in an effort to maintain flange stability and to control the size of welds, FEMA 350 (2000) places an upper limit on beam flange thickness of 25.4 mm (1 inch).

To ensure beam web stability, the AISC Seismic Provisions (2005) limit the web height-to-thickness ratio for seismic compactness

$$\frac{h}{t_{wb}} < 2.45\sqrt{\frac{E}{F_{yb}}} \tag{3.2}$$

where

h = clear distance between flanges less the fillet at each flange
t_{wb} = thickness of the web of the beam, referred to as t_w in the Provisions

Beams with low span-to-depth ratios have a steeper moment gradient and thus a reduced length of the plastic hinge. FEMA 350 (2000) requires a minimum span-to-depth ratio of the beam of 7 to prohibit this behavior. (Note that the specimen in this research includes only half of the beam span length). FEMA 350 (2000) also limits the depth of the beam by specifying sections must be W36 and shallower since deep beams experience more straining that shallow beams.

3.2.1.2 Column-to-Beam Moment Ratio

The specimens were designed to meet the strong column – weak beam criteria of the AISC Seismic Provisions. The AISC Seismic Provisions require that ratio of the column moments to the beam moments, at the intersection of the beam and column centerlines, are

$$\frac{\sum M_{pc}}{\sum M_{pb}} > 1 \tag{3.3}$$

where the sum of the moments in the column was calculated based on material properties of the column.

$$\sum M_{pc} = \sum Z_c (F_{yc} - P_{uc}/A_g) \tag{3.4}$$

where

P_{uc} = required compressive strength of the column per LRFD load combinations
Z_c = plastic section modulus of the column
A_g = gross area of the column
F_{yc} = yield strength of the column

The sum of the moments in the beam was found by first determining the moment in the beam at the location of the plastic hinge. The plastic hinge was assumed to act at a distance of half the depth of the beam from the column face (FEMA 350). The probable plastic moment, M_{pr}, at this hinge location is defined in the AISC Seismic Provisions (2005)

$$M_{pr} = C_{pr} R_y Z_b F_{yb} \tag{3.5}$$

where

C_{pr} = factor to account for overstrength including strain hardening, taken to be 1.15

R_y = ratio of the expected yield stress to the specified minimum yield stress; for A992 Grade 50 steel R_y = 1.1 (AISC Seismic Provisions, 2005)

Z_b = plastic section modulus for the beam

3.2.1.3 Panel Zone Shear Strength

Panel zone shear strength was first calculated based on the column web geometry (AISC Specification, 2005)

$$\phi_v R_n = 0.6 F_{yc} d_c t_{wc} \tag{3.6}$$

where

ϕ_v = 1.0 as per the AISC Seismic Provisions (2005)

d_c = depth of the column

t_{wc} = thickness of the column web

Panel zone shear strength proved insufficient based on the thickness of the column web alone. Doubler plates were then added to each side of the column web and panel zone strength determined based on the thickness of the web plus the additional thickness from the doubler plates.

$$\phi_v R_n = 0.6 F_{yc} d_c t_p \tag{3.7}$$

where

t_p = thickness of the panel zone, column web thickness plus doubler plates

The panel zone thickness must also meet minimum requirements to prevent local buckling based on the depth and width of the panel zone

$$t_p > \frac{d_z + w_z}{90} \tag{5.8}$$

where

d_z = panel zone depth between continuity plates

w_z = panel zone width between column flanges

FEMA 350 (2000) requires the use of continuity plates if the thickness of column flange, t_{cf}, does not meet either of the following

$$t_{cf} > 0.4 \sqrt{1.8 b_{fb} t_{fb} \frac{F_{yb} R_{yb}}{F_{yc} R_{yc}}} \tag{3.9}$$

$$t_{cf} > \frac{b_{fb}}{6} \tag{3.10}$$

where

b_{fb} = width of the beam flange

t_{fb} = thickness of the beam flange

R_{yb} = ratio of the expected yield strength to the minimum required yield strength of the beam

R_{yc} = ratio of the expected yield strength to the minimum required yield strength of the column

For exterior columns, continuity plates must be at least half the thickness of the beam flange.

3.2.1.4 Shear Tab and Bolts

The shear tab thickness was chosen to match the beam web thickness (FEMA 350, 2000). Shear strength of the tab was determined as per the AISC Specification (2005)

$$\phi_v V_n = \phi_v 0.6 F_{ytab} A_{tab} C_v \tag{3.11}$$

where

ϕ_v = 1.0 as per the AISC Specification (2005)
A_{tab} = area of the shear tab
F_{ytab} = yield strength of the tab
C_v = web shear coefficient, taken as 1.0

Shear strength of the beam web was found similarly

$$\phi_v V_n = \phi_v 0.6 F_{yb} A_w C_v \tag{3.12}$$

where

A_w = area of the beam web

Erection bolts were designed for the shear force at the face of the column, V_f due to the factored dead load of the beam (AISC Specification, 2005)

$$V_f = 1.4 DL \tag{3.13}$$

where

DL = factored dead load, equal to the self weight of the beam

3.2.1.5 Weld Details

Modified weld access geometry as defined in FEM 350 (2000) was used. Figure 3.2 shows the modified weld access geometry and weld details. All electrodes were specified as E7018 electrode.

3.2.1.6 Wall Fixture Design

Wall fixtures were designed based on the capacity of the actuator, 445 kN (100 kips). Details are shown in Figure 3.3.

3.2.1.7 Beam Requirements at Point of Load Application

Figure 3.4 shows the actuator in elevation. The actuator used for testing had a 610 mm total stroke (+/- 305 mm) and a 445 kN capacity. It was clamped onto a 932 mm column with 50.8 mm plates on top and bottom to raise the actuator to the proper height. Flange local buckling, web local yielding, web crippling, and compression buckling were considered when designing the transverse stiffener at the point of load application. The

transverse stiffener provided additional strength for the beam to resist a concentrated force from the maximum actuator load of 445 kN.

The design strength of the beam based on flange local buckling was defined in the AISC Specification (2005)

$$\phi R_n = 6.25 t_{fb}^2 F_{yf} \qquad (3.14)$$

where

ϕ = 0.90 for flange local buckling

F_{yf} = minimum yield stress of the loaded flange

The design strength of the beam based on web local yielding was defined in the AISC Specification (2005)

$$\phi R_n = (5k + N) F_{yw} t_{wb} \qquad (3.15)$$

where

ϕ = 1.00 for web local yielding

k = distance from the outer face of the flange to the web toe of the fillet

N = length of the bearing

F_{yw} = minimum yield stress of the beam web

The design strength of the beam based on web crippling was defined in the AISC Specification (2005) based on the distance between the member end and the load point. For members loaded at a distance of less than half the depth of the beam and a ratio of the length of bearing to the depth of the beam (N/d) of larger than 0.2

$$\phi R_n = 0.40 t_{wb}^2 \left[1 + \left(\frac{4N}{d_b} - 0.2 \right) \left(\frac{t_{wb}}{t_f b} \right)^{1.5} \right] \sqrt{\frac{E F_{yw} t_{fb}}{t_{wb}}} \qquad (3.16)$$

where

ϕ = 0.75 for web crippling

d_b = depth of the beam

The design strength of the beam based on web compression buckling was defined in the AISC Specification (2005)

$$\phi R_n = \frac{24 t_{wb}^3 \sqrt{E F_{yw}}}{h} \qquad (3.17)$$

where

ϕ = 0.90 for web compression buckling

3.2.2 Bracing Requirements

Lateral bracing of the column beyond the panel zone is required if the column does not remain elastic outside of the panel zone. The AISC Seismic Provisions (2005) define a column as elastic when the ratio of the sum of the column moments to the sum of the beam moments, calculated in the same manner as Equation 3.3, is greater than 2.

19

$$\frac{\sum M_{pc}}{\sum M_{pb}} > 2 \qquad (3.18)$$

For this testing, the column is designed to remain elastic, therefore bracing is only required at the levels of the top and bottom flanges of the beam. However, bracing in this region would interfere with the performance of the SFRM in the panel zone, which is of interest in this research. The column was therefore braced at the end points to prevent lateral and torsional displacements in the column.

The required brace strength for the column, P_{brc}, is defined in the AISC Seismic Provisions (2005) based on 2% of the available beam flange strength

$$P_{brc} = 0.02 F_{yb} b_{fb} t_{fb} \qquad (3.19)$$

The bracing system used for the column, shown previously in the wall fixture details in Figure 3.3 was designed as a truss. Members were checked for axial load capacity based on the required brace strength as well as buckling.

Lateral bracing of the beam is required at a minimum spacing, L_b, defined by the AISC Seismic Provisions (2005)

$$L_b = 0.086 r_{yb} \frac{E}{F_{yb}} \qquad (3.20)$$

where

r_{yb} = radius of gyration about the y axis of the beam

Figure 3.5 shows the spacing of the bracing for the assembly tests. Half round steel was used to reduce contact between the beam specimen and the columns in the braces.

The required strength of the beam lateral bracing, P_{brb}, is defined in the AISC Specification (2005) for nodal bracing as 2% of the beam flange force

$$P_{brb} = 0.02 M_r \frac{C_d}{h_0} \qquad (3.21)$$

where

M_r = the required flexural strength of the beam $M_r = M_u = R_y Z F_y$ (LRFD)
C_d = double curvature factor, 1.0 for single curvature in bending
h_o = distance between flange centroids

The required brace stiffness, β_{br}, is defined in the AISC Specification (2005)

$$\beta_{br} = \frac{1}{\phi} \left(\frac{10 M_r C_d}{L_b h_o} \right) \qquad (3.22)$$

where ϕ is taken as 0.75 for LRFD.

3.2.3 Specimen Fabrication

All steel fabrication was performed in house at Lehigh University's ATLSS laboratory. Figure 3.6 shows both specimens after fabrication was complete, before the application of SFRM and Figure 3.7 shows the details of the connection. When fabrication was complete, ultrasonic testing was performed in the connection region to ensure quality of the welds as seen in Figure 3.8. Results of the ultrasonic testing can be found in Appendix A.3. There were no defects found in the welds and the connection was found satisfactory.

3.2.4 Instrumentation

The instrumentation for each test specimen included: (1) a load cell to measure the applied load at the beam tip; (2) 8 strain gages to measure beam flange strains; (3) one 3-strain gage rosette placed at the center of the panel zone to measure panel zone deformations; (4) and a displacement transducer at the end of the beam to measure beam tip displacement.

Figure 3.9 shows the layout of the strain gages. One gage is placed on the top and bottom of each flange at 152 mm from the column face and 457 mm from the column face to measure flange deformations. Care was taken to ensure that the strain gages were not damaged during the application of the SFRM. This included application of silicon rubber, Teflon, and waterproofing on the gages. These protective materials remained in place during SFRM application, and then when the SFRM was sufficiently dry, these layers were carefully peeled away effectively leaving a void in the SFRM on top of each gage

The strain gages were applied at the top and bottom of each flange at 152 mm from the column face and 457 mm from the column face with the goal of tracking yielding and buckling of the flanges since the steel surface of the members was visually obscured by the SFRM.

The difference in the strains in the top and bottom of each flange was used as a measure of local flange buckling. As the top and bottom of the flange began to strain (and elongate) at different rates, the flange tended to deform out of plane. When the difference in the strains at the top and bottom of each flange grew large, the flange was no longer only experiencing axial elongation and shortening, but it was also bending and locally buckling out of plane.

The difference in the strains of the flanges was calculated such that the strain at the bottom of the flange is subtracted from the strain at the top of the flange. In this way, a positive difference described a larger strain at the top of the flange than at the bottom of the flange. When this difference became large, the flange buckled upward, in a concave downward shape. Likewise, a negative difference indicates downward buckling in a concave upward shape. However, since the gage locations are actually at the outer edge of the buckled area, the concavity at the gages is opposite to the concavity at the peak in the center.

21

The gages were successful in capturing yielding in the flanges. However, the peak of the flange buckling occurred approximately halfway between the two sets of strain gages, preventing easy recognition of local flange buckling.

3.3 SPRAYED FIRE RESISTIVE MATERIALS

The same two SFRMs used in the tensile plate tests (DM and WM) were also used in the assemblage tests. The steel surfaces of the assemblage were not sandblasted but were cleaned to remove dirt and oil using a general household cleaner.

3.3.1 Sprayed Fire Resistive Material Thickness

The thicknesses of the SFRMs were determined based on the required fire resistance ratings for a typical multi-story steel structure. Fire resistance ratings are determined based on the time for which an element can meet a certain criteria during a standard fire test. For the assemblage test specimens, the required fire resistance ratings were based on the International Building Code (IBC, 2003) and determined based on the type of construction, the type of building element, the use and occupancy of the building, and the fire separation distance.

The beam-column assemblage that was tested was based on the prototype frame introduced in Section 2.3.1. It is a six story, six bay structure approximately 22.9 m in height. Based on this height, the type of construction was either Type 1A or Type 1B (IBC, 2003). Type 1 building elements must be noncombustible materials, typically steel or concrete. Group B is the business group, including office space, professional services, and other similar use spaces, with a maximum height of 11 stories for Type 1B with unlimited building area. The typical structure fits into Type 1B construction and thus required a 2 hour fire protection rating.

The manufacturer provides a design manual to specify SFRM thicknesses based on Underwriters Laboratories (UL) Fire Resistance Ratings and the IBC (2003). The IBC defines the minimum thickness for fire protective materials on columns

$$h_{SFRM} = \frac{R}{C_1(W/D) + C_2} \tag{3.23}$$

where

h_{SFRM} = required thickness of the SFRM (in)
R = required fire rating (minutes)
W = weight of the steel column (lb/ft)
D = heated perimeter of steel column (in)
C_1, C_2 = material constants defined in UL Fire Resistance Ratings

This equation was adapted for consistent units in this research

$$h_{SFRM} = \frac{25.4R}{C_1\left(\dfrac{W/D}{58.589}\right) + C_2} \tag{3.24}$$

22

where
h_{SFRM} = required thickness of the SFRM, mm
R = required fire rating, minutes
W = weight of the steel column, kg/m
D = heated perimeter of steel column, m
C_1, C_2 = material constants defined in UL Fire Resistance Ratings

For columns protected with DM, UL (2008) specifies SFRM thickness

$$h_{DM} = \frac{25.4R}{1.034(W/D)+39.6} \qquad \text{for } 32.2 < W/D < 410.1 \qquad (3.25)$$

where
h_{DM} = required thickness of the DM, mm

For the columns protected with WM, UL (2009) specifies SFRM thickness

$$h_{WM} = \frac{25.4R}{1.280(W/D)+32} \qquad \text{for } 19.3 < W/D < 147.1 \qquad (3.26)$$

where
h_{WM} = required thickness of the WM, mm

The IBC (2003) specifies the thickness of SFRM on steel beams based on a series of approved beams and their associated thicknesses in the UL Fire Resistance Ratings

$$h_2 = \frac{\frac{(W_1/D_1)}{58.589}+0.60}{\frac{(W_2/D_2)}{58.589}+0.60}h_1 \qquad (3.27)$$

where
h_1 = thickness of the SFRM in the approved beam, mm
h_2 = required thickness of SFRM in the substitute beam, mm
W_1/D_1 = weight to heated perimeter of approved beam, kg/m^2
W_2/D_2 = weight to heated perimeter of substitute beam, kg/m^2

The required thicknesses for the beam-column assemblages used in this research are shown in Table 3.2.

3.3.2 Sprayed Fire Resistive Material Application
Application of the SFRM was done on-site at Lehigh University's ATLSS Center laboratory by a local contractor with mobile SFRM application equipment. Application was done over 3 days. Each type of SFRM required different application equipment as the DM is a dry-mix material and the WM is a wet-mix material. The DM was applied on the first day and the WM was applied over the next two days due to the thickness of SFRM required and required drying time.

The DM applicator is seen in Figure 3.10, and Figure 3.11 shows the contractor filling the applicator with the DM. The DM is a dry-mix material, requiring only a one step

application process. The dry materials are pumped through an applicator and a separate water jot moistens the material as it as applied to the specimen. Figure 3.12 shows the working area for application, with the DM applicator located on the ground level below the specimens. The DM was applied in one application, in contrast to the 2-day application of the WM.

The WM was first mixed with water in a mixer, shown in Figure 3.13. This mixture of the WM dry materials and water was then brought by wheel barrow over to the WM spray applicator, shown in Figure 3.14. WM was then pumped to the work area and sprayed on the specimen, shown in Figure 3.15. The WM had to be applied in two coats to allow for proper drying of the materials. Figure 3.16 shows the specimen after the first coat of WM.

Figure 3.17 shows the regions of the specimen that were sprayed with the SFRM. The SFRM was applied on the beam only up to the first lateral brace, approximately 1 m from the face of the column so that the bracing would not interfere with the SFRM. The SFRM was applied 0.61 m above and below the panel zone on the column. Thicknesses for the specimens were checked during application to ensure proper material had been applied as seen in Figure 3.18.

3.4 LOADING HISTORY
The loading history for each of the beam-column assemblage experiments was based on the Interim Protocol I- Quasi-Static Cyclic Testing of FEMA 461: Interim Testing Protocols for Determining the Seismic Performance Characteristics of Structural and Nonstructural Components (2007). In this report, the loading history is referred to as the FEMA 461 loading history. Testing was performed under displacement control as the beams were expected to experience inelastic deformations. Beam tip displacement was the control parameter, which can then be related to story drift ratio.

Testing was performed by cycling beam tip displacements in the vertical direction. Figure 3.19 shows FEMA 461 step-wise increasing cycles for deformation-controlled loading histories. Each step consists of 2 cycles at the same amplitude. Relative step amplitudes were defined as ratios of the step amplitude to the last planned amplitude. The last planned amplitude was chosen to be close to the targeted maximum deformation, Δ_m, corresponding to a severe damage state. For this testing a story drift index of 0.03 was selected on the basis that significant yielding in the beam is expected, and the smallest deformation amplitude Δ_o was chosen such that it corresponded to a story drift of 0.0015 since prior monotonic testing did not exist.

Figure 3.20 shows the story drift ratio, θ, as related to the ratio of the displacement at the top of the column, δ, to the height of the column, H. Story drift ratio is typically associated with displacement at the top of the column and the column height. For this experiment the story drift ratio was compared to the beam tip displacement and the length of the beam. Assuming that the beam and column remain orthogonal, this ratio, θ, is also equal to the ratio of the beam tip displacement, Δ, to the length of the beam, L_{beam}. The

beam tip displacements associated with story drift ratios of 0.0015 and 0.03 – the smallest and largest expected deformations – were calculated based on the length of the beam.

$$\Delta_o = 0.0015 \cdot L_{beam} = 0.0015 \cdot 4.267m = 6.4mm \tag{3.28}$$

$$\Delta_m = 0.03 \cdot L_{beam} = 0.03 \cdot 4.267m = 128mm \tag{3.29}$$

The relative amplitudes for a 10 step loading history are shown in Table 3.3. The amplitude of each step, a_i, is increased by 40% with each step until the final amplitude, a_n, is reached. It was recommended that at least 10 steps be used during the loading history.

The final amplitude, a_n, was set equal to the maximum deformation, Δ_m, of 128 mm and the relative amplitudes previously defined were used to define the loading amplitudes for each step. This is shown in Table 3.4 and also plotted graphically in Figure 3.21. If sufficient damage was not found after the maximum deformation of 128 mm, the amplitude was increased at a rate of $0.3\Delta_m$ per step.

$$0.3 \cdot \Delta_m = 0.3 \cdot 128mm = 38.4mm \tag{3.30}$$

For the DM assemblage testing, damage to the SFRM resulting in exposed steel on the beam occurred during step 10 and the testing was terminated at the end of step 10. For the WM testing, the SFRM was sufficiently intact at the end of step 10 and testing continued to step 11. During step 11, damage to the SFRM resulting in exposed steel occurred and testing was then stopped.

In general, the duration of step time was chosen such that the rate of loading was constant throughout the test. Due to some time constraints, step 11 was loaded at a slightly faster rate, by keeping the duration of the loading step the same as was used for step 10.

Table 3.1 – Specified member properties

	d (mm)	b_f (mm)	t_f (mm)	t_w (mm)	Z (mm^3)	F_y (MPa)	A (mm^2)
W24 x 55 Beam	599.4	178.1	12.8	10.0	2195867	344.7	10452
W12 x 120 Column	332.7	312.4	28.2	18.0	3047994	344.7	22774

Table 3.2 – Specified sprayed fire resistive material thicknesses for assemblage testing

SFRM Type	W12x120 Column	W24x55 Beam
DM	22.2 mm	19.1 mm
WM	20.6 mm	25.4 mm

Table 3.3 – Relative amplitudes of deformation based on FEMA 461

Step	1	2	3	4	5	6	7	8	9	10
a_i/a_n	0.048	0.068	0.095	0.133	0.186	0.260	0.364	0.510	0.714	1.000

Table 3.4 – Specified beam tip displacement amplitude of loading for each step

Step	Displacement (mm)	% Story drift
1	±6.1	±0.14%
2	±8.7	±0.20%
3	±12.2	±0.29%
4	±17.0	±0.40%
5	±23.8	±0.56%
6	±33.3	±0.78%
7	±46.6	±1.09%
8	±65.3	±1.53%
9	±91.4	±2.14%
10	±128.0	±3.00%
11	±166.4	±3.90%
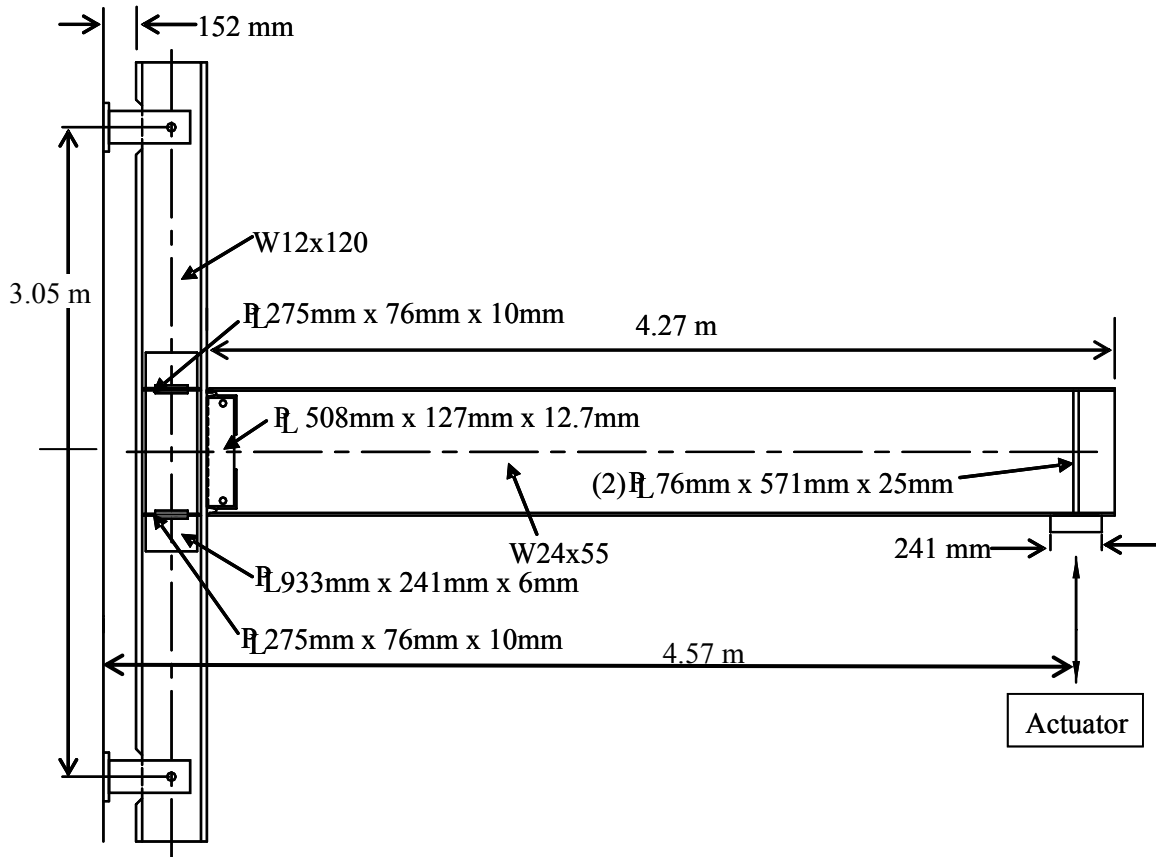
Figure 3.1 – Overall specimen geometry and setup
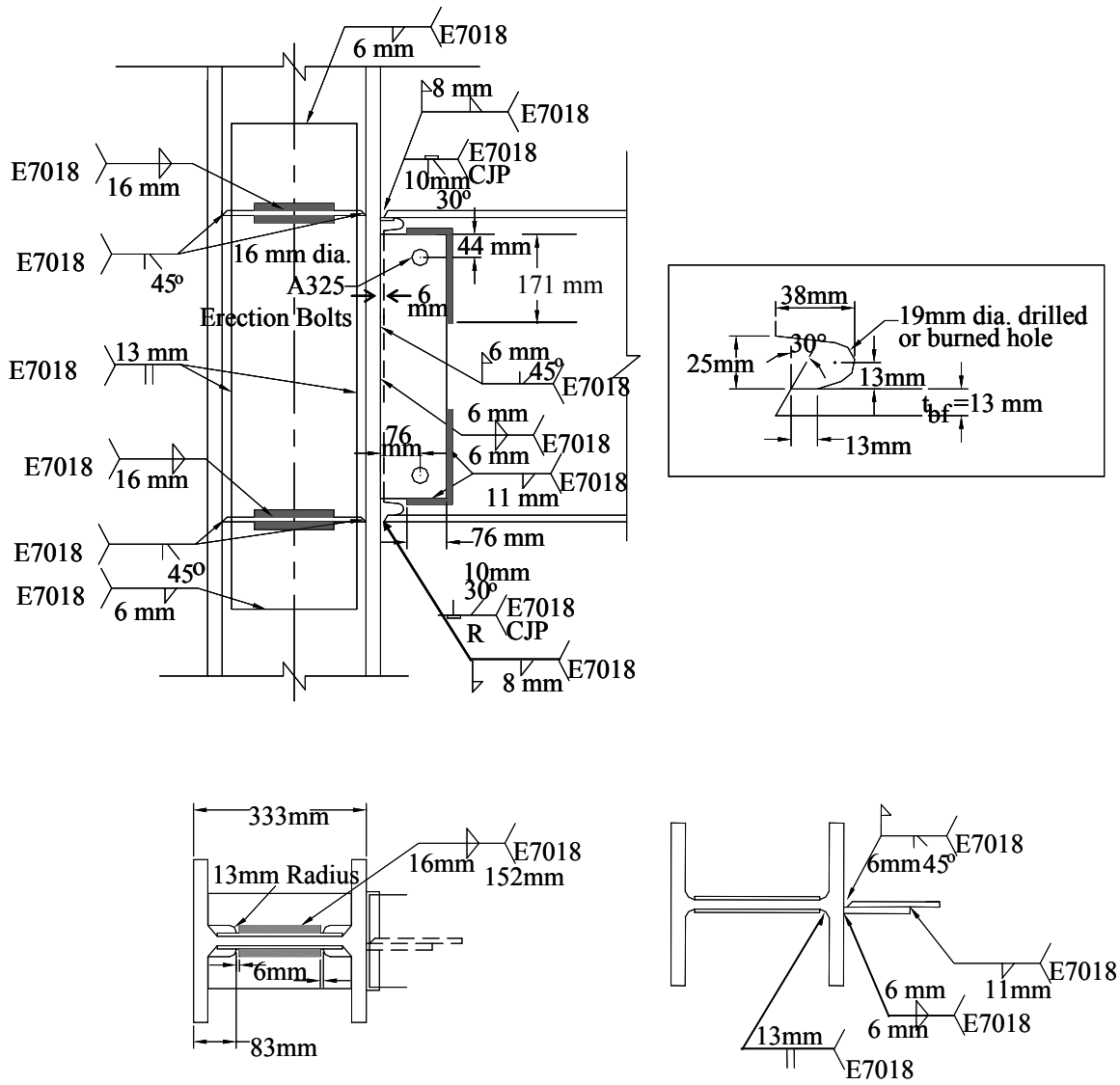
Figure 3.2 – Weld details for connection in assemblage tests

(a)

(b)

Notes:
-All bolts are 16mm A325
-Use filler plate to close gap
  at bolt locations
-All welds E7018
-All Angles 51mmx51mmx6mm

(c)
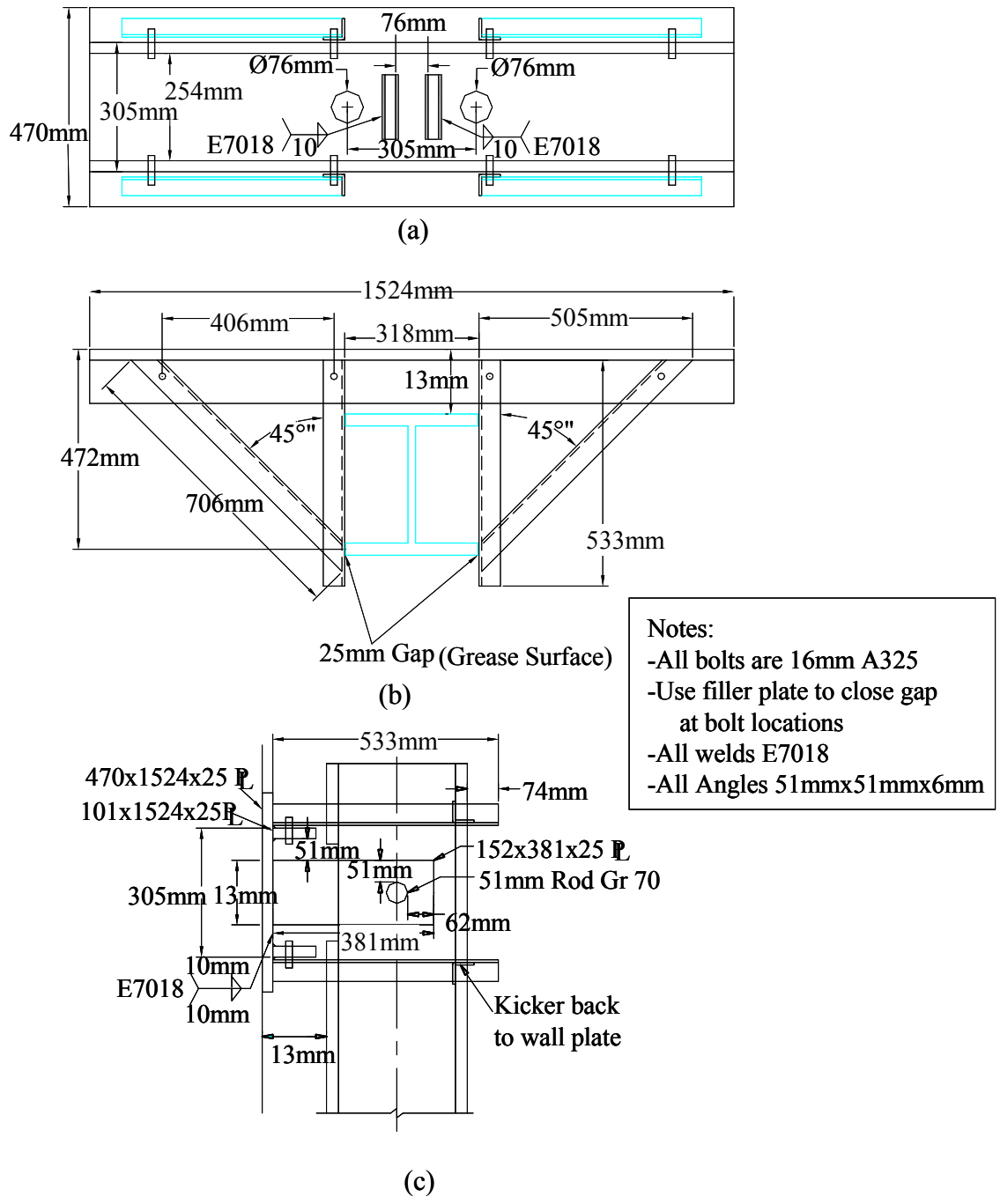
Figure 3.3 – Clevis details for wall fixture: (a) front view; (b) top view; and (c) side view
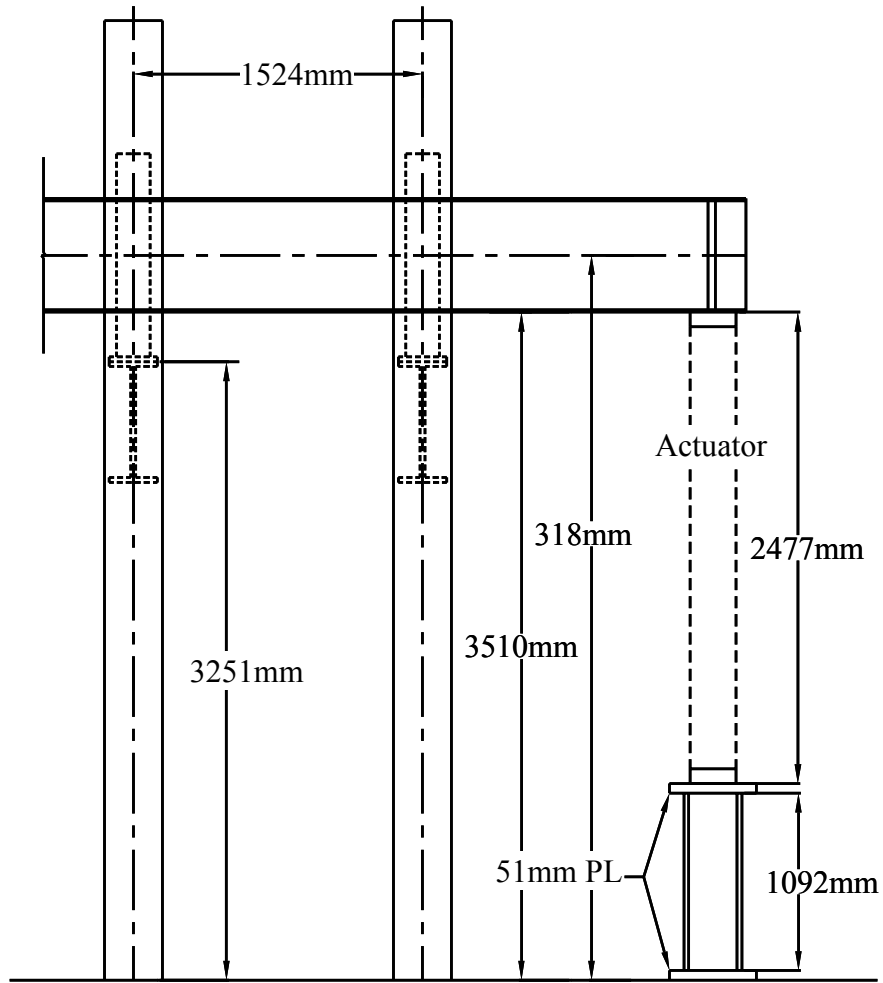
Figure 3.4 – Actuator base details
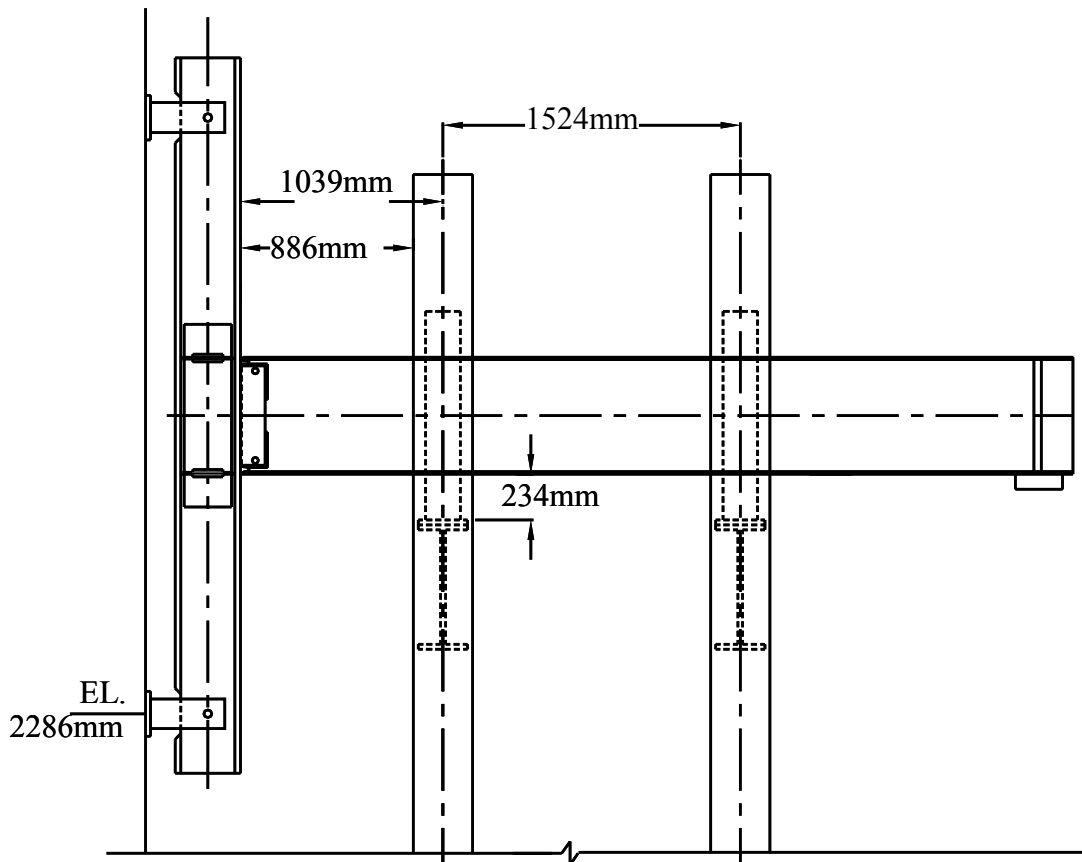
Figure 3.5 – Beam bracing layout

Figure 3.6 – Specimens after steel fabrication and before sprayed fire resistive material application

Figure 3.7 – Photograph of connection region after steel fabrication

Figure 3.8 – Ultrasonic testing of specimen
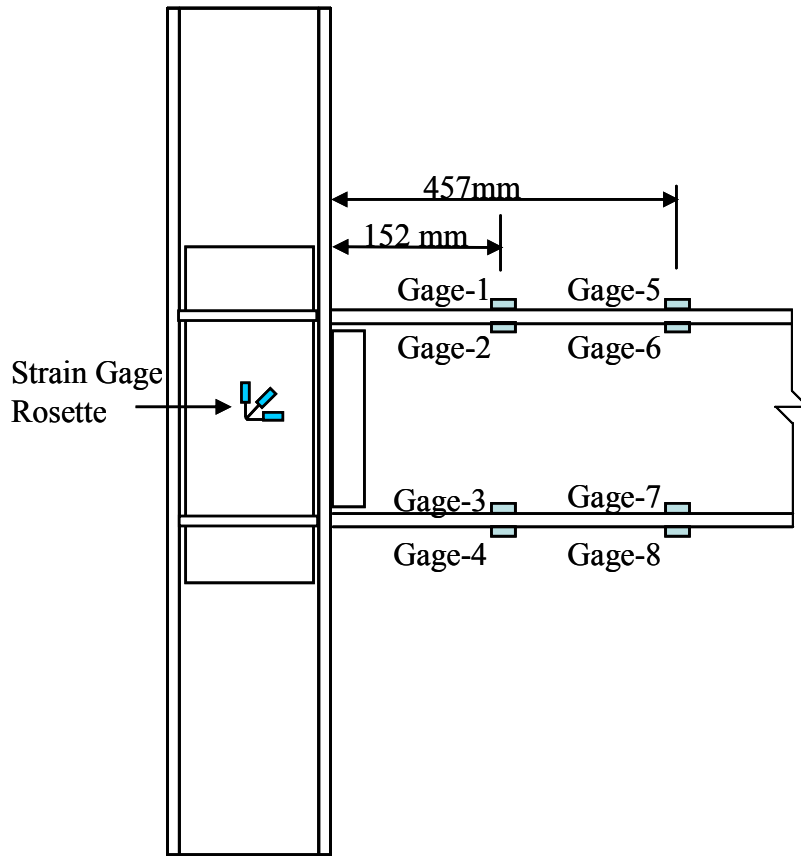
Figure 3.9 – Strain gage layout for assemblage testing

Figure 3.10 – Spray applicator for DM
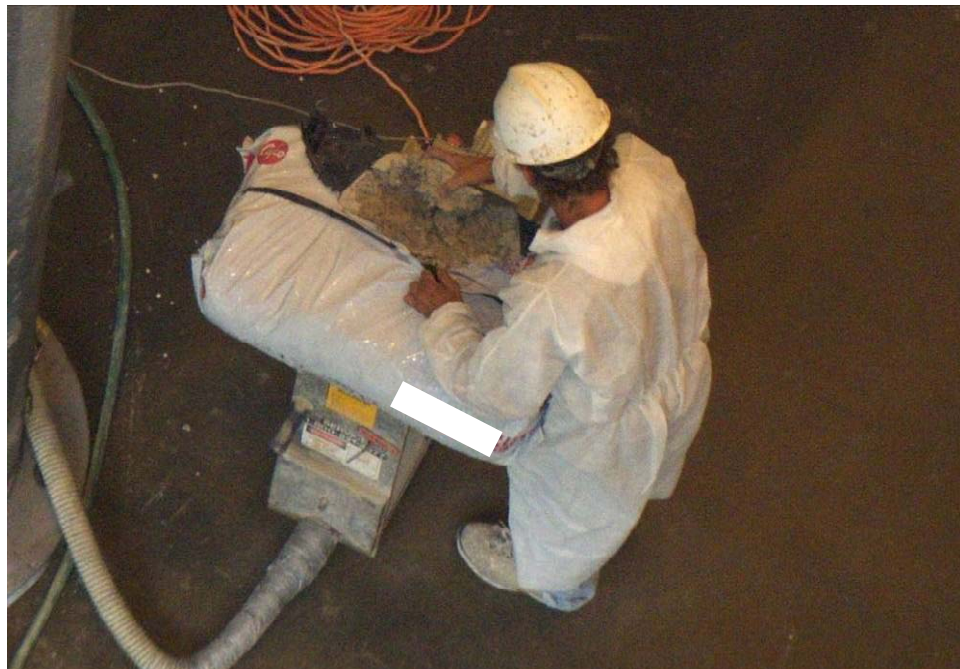
Figure 3.11 – Contractor filling applicator with DM

Figure 3.12 – Staging area for application

Figure 3.13 – Mixing WM with water

Figure 3.14 – WM spray applicator

Figure 3.15 – Application of WM

Figure 3.16 – Specimen after first coat of WM
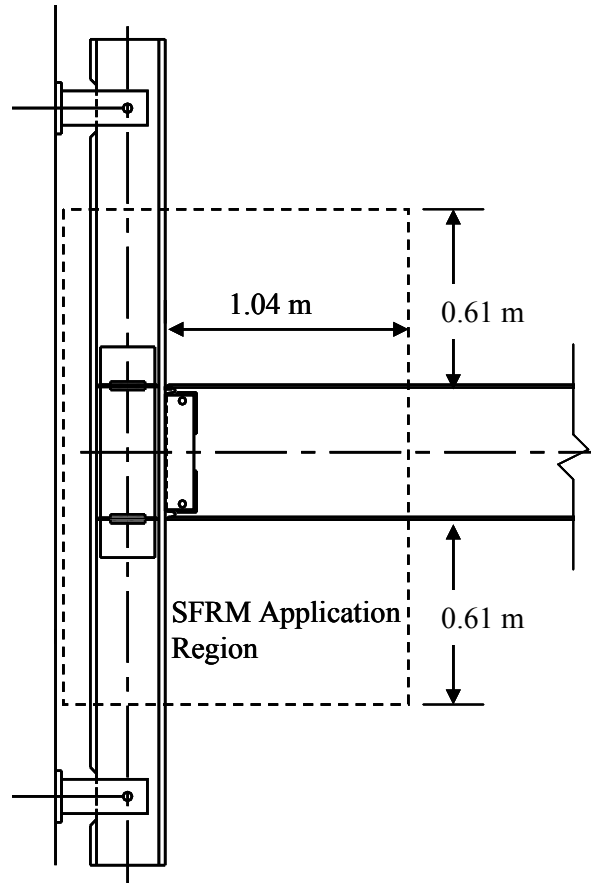
Figure 3.17 – Sprayed fire resistive material application regions

Figure 3.18 – Technician checking the thickness of the WM
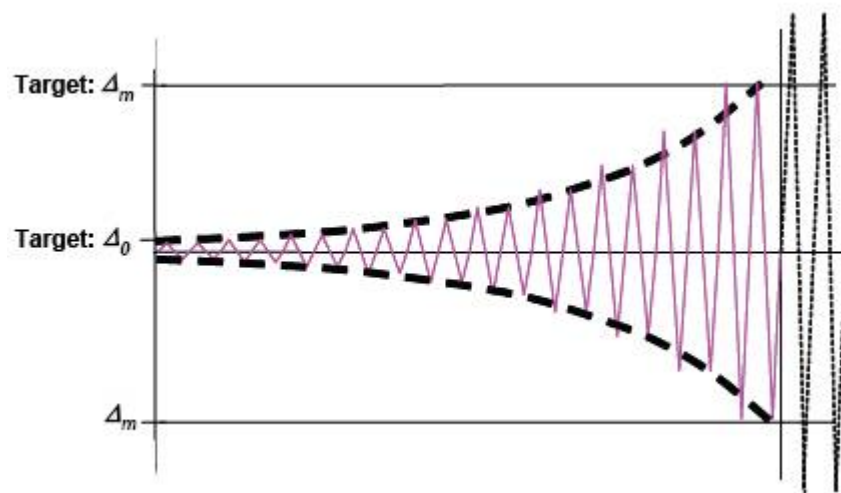
Figure 3.19 – FEMA 461 recommended deformation controlled loading history (FEMA 461, 2007)
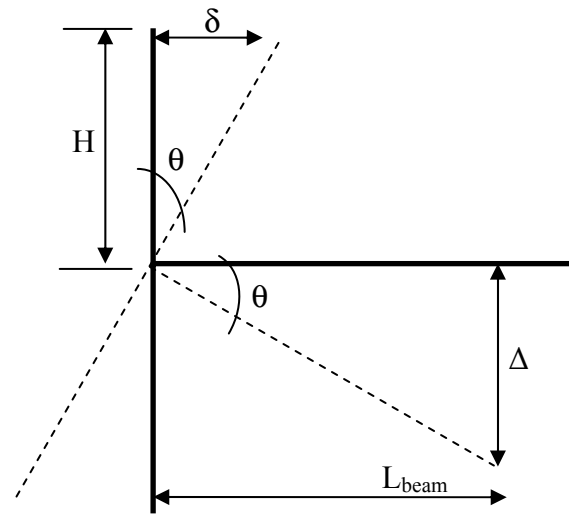
Figure 3.20 – Interstory drift relationships
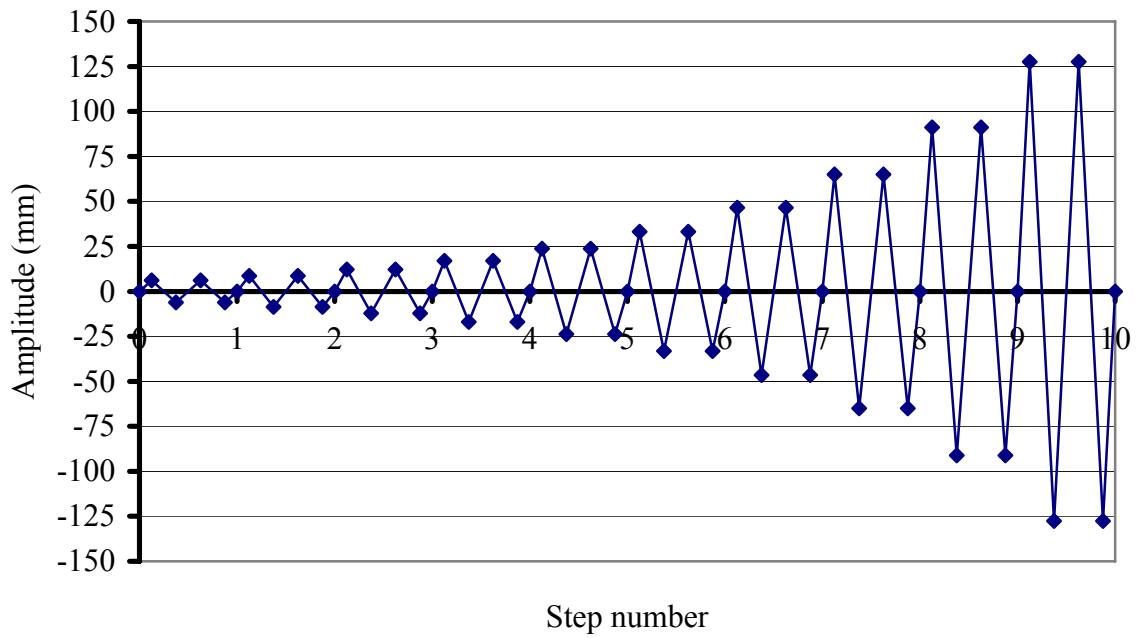
Figure 3.21 – Loading history for assemblage test

CHAPTER 4
ASSEMBLAGE TEST RESULTS AND DISCUSSION

4.1 INTRODUCTION

This chapter presents the results and discussion of the beam-column assemblage tests. The results from the DM assemblage test are presented in Section 4.2, and the results from the WM assemblage test are presented in Section 4.3. The presentation of results includes a description of the overall behavior of the specimen, beam behavior, panel zone behavior, and SFRM response.

For both the DM and WM specimens, the load expected to cause first yield in the beam, was 157 kN and the load expected to cause plastic moment in the beam section was 254 kN. This is based on the nominal cross-section dimensions, overall specimen geometry, and nominal material properties reported in the mill test reports.

4.2 DRY-MIX RESULTS AND DISCUSSION
4.2.1 Overall Behavior of Dry-mix Assemblage

The target beam tip displacement history used for the testing was presented in Chapter 3. Table 4.1 shows the actual load and displacement history that was applied during the DM assemblage testing. In this report, positive loads and positive displacements correspond to loading the beam tip in the upward direction. The associated story drift ratios at each step are also shown. The story drift ratio is calculated based on the average of the magnitude of the peak displacements.

Figure 4.1 shows a plot of load versus percent story drift for the duration of the DM assemblage test. The applied displacements ranged from -128 mm to +130 mm, which is equivalent to ±3% story drift, and the measured load ranged from -245.5 kN to +248.2 kN. The hysteresis loops show the energy dissipation in the system during the test and the system's ability to achieve large displacements.

Figure 4.2 shows a plot of load versus percent story drift for steps 1 through 6 of the DM assemblage testing. The plot shows linear elastic response and strain gage data from these steps, presented later in this chapter, confirm that the flanges of the beam remained elastic through step 4. The load in step 6 ranged from -108.1 kN to +106.8 kN, less than the load expected to cause first yield of 157.5 kN. There is a slight nonlinearity through zero load attributed to minor looseness in the loading and reaction hardware.

Figure 4.3 shows a plot of load versus percent story drift for step 7 of the DM assemblage testing. Slight hysteretic behavior is noticed in the graph. Strain gage data, presented in a later figure confirms that gages 2 and 3 yielded in compression. The load expected to cause first yield in the flanges of the beam was 157.5 kN and the maximum load reached in step seven was +/-152.6 kN. The displacement applied in this step is associated with 1% story drift, and is expected to be the onset of yielding in the steel beam.

Figure 4.4 shows a plot of load versus percent story drift for step 8 of the DM assemblage testing. Clear, but small, hysteretic behavior is now seen in the graph. Strain gage data, presented in later figures, confirms yielding in gages 1, 4, 5, 6, 7, and 8. The load ranged from -207.7 kN to +208.2 kN and the displacement ranged from -65.8 mm to +65.0 mm, which is associated with approximately 1.53% story drift.

Figure 4.5 shows a plot of load versus percent story drift for step 9 of the DM assemblage testing. The hysteresis loops have grown from the previous step and the beam tip displacement reached -91 mm and +92 mm, corresponding to an average story drift ratio of ±2.15%.   The loads ranged from -238.4 kN to +241.5 kN. The slope of the load-displacement curve started to decrease at higher loads as the section softened as it approached plastic moment capacity. The beam was expected to reach plastic moment capacity at an applied load of 253.5 kN.

Figure 4.6 shows the load versus percent story drift for step 10, the final step of the DM assemblage testing. The hysteresis loops are now large as energy was dissipated in the plastic hinge region and large deformations were experienced. The load during the first cycle of the step ranged from -245.5 kN to +248.2 kN and during the second cycle the step ranged from only -220.2 kN to +239.3 kN. This 10% reduction in the positive load and 4% reduction in the negative load were due to the softening of the system; larger displacements can be achieved under lesser loads. The unloading that is occurring in this step is attributed in part to the buckling of the beam flange. A plastic hinge formed in the beam near the face of the column allowing for plastic rotation of the beam and larger deformations. The specimen reached 3% story drift during this step.

A review of Figure 4.6 shows damage to the SFRM in step 10. During the first cycle of downward loading, a large tear in the SFRM was seen on the bottom flange when this flange is in compression, shown as point A in this figure and also shown in the photograph in Figure 4.7. During the second upward segment of loading, a large tear in the SFRM in the top flange was seen, also when the flange is in compression. This is shown as point B in Figure 4.6 and also shown in the photograph in Figure 4.8. Finally, during the second downward segment of loading at a displacement of -122.4 mm, a large portion of SFRM fell off of the bottom of the bottom flange of the specimen when that flange was in compression. This is shown as point C in Figure 4.6 and in the photograph in Figure 4.9. Details on the size and location of the damage to the SFRM are discussed further in Section 4.4.1.

4.2.2 Beam Results for Dry-mix Assemblage Test
4.2.2.1 Strains in the Beam Flanges
Table 4.2 shows the maximum strains at each step of the DM assemblage test and Table 4.3 summarizes the maximum strains in the beam flange gages for the entire test. Both tables also report the corresponding multiple of nominal yield strain, which is approximately 0.0019. In these tables and in all plots of strains, compressive strains are reported as negative values, and tension strains are reported as positive values.

Plots of beam strains versus applied load are shown in Figure 4.10 through Figure 4.14. All plots are shown to the same scale, with the overall scale dictated by the largest strain values reported during the test.

As shown in Figure 4.10, the first six steps of loading exhibit linear elastic response. Table 4.2 verifies that the steel at the locations of the strain gages has not yet yielded.

Figure 4.11 shows the DM assemblage test strain gage data for step 7 of loading. The steel at the locations of both Gage-2 and Gage-3, 152 mm from the column face, started to yield in compression but was still elastic in tension. The steel at the locations of the other six gages remained elastic in both compression and tension.

Figure 4.12 shows the DM assemblage test strain gage data for step 8 of loading. All the gages 152 mm from the column face (Gage-1, Gage-2, Gage-3, and Gage-4) show compressive yielding in the steel, and this is confirmed in the strain gage data presented in Table 4.2. The table also indicates that only the steel at the location of Gage-4, on the bottom of the bottom flange, is at the onset of tensile yielding, while the steel at other gages remained elastic in tension. In the group of gages 457 mm from the column face, Gage-5 indicated tensile yielding only, and the steel at the locations of Gage-6, Gage-7, and Gage-8 was still elastic in both compression and tension. This lag in yielding illustrates the decreasing in moment as the distance from the column face increases, and thus a decrease in flange force and strain at this location.

Figure 4.13 shows the DM assemblage test strain gage data for step 9 of loading. Gage-2 did not yet indicate tensile yielding and the steel at the location of Gage-3 was at the onset of tensile yielding. The steel at all of the other gages has yielded in both tension and compression. In general, the steel at the location of the gages 152 mm from the column face yielded further than the steel at the location of the gage 457 mm from the column face. Hysteretic behavior was clear in the steel at the location of several of the gages in this figure.

Figure 4.14 shows the DM assemblage test strain gage data for step 10, the final step of loading. The steel at the location of all the gages fully yielded, and hysteresis is clear in the steel at the location of all the gages in this figure. Gage-1 and Gage-2 on the top flange, 152 mm from the column face, show the strain ranged from -0.00436 to +0.00919 and -0.00893 to +0.01044 respectively, and at the end of the test there was residual tensile strain in the steel at both gage locations.

Gage-3 and Gage-4 were on the bottom flange, 152 mm from the column face. Gage-3 indicated a strain range of -0.01126 to +0.00586, however Gage-4 was damaged in the second cycle of step 10 when the SFRM fell off, and thus final strain readings are missing. At the end of the test there was residual compressive strain in Gage-3 and in can be deduced from the trend in the graph that there would also have been residual compressive strain in Gage-4.

44

Gage-5 and Gage-6 on the top flange indicate strains that ranged from -0.00997 to +0.00914 and -0.01926 to +0.00960 respectively. At the end of the test, there was residual tensile strain in Gage-5 and slight residual compressive strain in Gage-6. Gage-7 and Gage-8 on the bottom flange indicate the strain ranged from -0.03905 to +0.00323, and -0.01791 to +0.00321 respectively. Tensile yielding was more dominant than compressive yielding in Gage-7 and Gage-8 and at the end of the test there was large residual compressive strain in Gage-7. Gage-8 was damaged in the second cycle of step 10 when the SFRM fell off, so final strain readings are missing, but in can be inferred from the figure that residual compressive strain existed at the end of the test. Gage-7 also went out of range briefly near the end of the test.

4.2.2.2 Strain Difference in the Beam Flanges
The difference in strain over the thickness of the flanges is shown by comparing the gages at the top and bottom of the flange at each location. As a reminder, a positive difference described a larger strain at the top of the flange than at the bottom of the flange and an upward buckle in a concave downward shape. Likewise, a negative difference indicates downward buckling in a concave upward shape.

Figure 4.15 shows the DM assemblage test difference in strain at all four flange locations for steps 1 through 4. There was negligible difference in the strains at all locations, and the flanges were known to still be elastic at this point. Therefore flange buckling was not yet a factor up through step 6.

Figure 4.16 shows the DM assemblage test difference in strain at all four flange locations for step 7. The flange locations closer to the column face (152 mm) show small strain differences – positive on the top flange and negative on the bottom flange. The differences in strain are not thought to be large enough however to clearly indicate buckling. The difference in strain in the flanges further from the column face (457 mm) was still negligible, and strains were still elastic. Therefore flange buckling was not a factor through step 7.

Figure 4.17 shows the DM assemblage test difference in strain at all four flange locations for step 8. The flange locations closer to the column face now show larger strain differences, again positive on the top flange, negative on the bottom flange, indicating possible initiation of flange buckling. However, the flange locations further from the column face still show negligible strain difference and thus flange buckling was not a factor for the steel under the strain gage 457 mm from the column face through step 8.

Figure 4.18 shows the DM assemblage test difference in strain at all four flange locations for step 9. The magnitude of strain difference is similar in the closer gages to the magnitude of the strain difference in the previous step. The top flange, further from the column now exhibits a positive strain difference on the top flange, but still shows negligible difference in the bottom flange. The data from the top flange at this location shows possible initiation of flange buckling.

45

Figure 4.19 shows the DM assemblage test difference in strain at all four flange locations for step 10, the final step of loading. As a reminder, damage to the SFRM occurred during this step. The strain difference at all four locations are substantial and buckling was assumed to have occurred. The strain gages at the top flange at both locations indicated predominately a positive strain difference, and thus downward concavity at both gage locations. The strain gages on the bottom flange at both locations indicated negative strain differences, and thus positive concavity at both gage locations.

Figure 4.20 shows the bottom flange at the end of the DM assemblage test and Figure 4.21 shows the magnitude of the buckle in the bottom flange to be approximately 50 mm. The SFRM fell off in this region and the steel structure was exposed, revealing a local flange buckle partway between the Gage-4 and Gage-8. Strain difference data for the bottom flange indicated negative strain differences in the steel at both gage locations, consisted with the upward concavity at the gage locations. However at the peak of the buckle, the steel in concave downward and no strain data exists for this location. As a reminder, Gage-4 and Gage-8 data is incomplete due to damage in the second cycle of step ten of loading, and thus the difference in strain is not applicable for the end of the step for either location on the bottom flange.

Figure 4.22 shows the top flange during the post-testing inspection. The SFRM on the top flange of the beam did not fall off of the specimen during the testing. However, examination of this region after the experiment revealed that the SFRM was debonded. In order to inspect the steel substructure the loose SFRM was carefully removed from the flange. The inspection revealed a local flange buckle partway between Gage-5,6 and Gage-1,2. The strain gage data from these locations indicated positive strain differences at both locations, consisted with the downward concavity at the gage locations. Again, the peak of the buckle occurred between the gages and no strain data exists for this location.

In retrospect, positioning a pair of gages midway between the existing gages, at approximately 305 mm from the column face, would have resulted in more accurate detection of the onset of buckling.

4.2.3 Panel Zone Results
The column was designed in accordance with the strong column – weak beam philosophy. Panel zone strains were tracked with a strain gage rosette in the center of the panel zone on the doubler plate.

Figure 4.23 shows the principle stresses plotted against the principle strains in the panel zone for the DM assemblage test. Principle strains were calculated based on the rosette readings and principle stresses were determined based on linear-elastic, isotropic behavior. Linear-elastic response is clear. The maximum stress calculated was 241.3 MPa, approximately 70% of the yield strength of the material (344.7 MPa). Strains were not tracked in the upper and lower portions of the column, outside the panel zone, as the strains were expected to be lower in these regions.

4.3 WET-MIX RESULTS AND DISCUSSION
4.3.1 Overall Behavior of Wet-mix Assemblage
The target displacement history used for the testing was presented in Chapter 3. Table
4.4 shows the actual load and displacement history applied during the WM assemblage
testing. In this report, both positive loads and positive displacements correspond to the
upward direction. The associated story drift ratios at each step are also shown. Story
drift ratios were calculated based on the average magnitude of maximum displacement in
that step.

Figure 4.24 shows a plot load versus beam tip displacement for the duration of the WM
assemblage test. The applied displacements ranged from -167 mm to +165 mm, which is
equivalent to an average of ±3.9% story drift, and the measured load ranged from -255.6
kN to +257.1 kN. The hysteresis loops show the energy dissipation in the system during
the test and the system's ability to achieve large displacements. The load expected to
cause first yield, was 157 kN and the load expected to cause plastic moment in the
section was 254 kN. Both of these values are shown on the figure.

Figure 4.25 shows a plot of the load versus percent story drift for the first 6 load steps of
the WM assemblage testing. The plot shows linear elastic response, and strain gage data
from these steps presented later in this chapter, confirm that the flanges of the beam
remained elastic through step 6. The load in step 6 ranged from -107.7 kN to +107.0 kN,
less than the load expected to cause first yield of 157.5 kN.

Figure 4.26 shows a plot of the load versus percent story drift for step 7 of the WM
assemblage testing. The behavior looks close to linear elastic, and strain gage data
presented later in this chapter confirms that only the steel at Gage-4 began to yield in
tension. The load expected to cause first yield in the flanges of the beam was 157.5 kN
and the maximum load reached in step 7 was only 153.1 kN. The specimen reached
approximately 1% story drift in this step.

Figure 4.27 shows a plot of the load versus percent story drift for step 8 of the WM
assemblage testing. Clear, but small, hysteretic behavior is now seen in the graph. Strain
gage data presented later in this chapter confirms yielding in the steel at all gages. The
load ranged from -210.2 kN to +210.7 kN and the displacement ranged from -64.6 mm to
+63.9 mm, which is associated with approximately 1.5% story drift.

Figure 4.28 shows a plot of the load versus percent story drift for step 9 of the WM
assemblage testing. The hysteresis loops have grown from the previous step and the
specimen reached -91.4 mm and +88.8 mm, corresponding to a story drift ratio of
±2.11%. The loads ranged from -243.7 kN to +244.7 kN. The slope of the load-
displacement curve has decreased at higher loads as the section softened. The beam is
expected to reach plastic moment capacity at an applied load of 253.5 kN.

Figure 4.29 shows a plot of the load versus percent story drift for step 10 of the WM
assemblage testing. The hysteresis loops are now large as energy was dissipated through

the system and large deformations were experienced. The load ranged from -255.6 kN to +257.1 kN and the displacement ranged from -128.7 mm to +126.5 mm, corresponding to approximately ±3% story drift. This was the story drift expected to cause damage in the structural steel system. Since the load and moment were still maintained, and the SFRM was still in place, the test was extended for an additional step as per the recommendations in FEMA 461.

Figure 4.30 shows a plot of load versus percent story drift for step 11, the final step of the WM assemblage testing. The hysteresis loops are large as energy was dissipated through the system and large deformations were experienced. Only one cycle of loading was performed as damage to the SFRM occurred in this first cycle. The load ranged from -234.3 kN to +254.7 kN and the displacement ranged from -167.0 mm to 165.0 mm, which corresponds to approximately 3.9% story drift. A reduction in moment occurred during the latter portion of both the upward and downward portions of loading in this step, as the system unloaded. During the upward loading segment, the moment decreased to 221.5 before the loading was reversed, a 14% drop. During the downward loading segment, the moment decreased to -201.6 before the loading was reversed, also a 14% drop. This reduction in load is due to possible flange buckling. A plastic hinge formed in the beam near the face of the column allowing for plastic rotation of the beam and larger deformations.

Figure 4.31 shows the damage to the SFRM that occurred during step 11.   Throughout the step, large cracks were seen on the specimen on both the web and flanges of the beam. During the downward loading cycle, when the bottom flange was in compression, a large portion of SFRM fell off, damaging Gage-4 in the process. This occurred at a displacement of approximately -150 mm. Further details of the SFRM damage are presented and discussed in Section 4.4.2.

4.3.2 Beam Results for Wet-mix Assemblage Test
4.3.2.1 Strains in the Beam Flanges
Table 4.5 shows the minimum and maximum strains at each step of the WM assemblage test and Table 4.6 summarizes the maximum strains in the steel at the locations of the beam flange gages for the entire test. Both tables also report the corresponding multiple of nominal yield strain, which is approximately 0.0019. In these tables and in all plots of strains, compressive strains are reported as negative values, and tension strains are reported as positive values.

Figure 4.32 shows the WM assemblage test strain gage data for steps 1 through 6 of loading. All gages exhibit linear-elastic behavior and Table 4.5 verifies that the steel at the strain gages did not yield.

Figure 4.33 shows the WM assemblage test strain gage data for step 7 of loading. The steel at all gages is still elastic.

Figure 4.34 shows the WM assemblage test strain gage data for step 8 of loading.   The steel at all the gages 152 mm from the column face (Gage-1, Gage-2, and Gage-4) was at the onset of yielding and this is confirmed in the strain gage data presented in Table 4.5. In group of strain gages located at 457 mm from the column face, the steel at the location of most of the gages was still elastic in both compression and tension.

Figure 4.35 and Figure 4.36 show the WM assemblage test strain gage data for step 9 and 10 of loading, respectively. The steel at all the gages has yielded and hysteretic behavior is now clear in both figures.

Figure 4.37 shows the WM assemblage test strain gage data for step 11, the final step of loading. Gage-1, 2, 7, and 8 appear to have failed during testing. Gage-1 and Gage-2 on the top flange, 152 mm from the column face, indicate strain ranges from -0.01169 to +0.00324 and -0.00329 to +0.00363, respectively, and at the end of the test there was residual compressive strain in the steel beneath both gages.

Gage-4 on the bottom flange, 152 mm from the column face, was damaged when the SFRM fell off during step 11 and final strain readings are missing. It is reasonable to assume from the trends in the figure that there would have been residual tensile strain in Gage-4 at the end of the test.

Gage-5 and Gage-6 on the top flange indicate that the strain ranged from -0.00671 to +0.00627 and -0.00262 to +0.00880, respectively.   At the end of the test, there was residual tensile strain in the steel at the location of both Gage-5 and Gage-6. Gage-7 and Gage-8 on the bottom flange indicate the strain ranged of -0.00644 to +0.00701 and -0.00505 to +0.01133, respectively. However, the data is inconclusive as the gages appear to have failed.

4.3.2.2 Strain Difference in Flanges
As a reminder, a positive difference described a larger strain at the top of the flange than at the bottom of the flange and an upward buckle in a concave downward shape. Likewise, a negative difference indicates downward buckling in a concave upward shape.

Figure 4.38 and Figure 4.39 show the WM assemblage test difference in strain at the three applicable flange locations for steps 1 through 6, and step 7, respectively. There was negligible difference in the strains at all locations and the flanges were known to still be elastic at this point. Therefore, flange buckling was not a factor up through step 7.

Figure 4.40 show the WM assemblage test difference in strain at the three applicable flange locations for step 8. The gages on the top flange closer to the column face, at 152 mm, show small negative strain differences. The differences in strain were not thought to be large enough however to clearly indicate buckling. The difference in strain in the flanges further from the column face (457 mm) were still negligible, strains were still elastic, and therefore buckling was not a factor through step 8.

Figure 4.41 show the WM assemblage test difference in strain at the three applicable flange locations for step 9. All three locations show small strain differences. Therefore flange buckling was not a factor through step 9.

Figure 4.42 show the WM assemblage test difference in strain at the three applicable flange locations for step 10. All three locations show larger strain differences. Therefore, it is probable that flange buckling was imminent.

Figure 4.43 show the WM assemblage test difference in strain at the three applicable flange locations for step 11. The data is largely inconclusive as failure appears to have occurred in the gages. However, it can be inferred from the data that the strain differences were negative, indicating concave upward deformations. As a reminder, significant damage occurred to the SFRM during this step.

Figure 4.44 shows the bottom flange of the WM assemblage at the end of the test. The SFRM fell off in this region and the steel structure was exposed, showing a local flange buckle between Gage-4 and Gage-8, approximately 50 mm at the peak, as shown in Figure 4.45. The flange is concave upward at each strain gage location, which is consistent with the negative strain difference in the bottom flange previously discussed.

Figure 4.46 shows the top flange during post-testing inspection. The SFRM on the top flange of the beam did not fall off of the specimen during testing, but it was discovered during inspection that it was debonded. In order to inspect the steel substructure the loose SFRM was carefully removed from the flange. The flange is only slightly concave upward at each strain gage location, which is consistent with the negative strain difference in the top flange previously discussed. Also the small magnitude of strain difference is indicative of the minor extent of buckling.

4.3.3 Panel Zone Results
Figure 4.47 shows the principle stresses plotted against the principle strains in the panel zone for the WM assemblage test and the linear-elastic response is clear. The column was designed in accordance with the strong column – weak beam philosophy. Panel zone strains were tracked with a strain gage rosette in the center of the panel zone on the doubler plate. Principle strains were calculated based on the rosette readings and principle stresses were determined based on linear-elastic, isotropic behavior. The maximum stress calculated was 146 MPa, approximately 42% of the steel's yield strength (344.7 MPa). Strains were not tracked in the upper and lower portions of the column, outside the panel zone, as the strains were expected to be lower in these regions.

4.4 SPRAYED FIRE RESISTIVE MATERIAL RESPONSE
The SFRM was visually inspected during testing and also carefully examined after the testing was complete. SFRM response is considered for three different regions in the assemblage: the beam flanges, the beam web, and the panel zone.

4.4.1 Dry-mix Response

4.4.1.1 Beam Flange Response

Figure 4.48 shows longitudinal splitting in the SFRM on the top flange that was observed during step 10 of testing. These tears appeared when the flanges were in compression and were approximately 300 mm long.

Figure 4.49 shows a large transverse crack that was found in the SFRM on the top flange at the end of the test, 203 mm from the face of the column SFRM.

Figure 4.50 shows the top of the top flange after the loose SFRM was removed during post-testing inspection. The SFRM on the top flange of the beam was debonded at the end of the test. However, due to the geometry of the specimen, the SFRM did not fall off. The damaged area is 430 mm on the far side of the flange and 350 mm on the near side and covers the full width of the flange. The damaged area is approximately 50 mm from the face of the column SFRM.

Figure 4.51 shows the underside of the top flange after the loose SFRM was removed. The damaged portion of the underside of the flange is 305 mm in length and approximately 50 mm in depth.

Figure 4.52 show longitudinal splitting in the bottom flange SFRM that was noticed during the step 10 of testing, during the first downward loading cycle when the bottom flange was in compression. These tears were approximately 300 mm long.

Figure 4.53 and Figure 4.54 shows a more detailed view of the large portion of SFRM that fell off of the bottom flange during the second downward cycle of loading in step 10, when the bottom flange was in compression. The exposed steel area was 305 mm long and 178 mm wide.

Figure 4.55 shows the final damaged section on the underside of the bottom flange. By the time the test was complete, a smaller portion of SFRM also became detached from the specimen. The damaged section is 100 mm from the face of the column SFRM and measures 483 mm on the far side of the flange and 431 on the near side, and covers the full width of the beam flange which is 178mm.

4.4.1.2 Beam Web Dry-mix Response

The SFRM on the beam web remained intact throughout the duration of the test. When inspecting the SFRM after testing was complete, it was found that it was actually debonded over most of the web. However, due to the geometry of the web and the proximity of the SFRM on the flanges the SFRM was able to remain attached to the specimen. The fibrous DM also has a tendency to remain contiguous.

4.4.1.3 Panel Zone Dry-mix Response

The SFRM remained fully intact in the panel zone region of the DM specimen. After the test had been performed, a sample of the SFRM was taken from the panel zone and after

cutting into the material it was found that the SFRM was still bonded to the steel. This was the expected result as the column was designed to remain elastic.

4.4.2 Wet-mix Response
4.4.2.1 Beam Flange Wet-mix Response
Figure 4.56 shows the damage of the SFRM in the WM specimen that occurred during the step 11 of loading, near the end of the downward loading cycle at a beam tip displacement of approximately 149 mm. The damaged area covered the width of the beam flange and extended from the face of the column SFRM outward for 381 mm. Figure 4.57 shows the extensive cracking present at the completion of testing on the top of the top flange and Figure 4.58 shows the area of steel exposed once the loose SFRM was removed during post-testing inspection. Cracking in the SFRM was present throughout the duration of the test. At the end of the test there were areas where the SFRM was debonded, but still attached to the beam flange. These areas were carefully removed at the end of the test to further investigate SFRM damage. The damage extends the full width of the flange and progresses from 76 mm from the face of the column SFRM outward for 305 mm.

4.4.2.2 Beam Web Wet-mix Response
Figure 4.59 shows the extensive cracking in the beam web that occurred throughout the WM assemblage test.

Figure 4.60 shows the damage to the web near the top flange of the WM specimen found during the post-inspection testing. When the loose SFRM was removed from the top flange, it was found that the loosened SFRM extended into the upper portion of the web of the beam.

Figure 4.61 shows the damage to the web near the bottom flange of the WM specimen found during the post-inspection testing. Likewise, when the loosened SFRM was removed from the top of the bottom flange, it was found that the damage extended into the lower portion of the beam web.

4.4.2.3 Panel Zone Wet-mix Response
The SFRM remained fully intact in the panel zone region of the WM test specimen. After the test had been performed, a sample of the SFRM was taken from the panel zone and after cutting into the material it was found that the SFRM was still bonded to the steel. This was the expected result as the column was designed to remain elastic.

4.5 BUILDING PERFORMANCE LEVELS
FEMA 450 (BSSC, 2003) defines performance levels of buildings in terms of the extent of damage that has occurred to structural and nonstructural systems. There are four main performance levels of importance: (1) operational; (2) immediate occupancy; (3) life safety; and (4) collapse prevention. The operational level is defined for structures that have negligible damage to the structural system and minor damage to the nonstructural system. The immediate occupancy level is defined for structures that have slight damage

to the structural system, but moderate damage to the nonstructural system. The structure retains its full strength, but may have a small reduction in stiffness, and remains safe to occupy. The life safety performance level is defined for structures that have significant structural damage, including yielding and buckling, and serious (but not hazardous) damage to the nonstructural systems. Finally, the collapse prevention level is defined for structures that have serious damage to their structural systems and have lost substantial strength and stiffness. Structures at the collapse prevention level are not likely repairable.

Structures are required to meet different performance levels for earthquakes of varying severity. Figure 4.62 shows the expected building performance for the different Seismic Groups under the different ground motion levels. For instance, general structures in Seismic Use Group 1 are expected to meet the life safety performance level requirements when exposed to a design earthquake. Design earthquakes have a 10% probability of exceedance in 50 years and have ground shaking levels that are 2/3 of that of the Maximum Considered Earthquake. Maximum Considered Earthquakes have a 2% probability of exceedance in 50 years.

The specimens in this research were displaced to approximately ±3% and ±3.9% story drift during the application of load and the steel was expected to start to yield at approximately ±1% story drift. For the steel moment frame considered in this research, 1% story drift would typically occur due to a design earthquake. Since the steel is expected to begin to yield, and thus damage to the steel is initiated, this is associated with the onset of the life safety performance level. The ±3% and ±3.9% story drift ranges associated with the displacements applied during the tests would typically occur due to a more intense design earthquake. Inelastic deformations are expected in the steel at these story drift levels as well as potential buckling in the beam flanges and beam web. This level of damage to the steel frame is again associated with the life safety performance level, but during the latter stages of the level, approaching collapse prevention.

4.6 SUMMARY OF BEAM-COLUMN ASSEMBLAGE TESTS
Damage occurred to the beam SFRM when large deformations were achieved in the beam adjacent to the column. This damage was present on the underside of the bottom flange in both the DM and WM tests and progressed into the web for the WM test. Damage also occurred on the top flange in both tests. However this damage may not arise in actual structures due to the presence of decking and/or a concrete slab in the floor system.

Damage occurred to the SFRM in the beam column assemblage at story drift levels associated with earthquake loading. At approximately ±3% story drift the DM specimen exhibited longitudinal as well as transverse tearing, and large portions of SFRM fell off the specimen. At approximately ±3.9% story drift during the WM assemblage test, large portions of SFRM fell off the specimen.

Longitudinal and transverse tearing occurred in the beam of the DM specimen prior to the final damaged state. These tears occurred on both the top and bottom flange of the beam.

Extensive cracking occurred throughout the duration of testing on the beam of the WM specimen, both on the flanges and the web. There was no visible cracking on the column of the WM specimen.

Damage in the WM specimen progressed into the beam web, while the DM remained intact on the web. The cracking in the WM allowed for localized damage in the web SFRM to occur, while the fibrous nature of the DM caused a tendency of the SFRM to remain fused together. During post-testing inspection, the DM was loose to the touch and it was assumed to lack adhesion to the steel in areas. However, it did not fall away from the specimen.

Buckling occurred in the bottom flange of the beam in both the DM and WM tests, as confirmed by the strain gage data presented in Chapter 6 and 7. The SFRM became detached over the full width of the bottom flange in this region. In the case of the DM specimen, the detachment occurred at a distance of approximately half the flange width from the column face. In the WM test specimen, the detachment extended to the face of the column SFRM. This could be due to the tendency of the WM to crack and the presence of a transverse crack at the interface between the beam and the column.

Web buckling was visible during post-testing inspection of both the DM and WM specimens, but there is no strain gage data present quantify strain in the web. Cracking was prominent over the web of the WM specimen but there was no visible cracking or tearing in the web of the DM specimen.

The column was designed to remain elastic during loading and strain gage data confirmed this behavior. The SFRM on the column remained intact throughout the duration of both the DM and WM tests. At the conclusion of testing, an area of SFRM was removed from the panel zone on the column for density and thickness testing. The SFRM was still fully bonded to the column on both the DM and WM specimens. This result agrees with the results of the flat plate tests, where the bond strength was reduced, but not diminished at elastic strains.

Damage occurred to the SFRM in the beam column assemblage specimens at story drift levels associated with earthquake loading. The degree of damage to the SFRM depends upon the earthquake intensity. Damage to the SFRM begins with debonding of the SFRM from the steel as the steel yields. This occurs at story drifts as low as 1%, which for the steel moment frame considered in this research, would be expected under the action of an earthquake in the early stages of the life safety performance level. However, even though the SFRM is debonded from the yielded portions of the connection at this story drift level, the three dimensional geometry of the SFRM in the beam-column connection prevents the SFRM from falling off the connection region.

Under the action design earthquakes causing story drifts of 3% to 4%, anticipated inelastic buckling (in the beam flanges in this study) creates tears in the SFRM at the locations of the buckling. The tears separate the SFRM in to sections that can then fall away from the connection, exposing the steel at those locations. The steel moment frame considered in this research is in the latter stages of the life safety performance level when this damage occurs.

Table 4.1 – Actual load and displacement history for DM assemblage test

	Load Range		Displacement Range		% Story drift
	min (kN)	max (kN)	min (mm)	max (mm)	
Step 1	-16.5	17.8	-5.6	6.6	±0.14%
Step 2	-24.5	25.4	-8.1	8.7	±0.20%
Step 3	-35.6	36.9	-11.9	11.8	±0.28%
Step 4	-51.6	53.4	-16.9	16.8	±0.39%
Step 5	-73.8	75.6	-23.9	23.5	±0.56%
Step 6	-106.8	108.1	-33.4	33.0	±0.78%
Step 7	-152.6	152.6	-47.1	46.3	±1.09%
Step 8	-207.7	208.2	-65.9	65.1	±1.53%
Step 9	-238.4	241.5	-91.1	92.1	±2.15%
Step 10	-245.5	248.2	-128.4	129.6	±3.02%

Table 4.2 – Strain ranges in strain gages for DM assemblage test [multiple of yield strain shown in brackets]

Step	Gage-1		Gage-2		Gage-3		Gage-4	
	minimum	maximum	minimum	maximum	minimum	maximum	minimum	maximum
1 - 6	-0.00095 [0.5]	0.00098 [0.5]	-0.00111 [0.6]	0.00096 [0.5]	-0.00111 [0.6]	0.00097 [0.5]	-0.00091 [0.5]	0.00099 [0.5]
7	-0.00127 [0.7]	0.00144 [0.8]	-0.00215 [1.1]	0.00087 [0.5]	-0.00277 [1.5]	0.00140 [0.7]	-0.00115 [0.6]	0.00154 [0.8]
8	-0.00269 [1.4]	0.00131 [0.7]	-0.00590 [3.1]	-0.00032 [0.2]	-0.00643 [3.4]	0.00108 [0.6]	-0.00274 [1.4]	0.00205 [1.1]
9	-0.00268 [1.4]	0.00240 [1.3]	-0.00598 [3.2]	0.00155 [0.8]	-0.01256 [6.6]	0.00195 [1.0]	-0.00639 [3.4]	0.00292 [1.5]
10	-0.00436 [2.8]	0.00919 [5.9]	-0.00893 [5.7]	0.01044 [6.7]	-0.01126 [7.2]	0.00586 [3.7]	-0.00532 [2.8]	0.00703 [4.5]

Step	Gage-5		Gage-6		Gage-7		Gage-8	
	minimum	maximum	minimum	maximum	minimum	maximum	minimum	maximum
1 - 6	-0.00099 [0.5]	0.00097 [0.5]	-0.00095 [0.5]	0.00092 [0.5]	0.00095 [0.5]	0.00089 [0.5]	0.00099 [0.5]	0.00092 [0.5]
7	-0.00136 [0.7]	0.00142 [0.8]	-0.00130 [0.7]	0.00136 [0.7]	0.00132 [0.7]	0.00132 [0.7]	0.00137 [0.7]	0.00136 [0.7]
8	-0.00183 [1.0]	0.00280 [1.5]	-0.00168 [0.9]	0.00206 [1.1]	0.00171 [0.9]	0.00195 [1.0]	0.00185 [1.0]	0.00194 [1.0]
9	-0.00331 [1.7]	0.00634 [3.3]	-0.00263 [1.4]	0.00416 [2.2]	0.00269 [1.4]	0.00250 [1.3]	0.00252 [1.3]	0.00245 [1.3]
10	-0.00997 [6.4]	0.00914 [5.8]	-0.01926 [12.3]	0.00960 [6.1]	0.03905 [24.9]	0.00323 [2.1]	0.01792 [11.4]	0.00321 [2.1]

Table 4.3 – Maximum strains in beam flange gages for DM assemblage test

Gage	max strain (mm/mm)		multiple of expected yield strain	
	compression	tension		
1	-0.00436	0.00919	2.8	5.9
2	-0.00893	0.01044	5.7	6.7
3	-0.01126	0.00586	7.2	3.7
4	-0.00532	0.00703	3.4	4.5
5	-0.00997	0.00914	6.4	5.8
6	-0.01926	0.00960	12.3	6.1
7	-0.03905	0.00323	24.9	2.1
8	-0.01792	0.00321	11.4	2.1

Table 4.4 – Actual load and displacement history for WM assemblage test

	Load Range		Displacement Range		% Story drift
	min (kN)	max (kN)	min (mm)	max (mm)	
Step 1	-15.9	16.5	-5.3	5.8	±0.13%
Step 2	-23.6	25.4	-7.8	8.7	±0.19%
Step 3	-34.4	36.1	-11.5	11.6	±0.27%
Step 4	-51.4	52.3	-16.5	16.3	±0.38%
Step 5	-74.5	75.0	-23.5	23.5	±0.55%
Step 6	-107.7	107.0	-32.3	32.7	±0.76%
Step 7	-154.6	153.1	-46.1	45.9	±1.08%
Step 8	-210.2	210.7	-64.6	63.9	±1.51%
Step 9	-243.7	244.7	-91.4	88.8	±2.11%
Step 10	-255.6	257.1	-128.7	126.5	±2.99%
Step 11	-234.2	254.7	-167.0	165.0	±3.89%

Table 4.5 – Strain ranges in strain gages for WM assemblage test [multiple of yield strain shown in brackets]

Step	Gage-1		Gage-2		Gage-3		Gage-4	
	Minimum	Maximum	Minimum	Maximum	Minimum	Maximum	Minimum	Maximum
1 - 6	-0.00091 [0.5]	0.00100 [0.5]	-0.00104 [0.6]	0.00101 [0.5]	NA	NA	-0.00087 [0.5]	0.00113 [0.6]
7	-0.00157 [0.8]	0.00118 [0.6]	-0.00140 [0.7]	0.00153 [0.8]	NA	NA	-0.00105 [0.6]	0.00178 [0.9]
8	-0.00245 [1.3]	0.00138 [0.7]	-0.00202 [1.1]	0.00215 [1.1]	NA	NA	-0.00211 [1.1]	0.00228 [1.2]
9	-0.00418 [2.2]	0.00324 [1.7]	-0.00325 [1.7]	0.00363 [1.9]	NA	NA	-0.00840 [4.4]	0.00457 [2.4]
10	-0.01169 [6.2]	0.00070 [0.4]	-0.01069 [5.6]	0.00063 [0.3]	NA	NA	-0.00939 [4.9]	0.01000 [5.2]
11	-0.00564 [3.0]	-0.00334 [1.8]	-0.00329 [1.7]	-0.00290 [1.5]	NA	NA	0.00057 [0.3]	0.02200 [11.6]

Step	Gage-5		Gage-6		Gage-7		Gage-8	
	Minimum	Maximum	Minimum	Maximum	Minimum	Maximum	Minimum	Maximum
1 - 6	-0.00095 [0.5]	0.00095 [0.5]	-0.00090 [0.5]	0.00089 [0.5]	-0.00094 [0.5]	0.00094 [0.5]	-0.00097 [0.5]	0.00098 [0.5]
7	-0.00135 [0.7]	0.00137 [0.7]	-0.00127 [0.7]	0.00129 [0.7]	-0.00130 [0.7]	0.00139 [0.7]	-0.00135 [0.7]	0.00144 [0.8]
8	-0.00175 [0.9]	0.00200 [1.1]	-0.00164 [0.9]	0.00193 [1.0]	-0.00162 [0.9]	0.00221 [1.2]	-0.00172 [0.9]	0.00212 [1.1]
9	-0.00207 [1.1]	0.00378 [2.0]	-0.00192 [1.0]	0.00465 [2.5]	-0.00163 [0.9]	0.00456 [2.4]	-0.00214 [1.1]	0.00464 [2.4]
10	-0.00364 [1.9]	0.00627 [3.3]	-0.00262 [1.4]	0.00824 [4.3]	-0.00644 [3.4]	0.00701 [3.7]	-0.00505 [2.7]	0.00878 [4.6]
11	-0.00671 [3.5]	0.00361 [1.9]	-0.00120 [0.6]	0.00880 [4.6]	-0.00066 [0.4]	0.00554 [2.9]	0.00039 [0.2]	0.01133 [6.0]

Table 4.6 – Maximum strains in beam flange gages for WM assemblage test

Gage	max strain (mm/mm)		multiple of expected yield strain	
	compression	tension		
1	-0.01169	0.00324	6.2	1.7
2	-0.01069	0.00363	5.6	1.9
4	-0.00094	0.02200	4.9	11.6
5	-0.00671	0.00627	3.5	3.3
6	-0.00262	0.00880	1.4	4.6
7	-0.00644	0.00701	3.4	4.7
8	-0.00505	0.01133	2.7	6.0
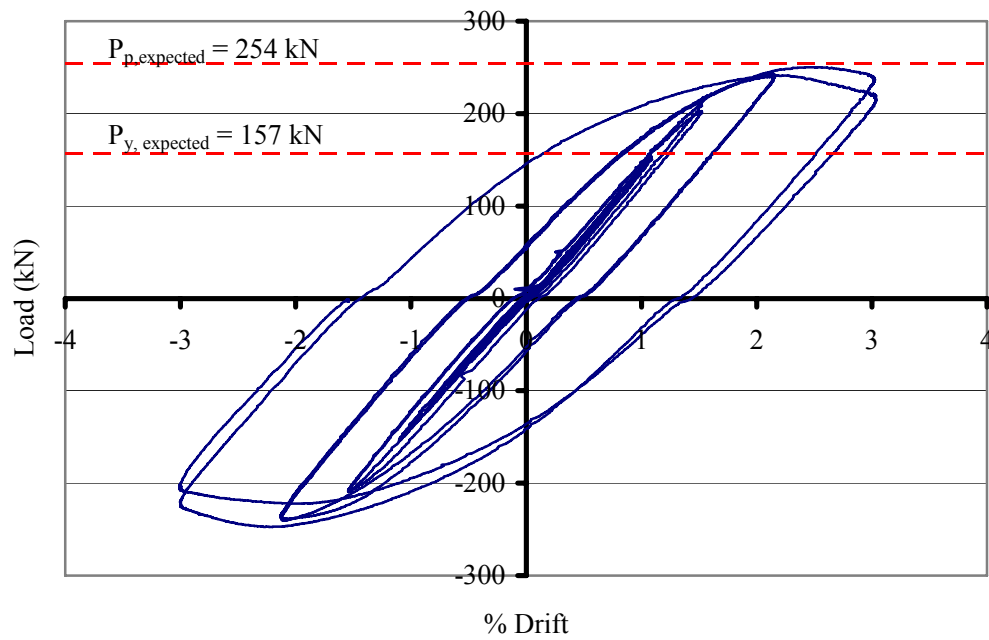
Figure 4.1 – Load vs. percent drift for DM assemblage test
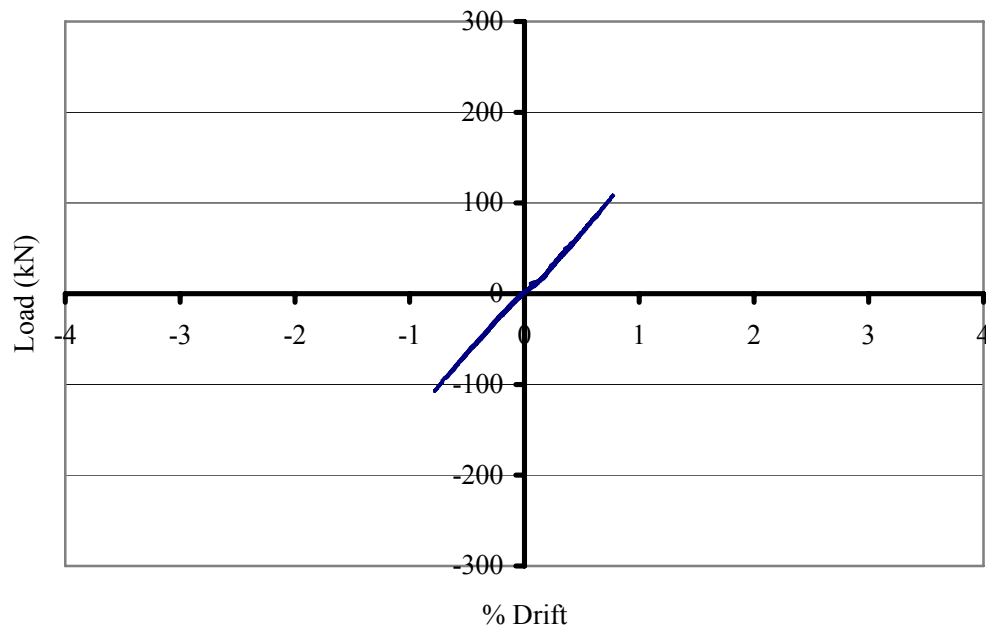
Figure 4.2 – Load vs. percent drift – steps 1 through 6 of DM assemblage test
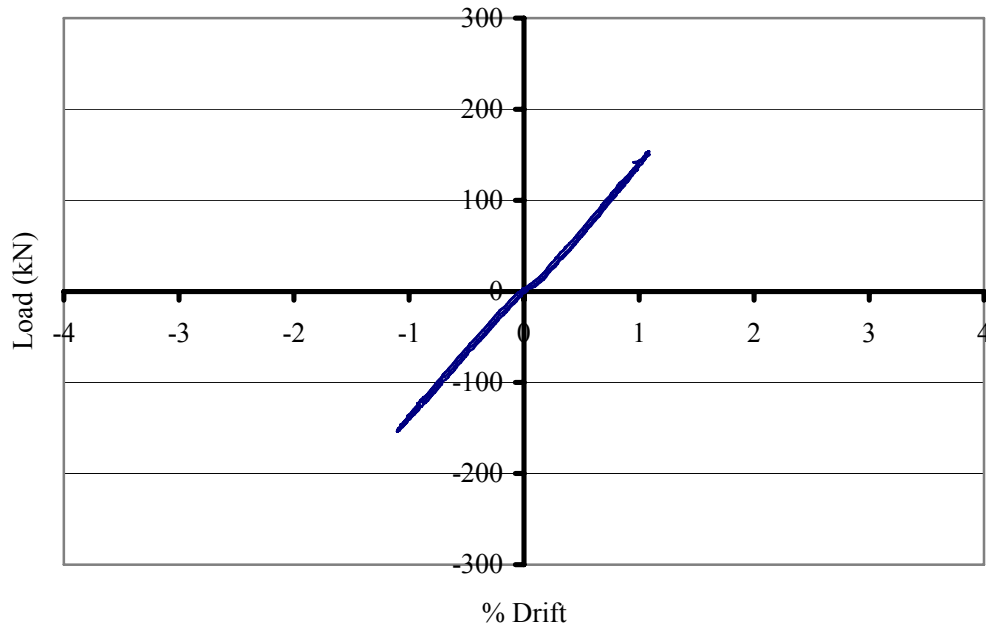
Figure 4.3 – Load vs. percent drift – step 7 of DM assemblage test
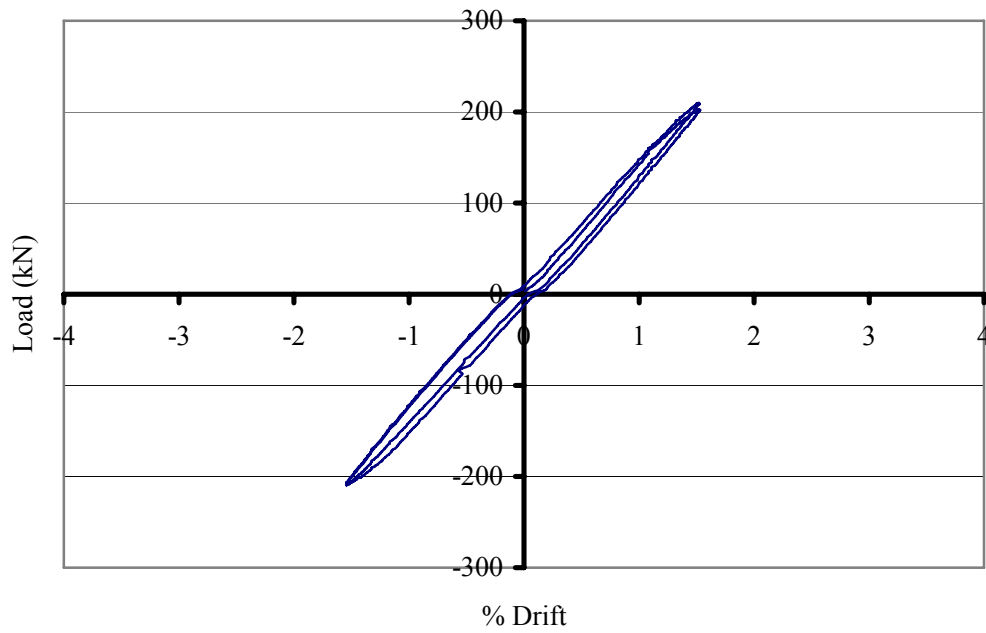
Figure 4.4 – Load vs. percent drift – step 8 of DM assemblage test
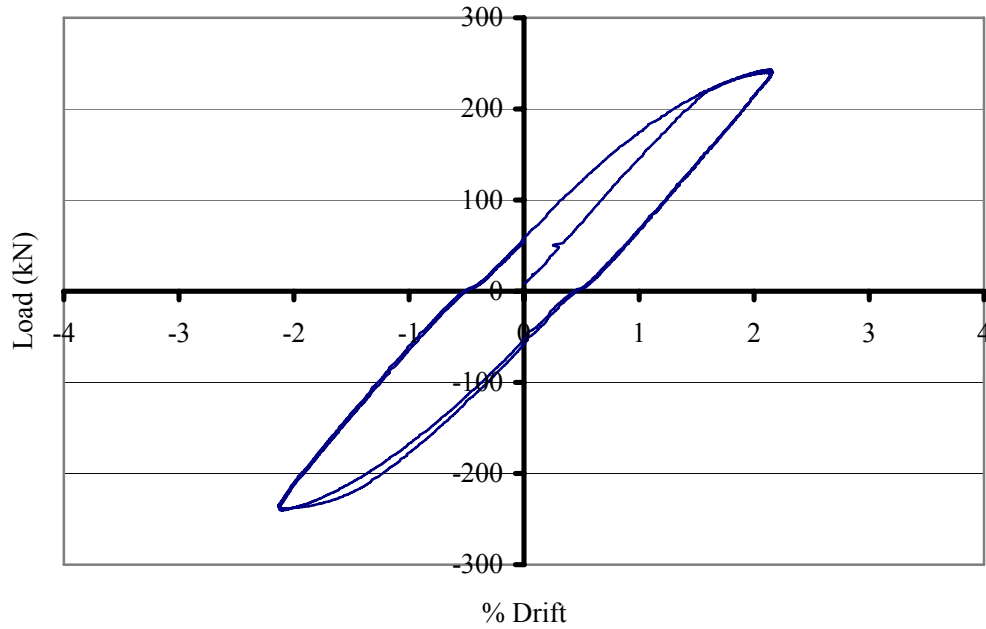
Figure 4.5 – Load vs. percent drift – step 9 of DM assemblage test
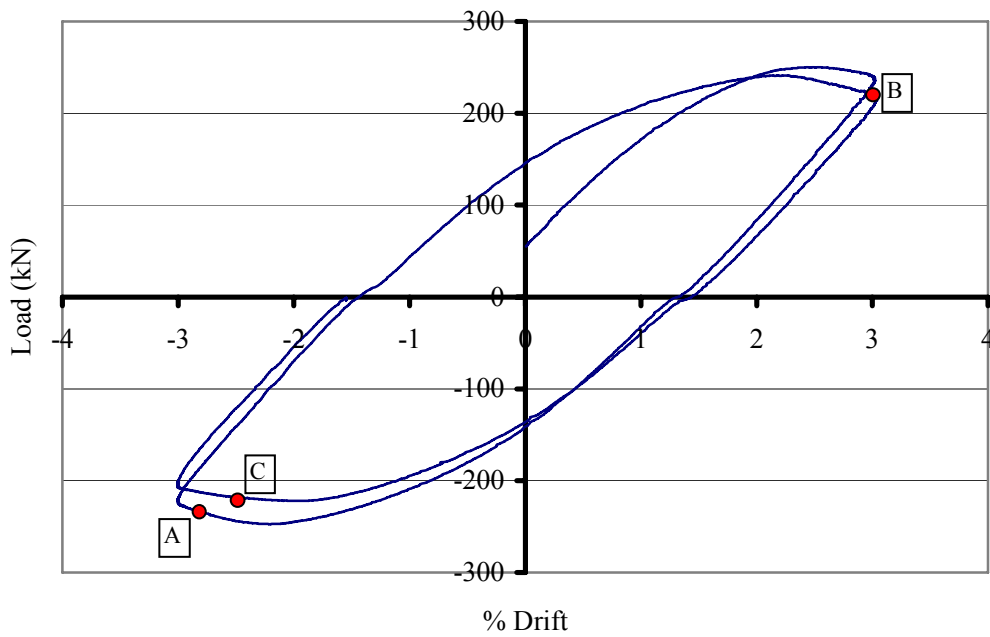
Figure 4.6 – Load vs. percent drift – step 10 of DM assemblage test

Figure 4.7 – Tear in bottom flange seen during step 10 of loading shown as Point A in Figure 4.6

Figure 4.8 – Tear in top flange seen during step 10 of loading shown as Point B in Figure 4.6
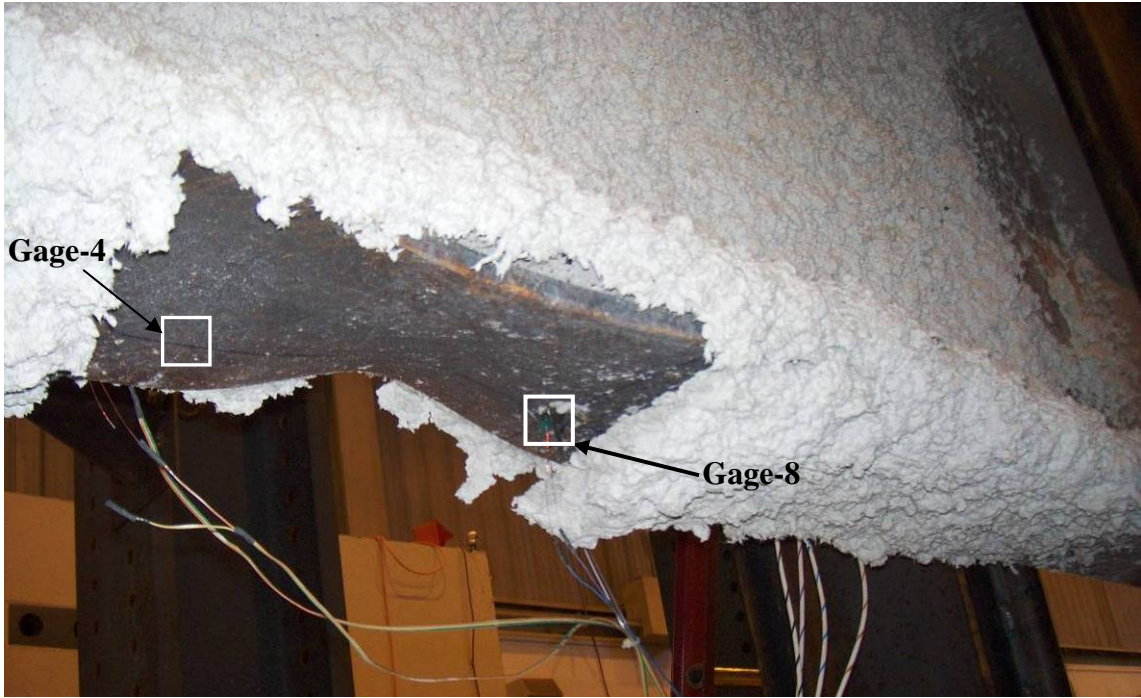
Figure 4.9 – Damage to the SFRM that occurred during step 10 of the DM test shown as Point C in Figure 4.6
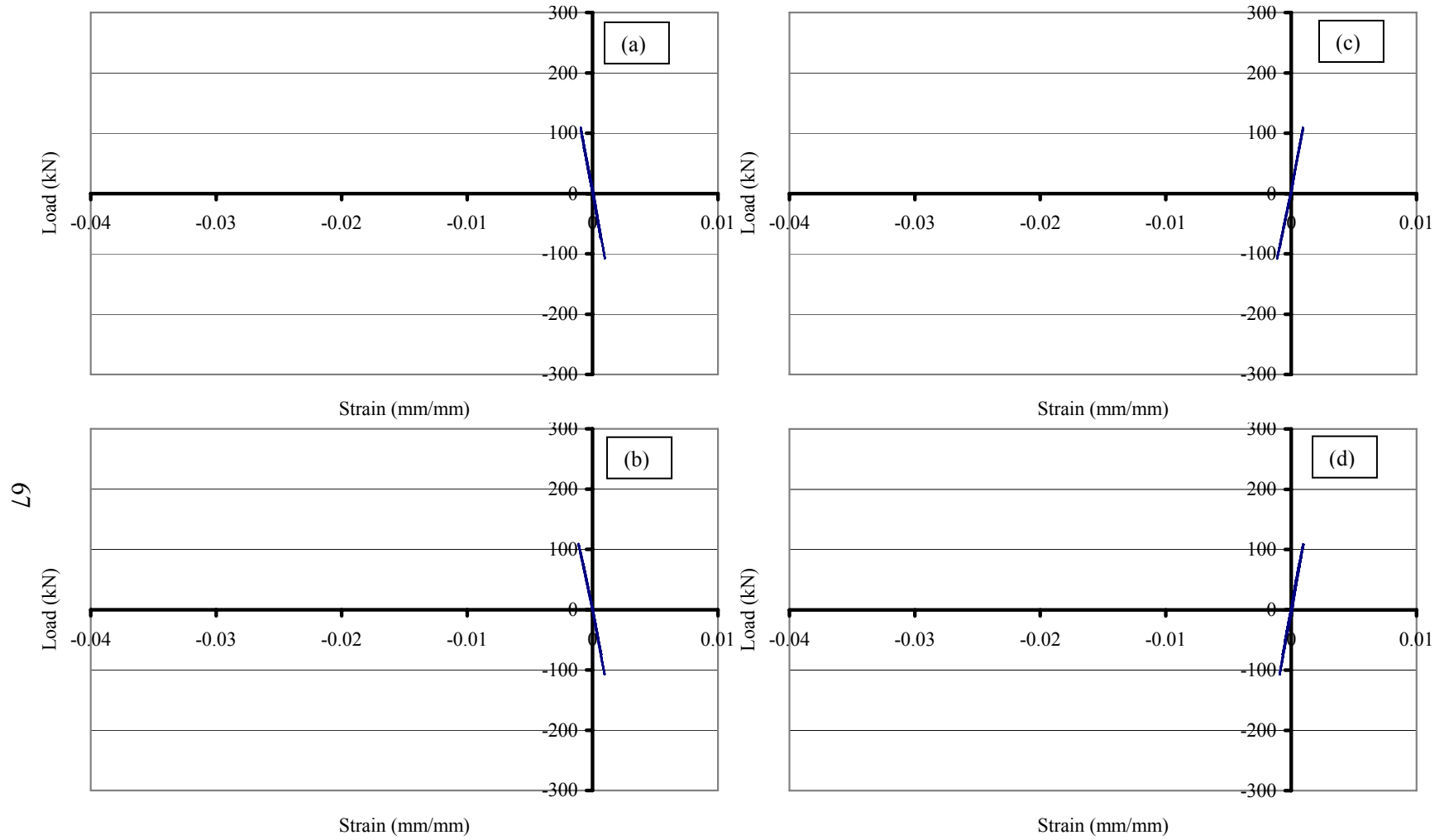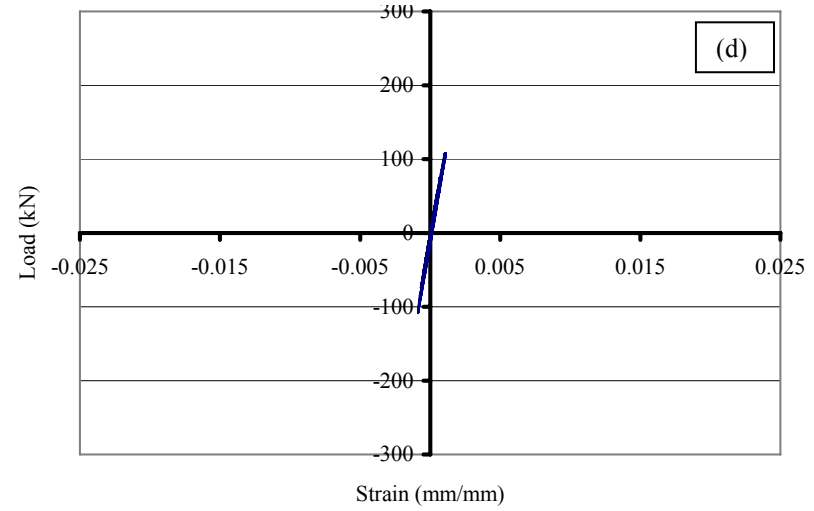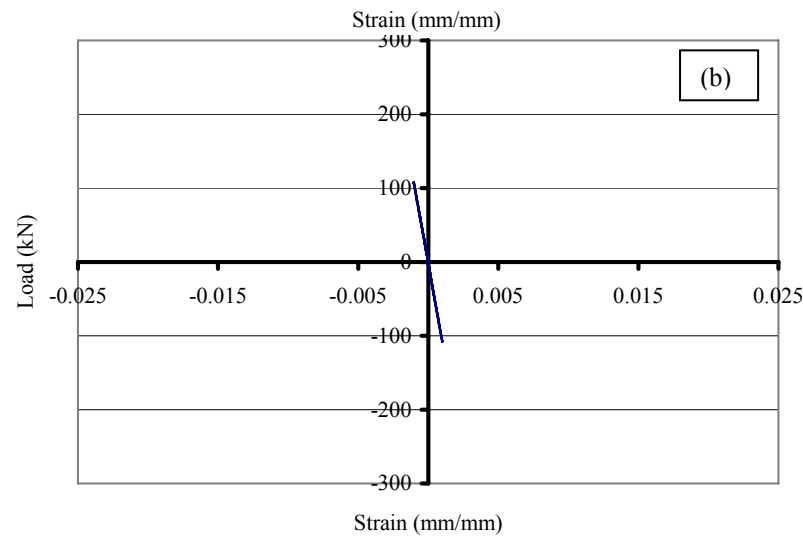
Figure 4.10 – DM assemblage test strain data – steps 1 through 6: (a) Gage-1; (b) Gage-2; (c) Gage-3; (d) Gage-4; [continued]
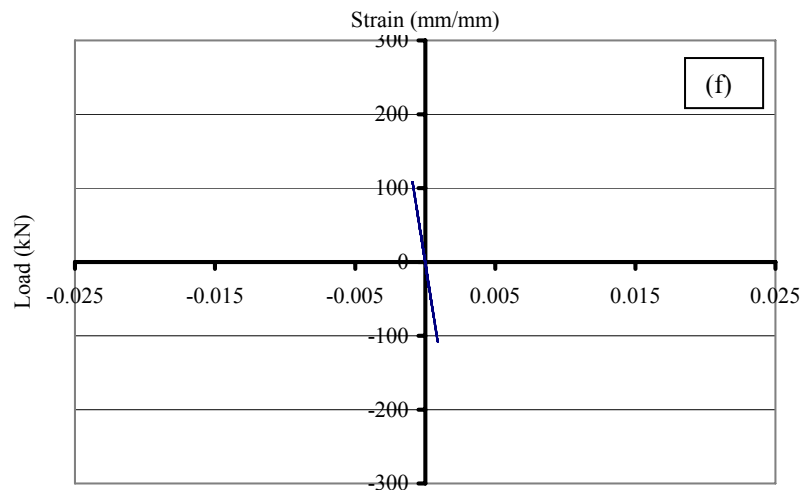
67
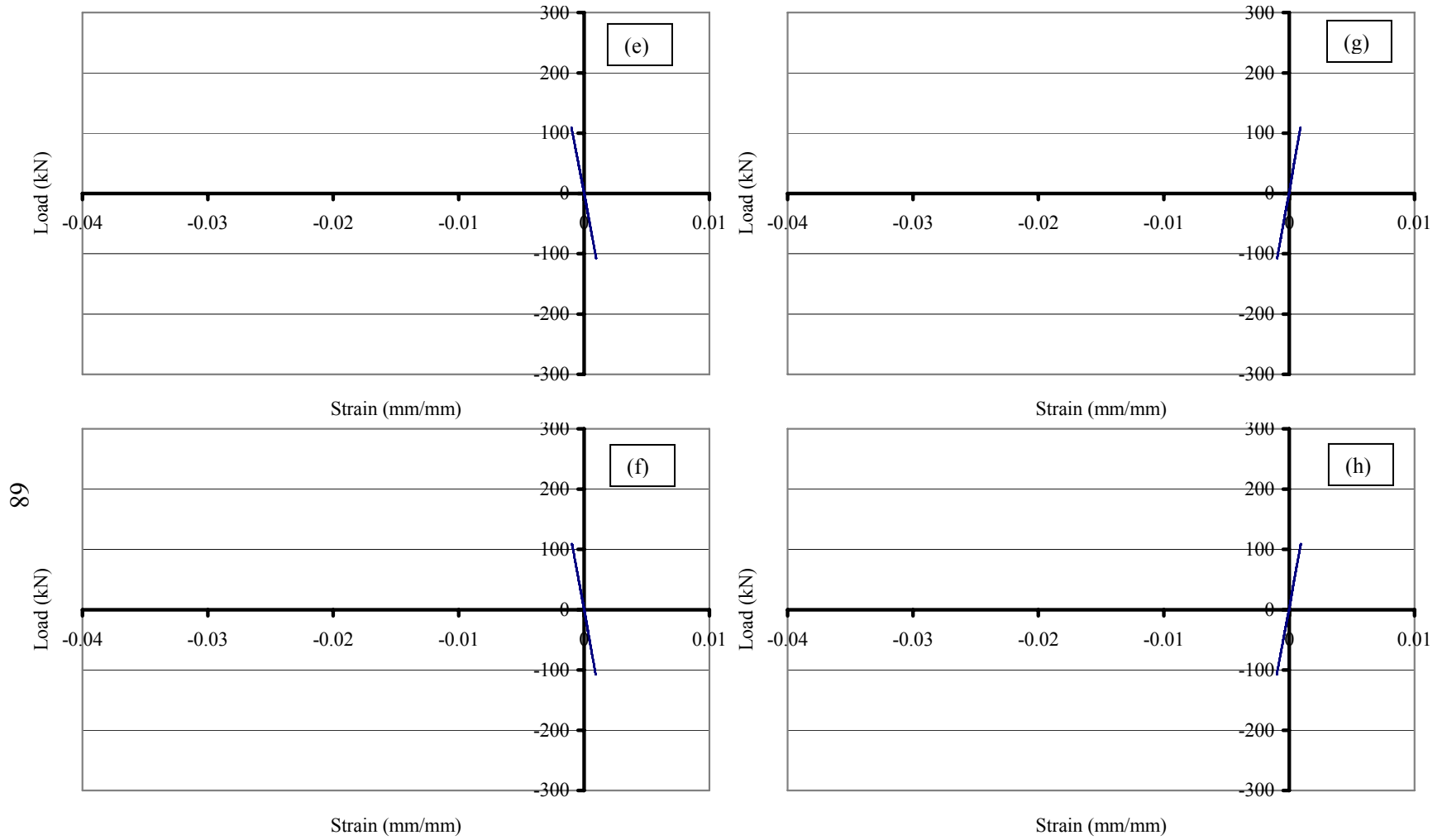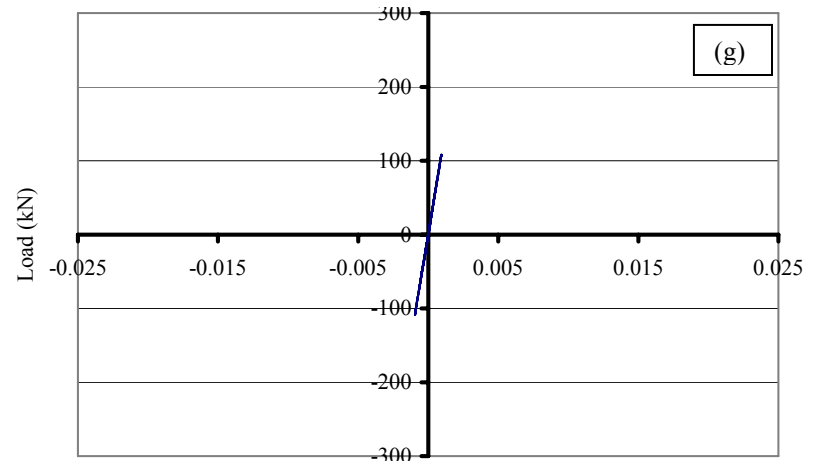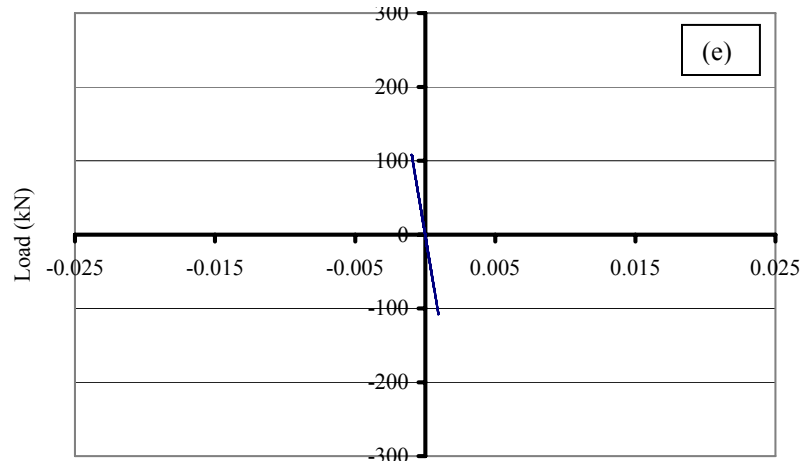
Figure 4.10 – [continued] DM assemblage test strain data – steps 1 through 6: (e) Gage-5; (f) Gage-6; (g) Gage-7; and (h) Gage-8

89
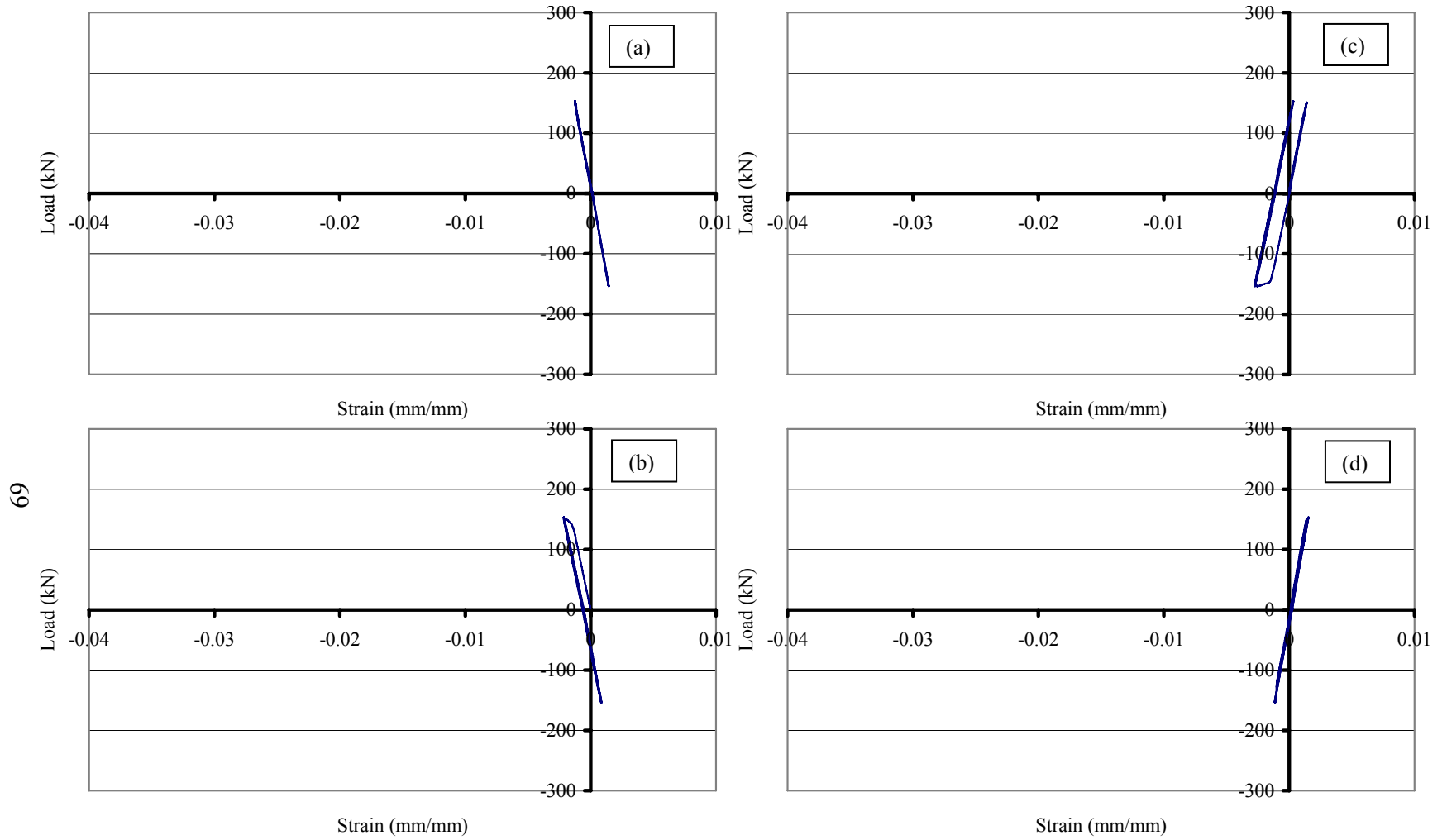
Figure 4.11 – DM assemblage test strain data – step 7: (a) Gage-1; (b) Gage-2; (c) Gage-3; (d) Gage-4; [continued]

69
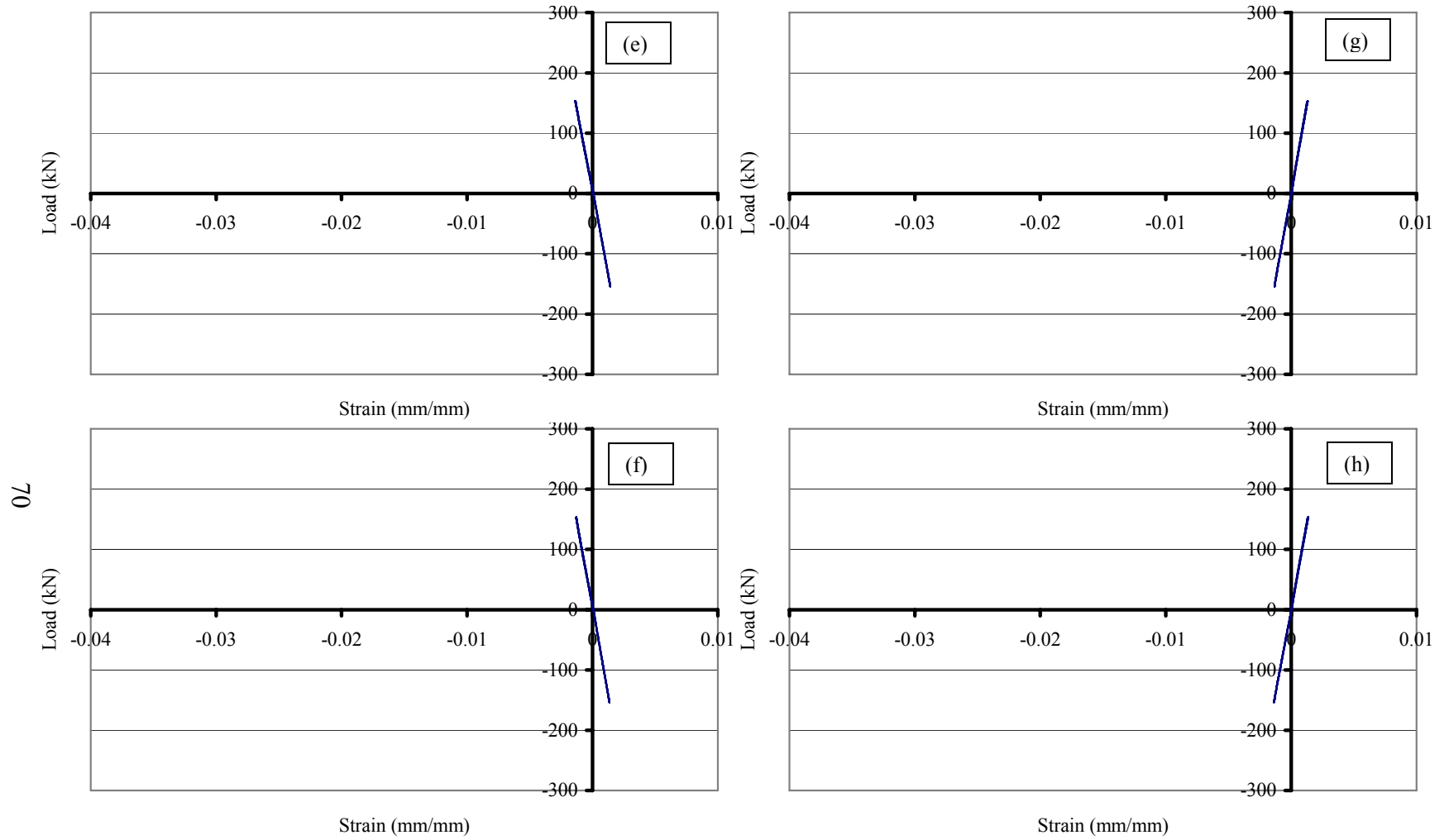
Figure 4.11 – [continued] DM assemblage test strain data – step 7: (e) Gage-5; (f) Gage-6; (g) Gage-7; and (h) Gage-8

70
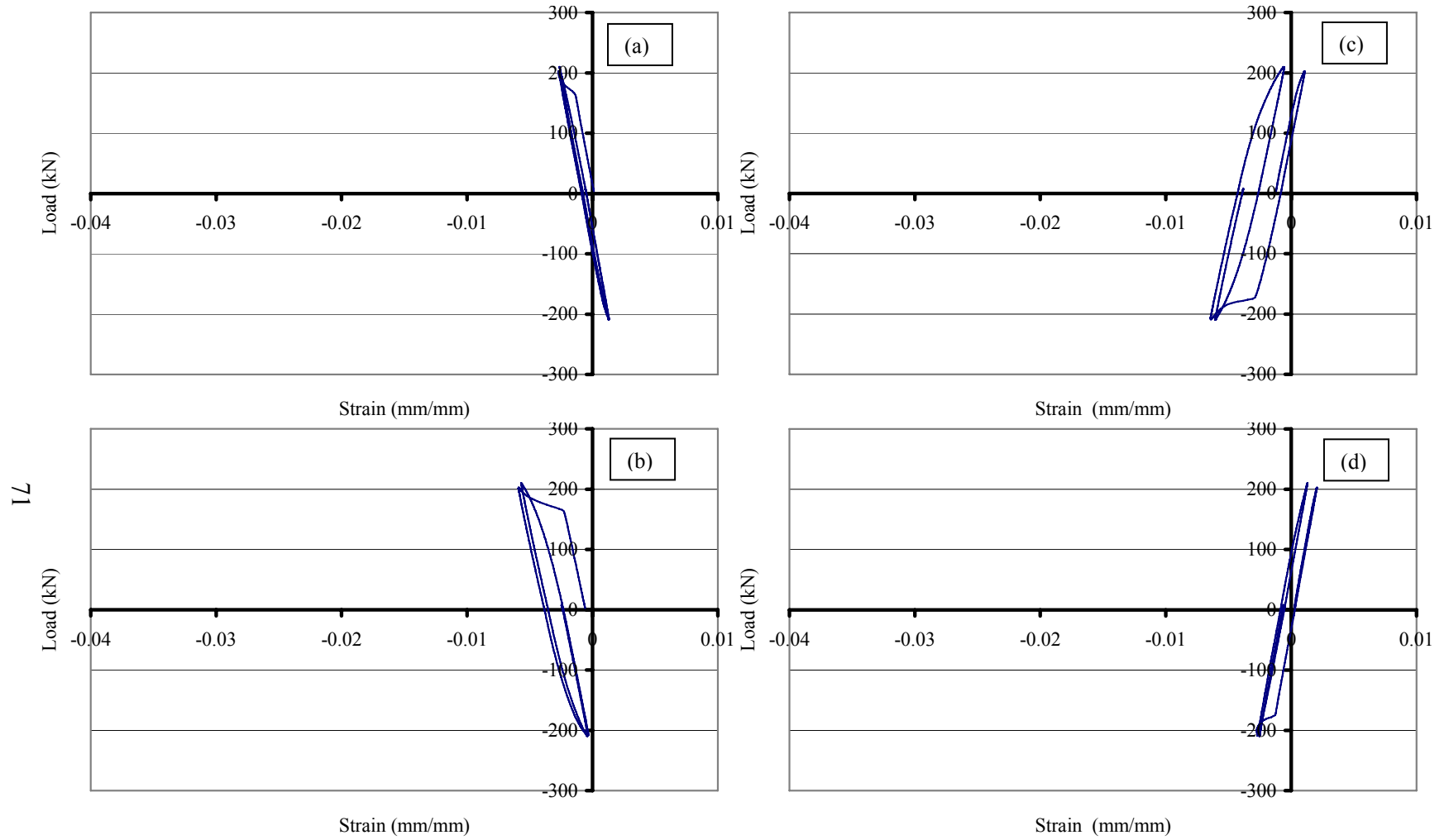
Figure 4.12 – DM assemblage test strain data – step 8: (a) Gage-1; (b) Gage-2; (c) Gage-3; (d) Gage-4; [continued]
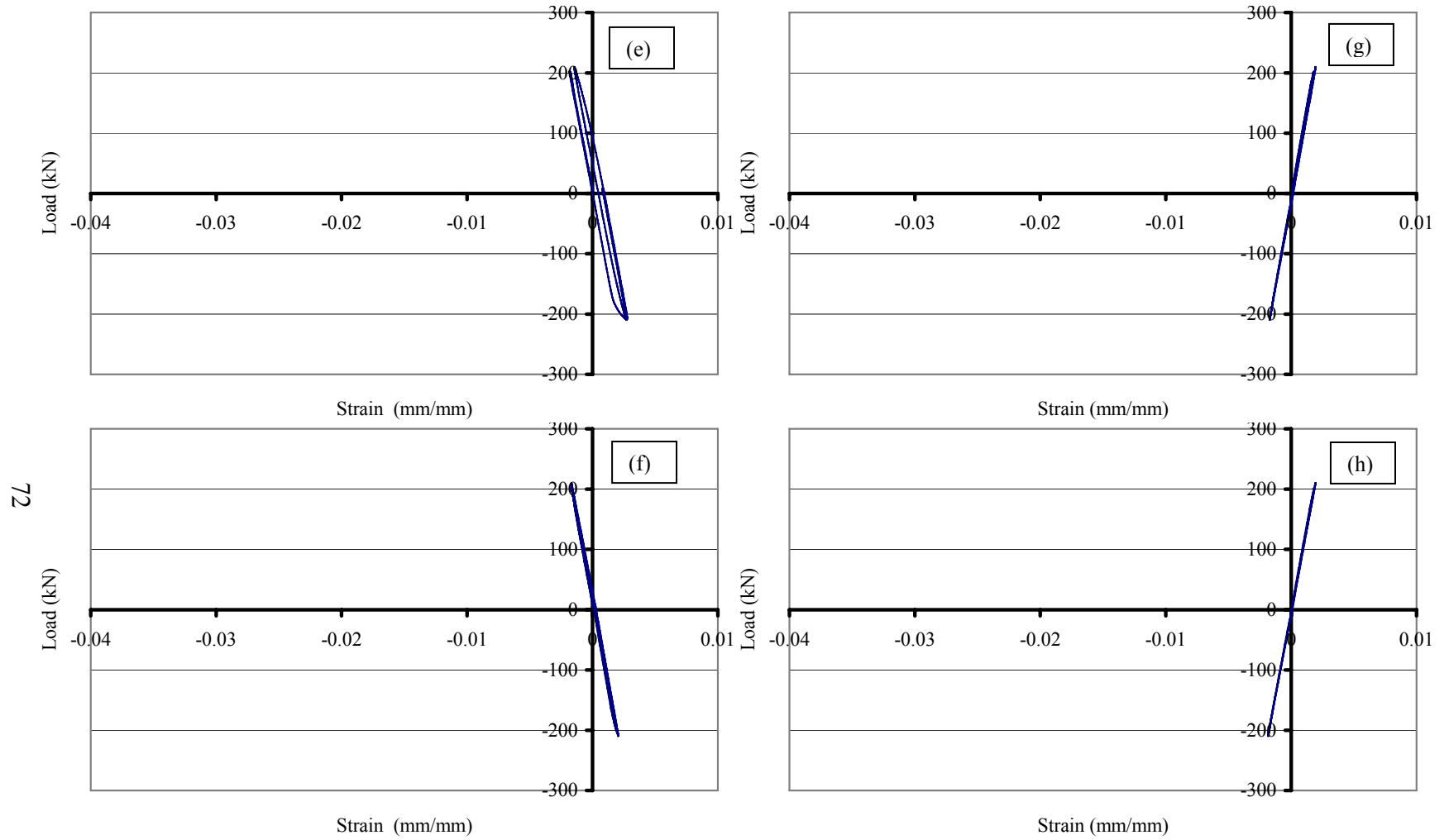
Figure 4.12 – [continued] DM assemblage test strain data – step 8: (e) Gage-5; (f) Gage-6; (g) Gage-7; and (h) Gage-8
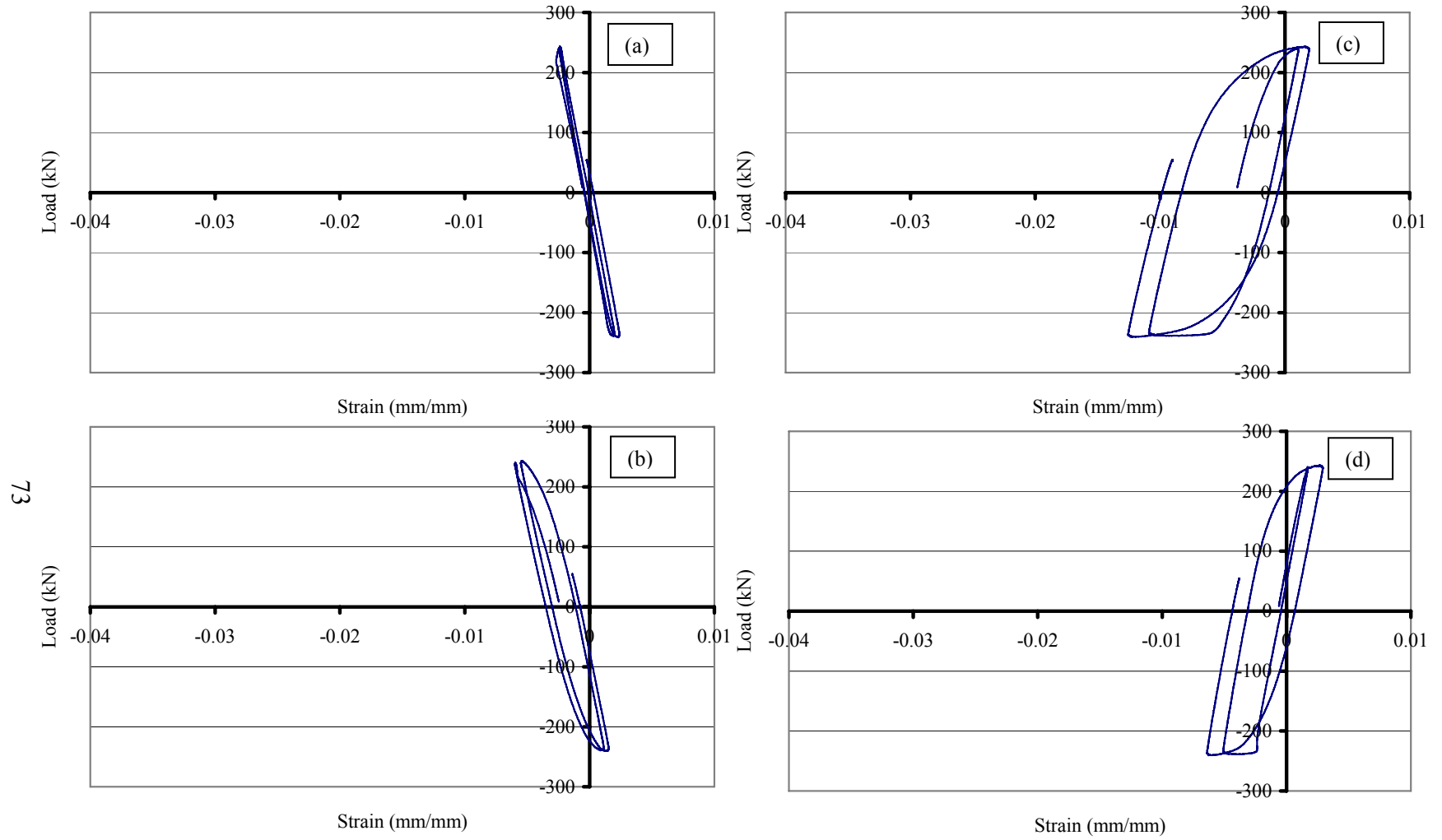
Figure 4.13 – DM assemblage test strain data – step 9: (a) Gage-1; (b) Gage-2; (c) Gage-3; (d) Gage-4; [continued]

73
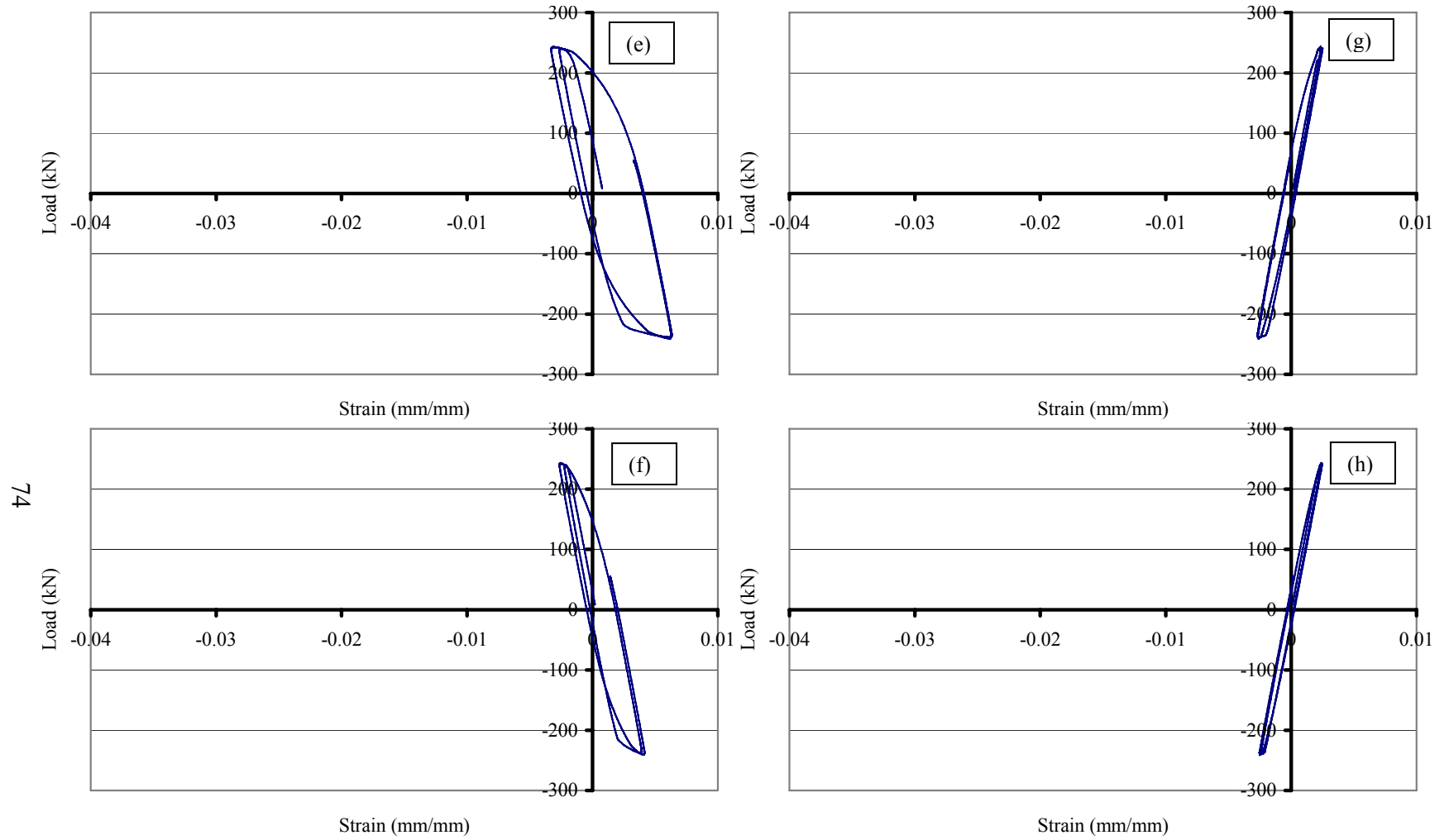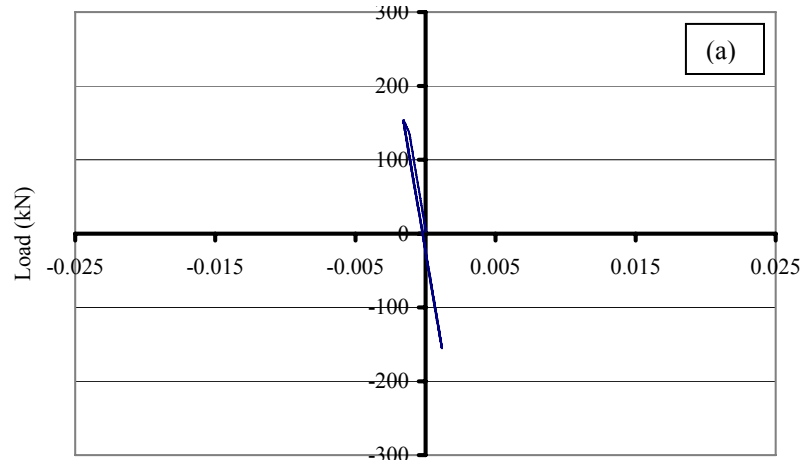
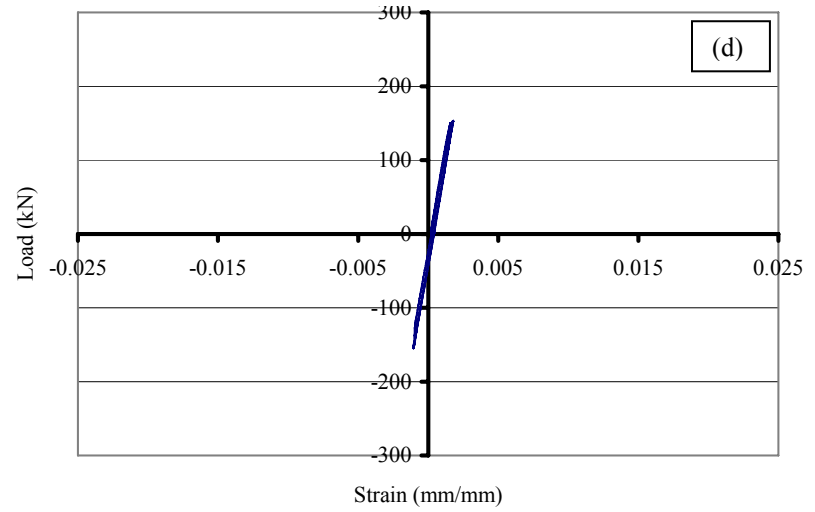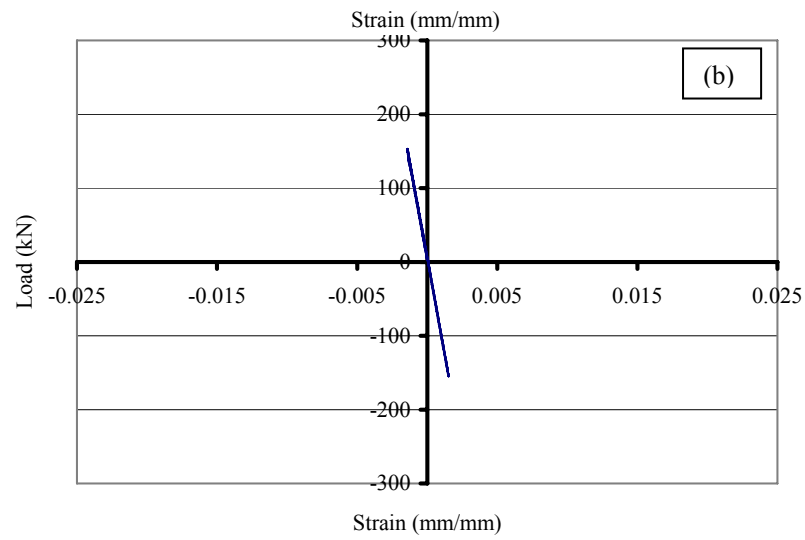Figure 4.13 – [continued] DM assemblage test strain data – step 9: (e) Gage-5; (f) Gage-6; (g) Gage-7; and (h) Gage-8
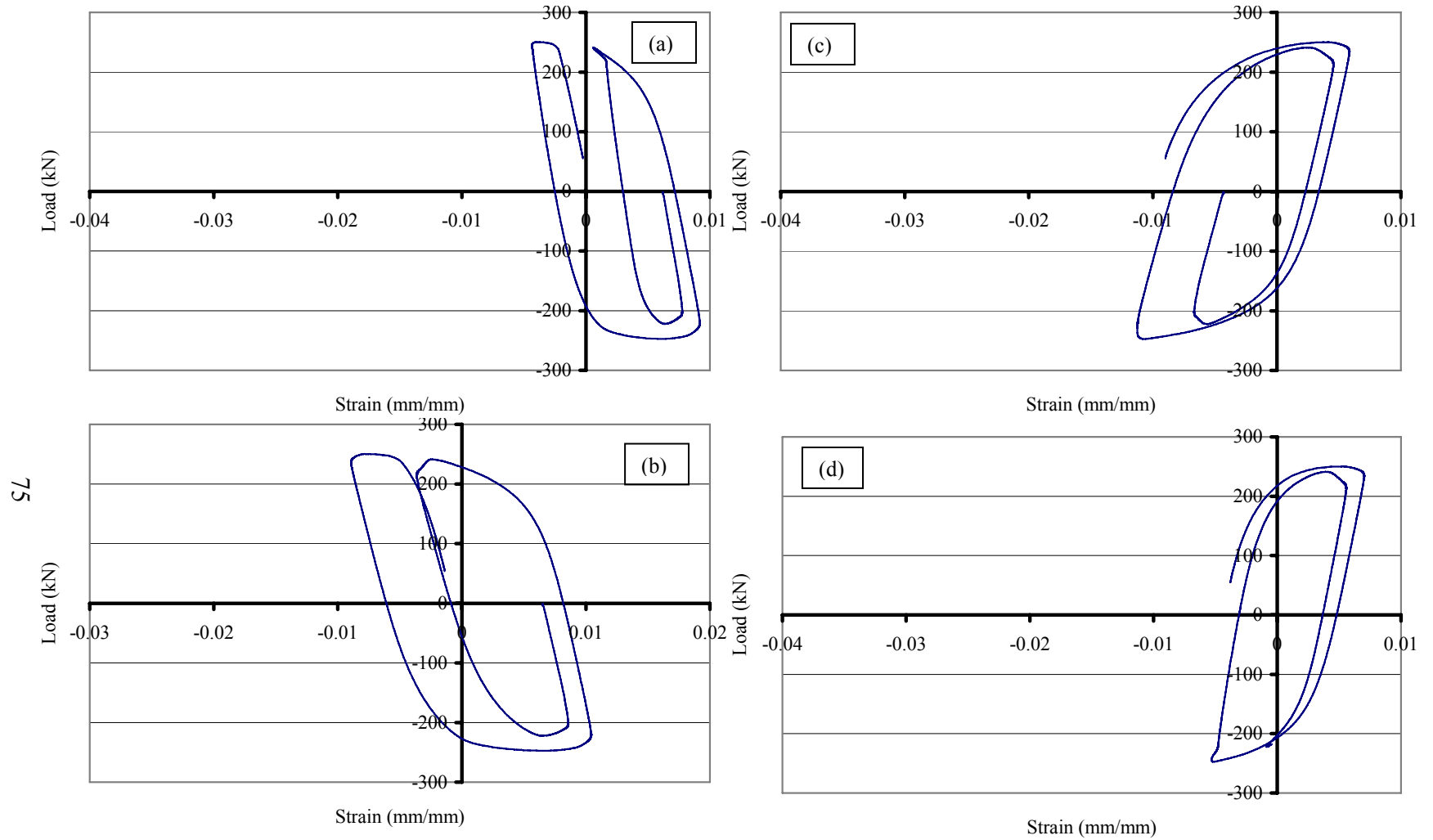
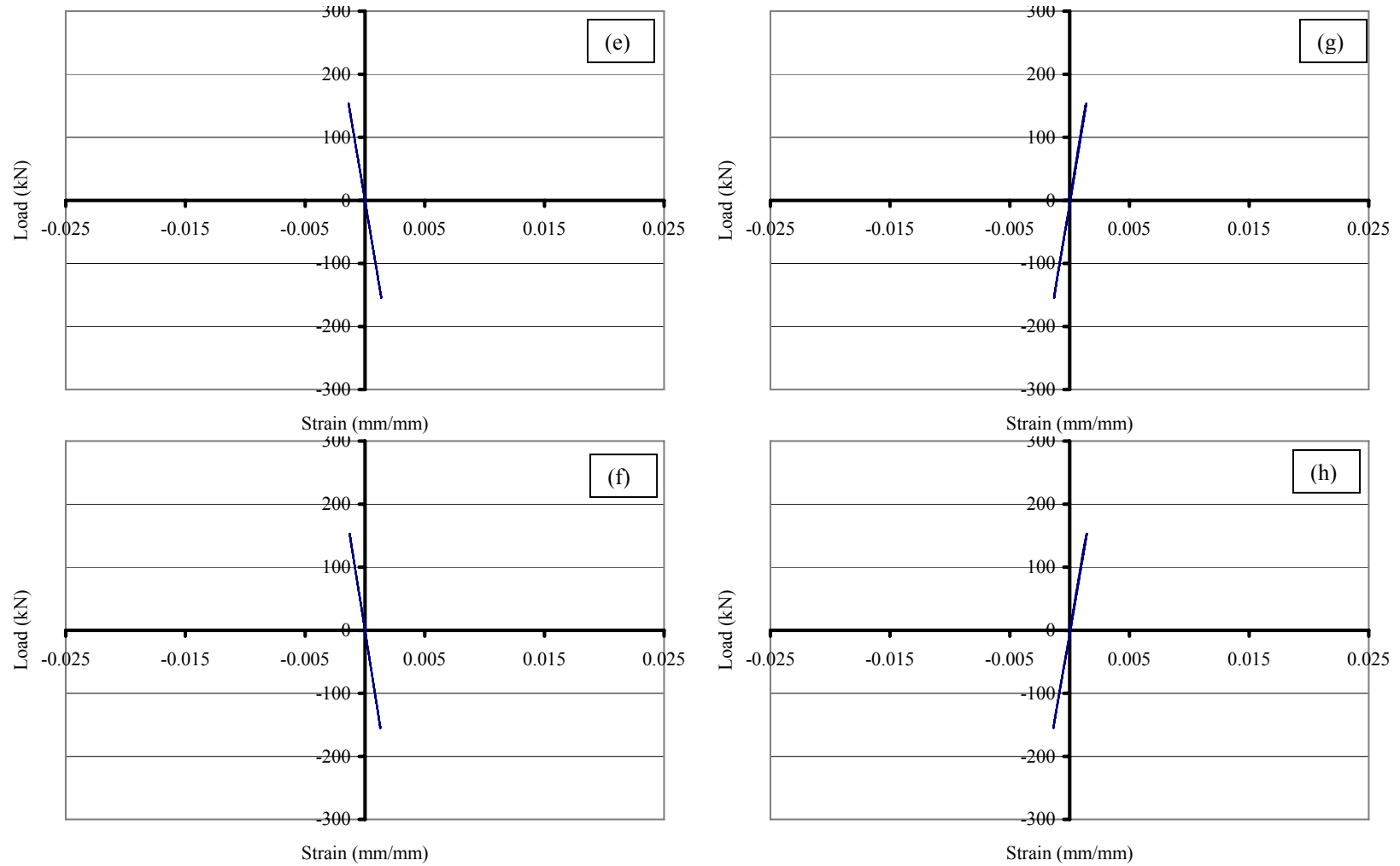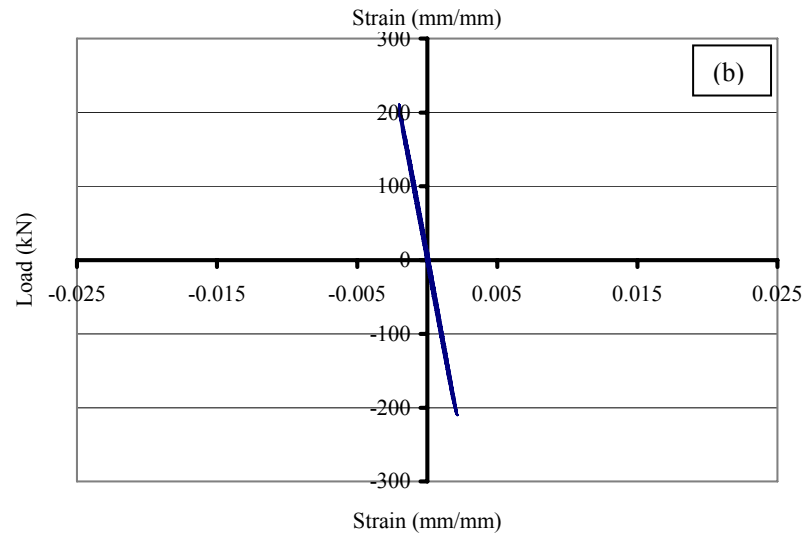Figure 4.14 – DM assemblage test strain data – step 10: (a) Gage-1; (b) Gage-2; (c) Gage-3; (d) Gage-4; [continued]
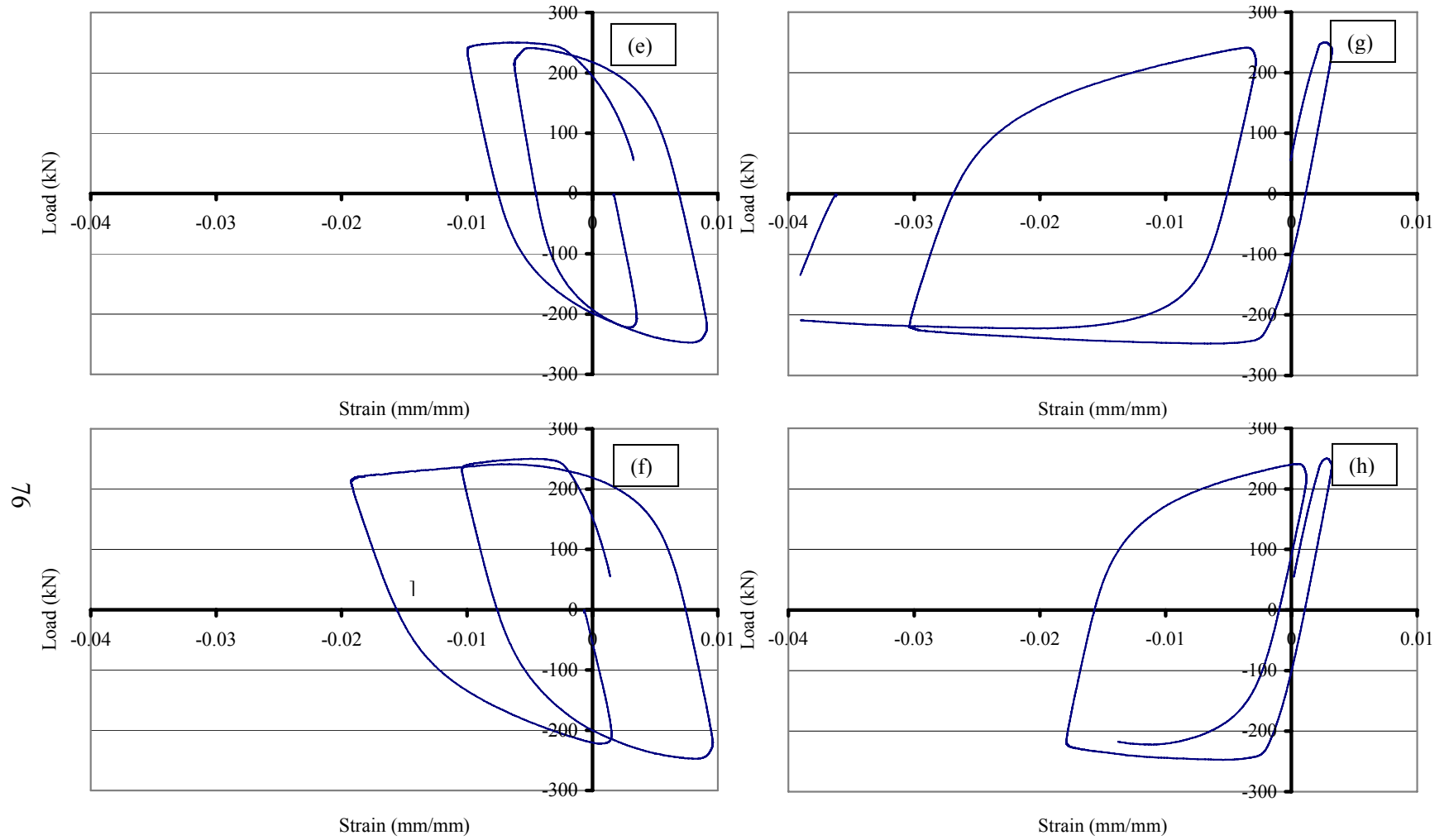
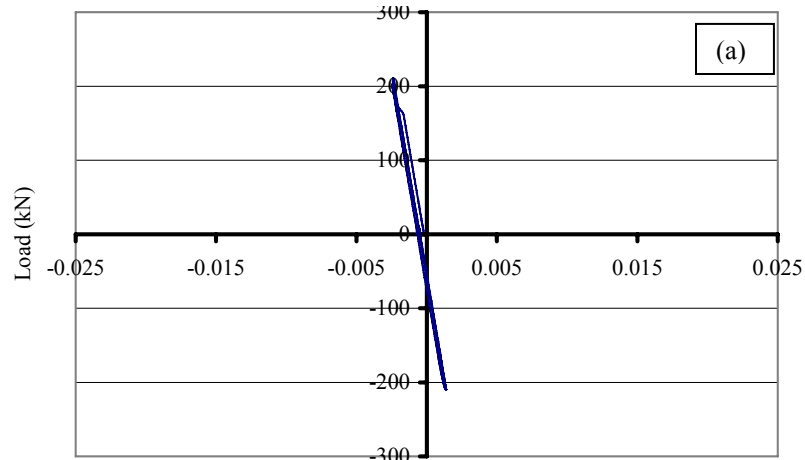Figure 4.14 – [continued] DM assemblage test strain data – step 10: (e) Gage-5; (f) Gage-6; (g) Gage-7; and (h) Gage-8
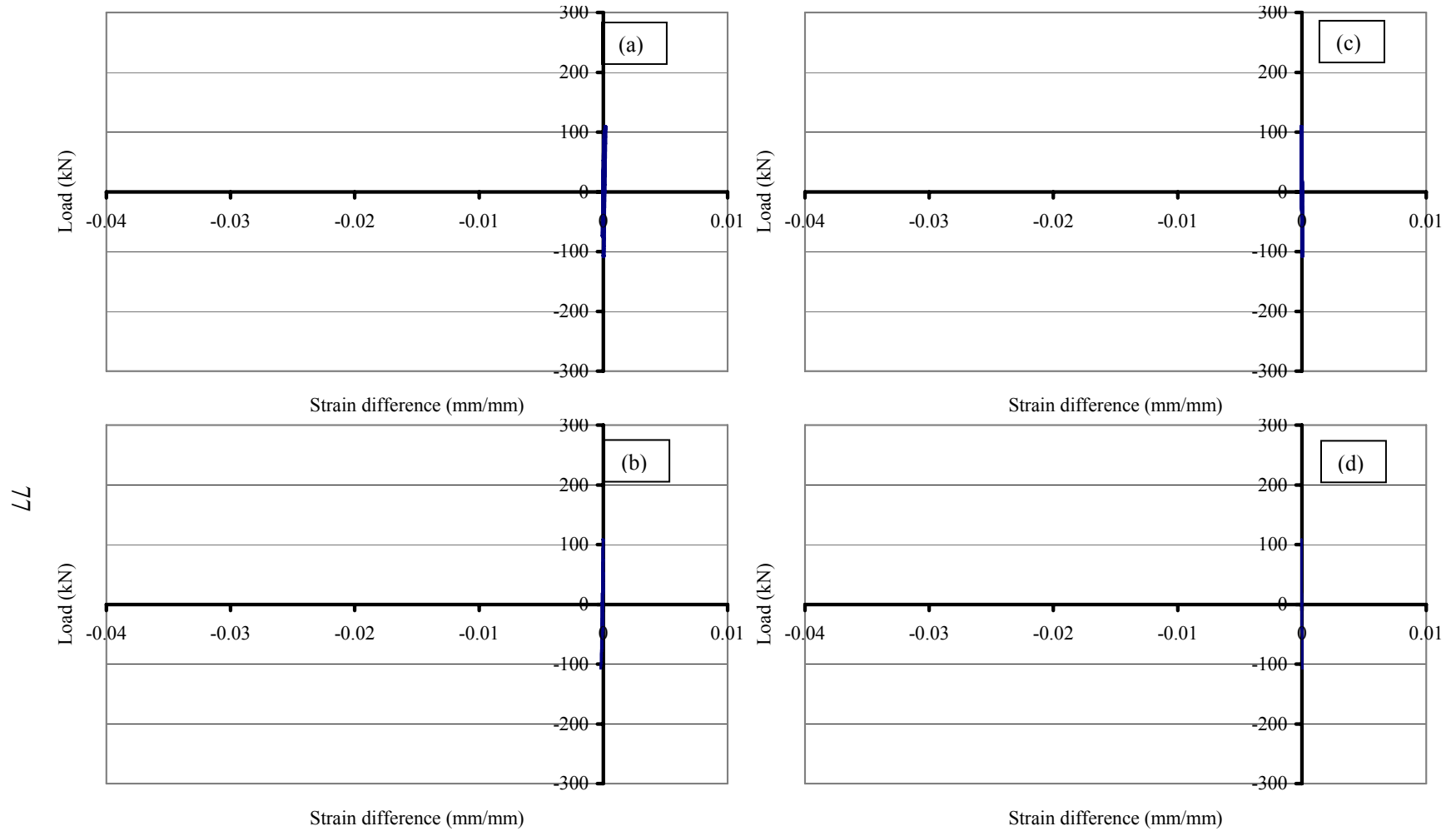
Figure 4.15 – Strain difference in flanges for DM assemblage test – steps 1 through 6: (a) top flange-152 mm; (b) bottom flange-152 mm; (c) top flange-457 mm; and (d) bottom flange-457 mm
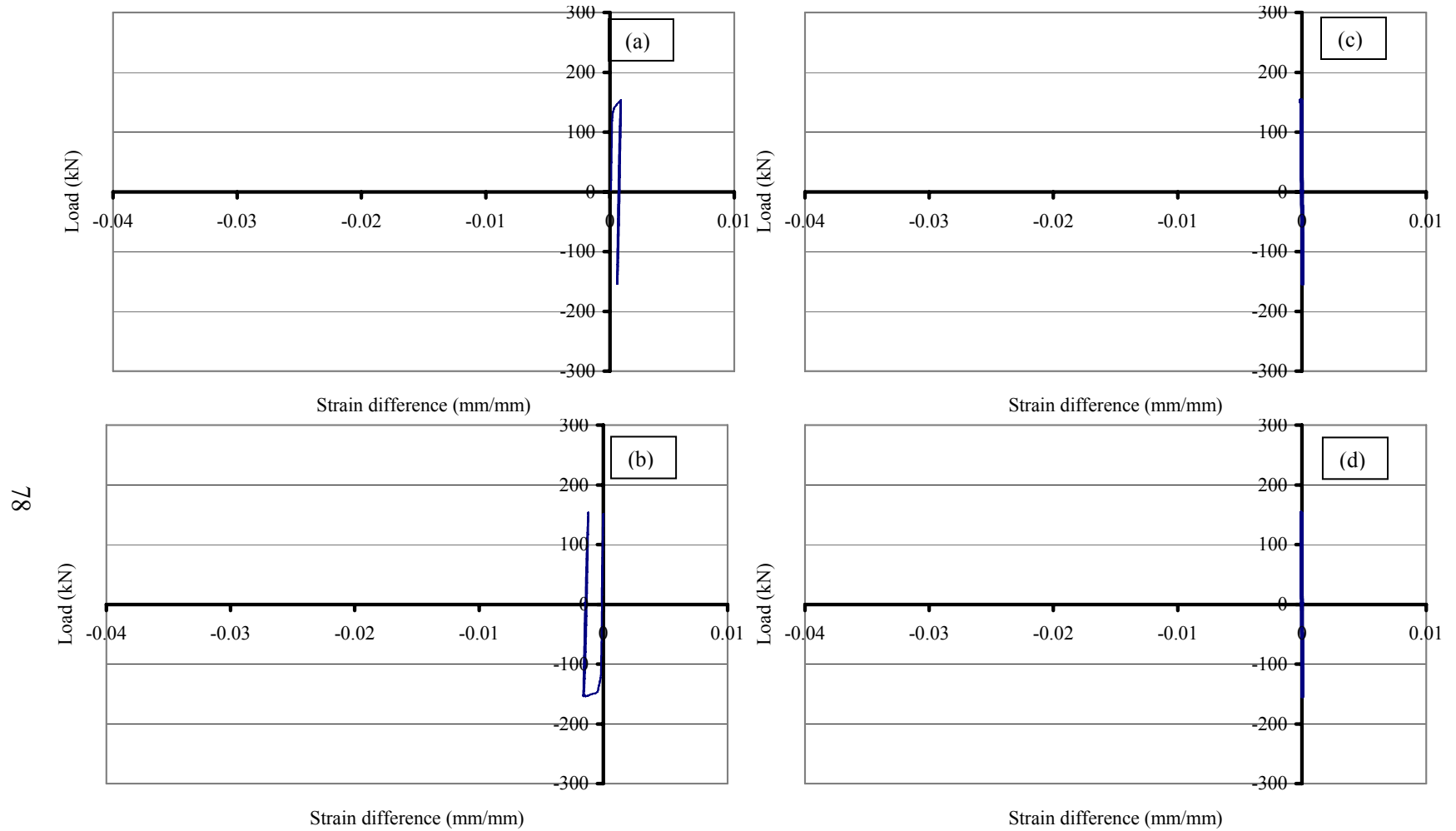
Figure 4.16 – Strain difference in flanges for DM assemblage test – step 7: (a) top flange-152 mm; (b) bottom flange-152 mm; (c) top flange-457 mm; and (d) bottom flange-457 mm
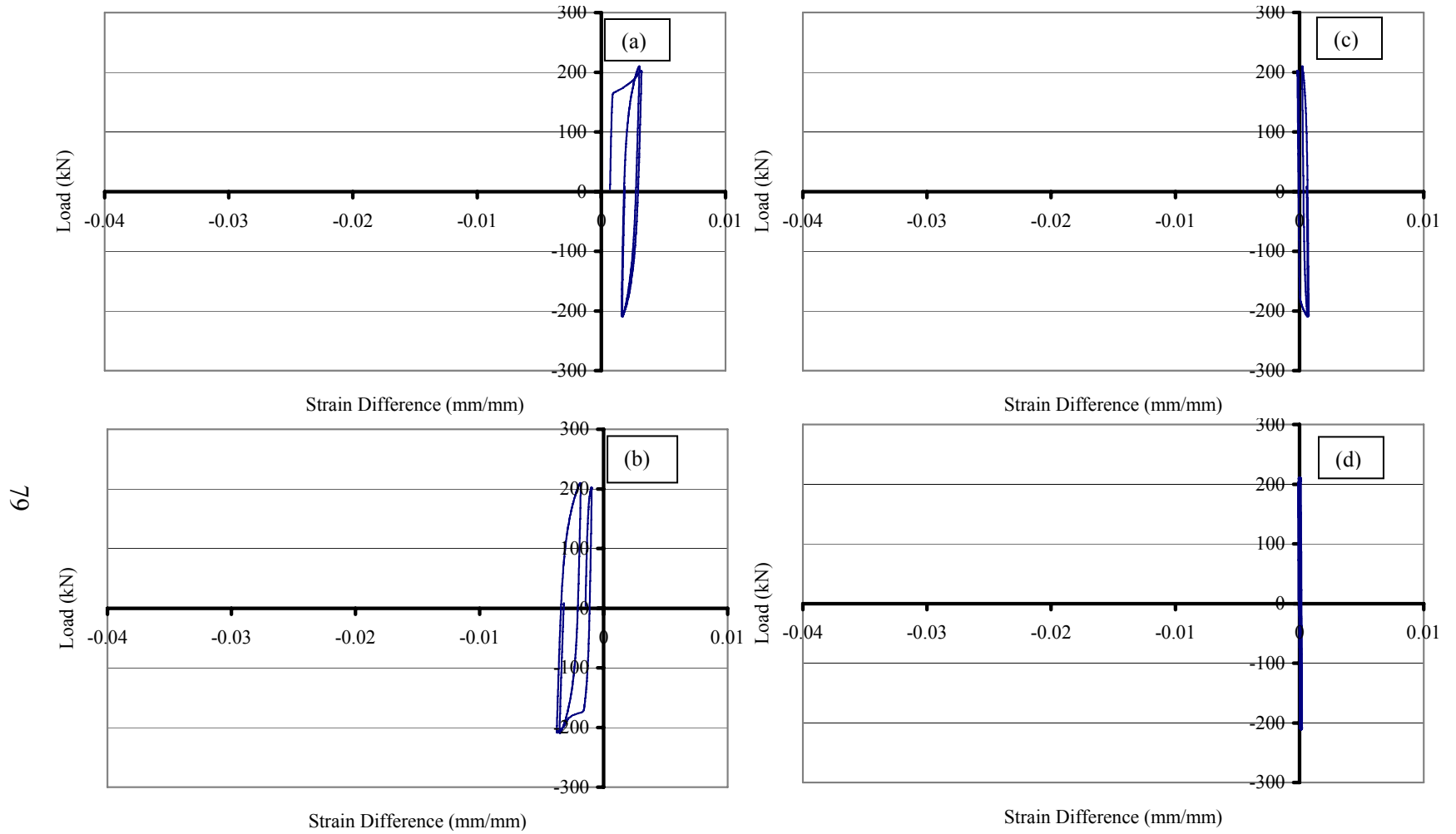
Figure 4.17 – Strain difference in flanges for DM assemblage test – step 8: (a) top flange-152 mm; (b) bottom flange-152 mm; (c) top flange-457 mm; and (d) bottom flange-457 mm
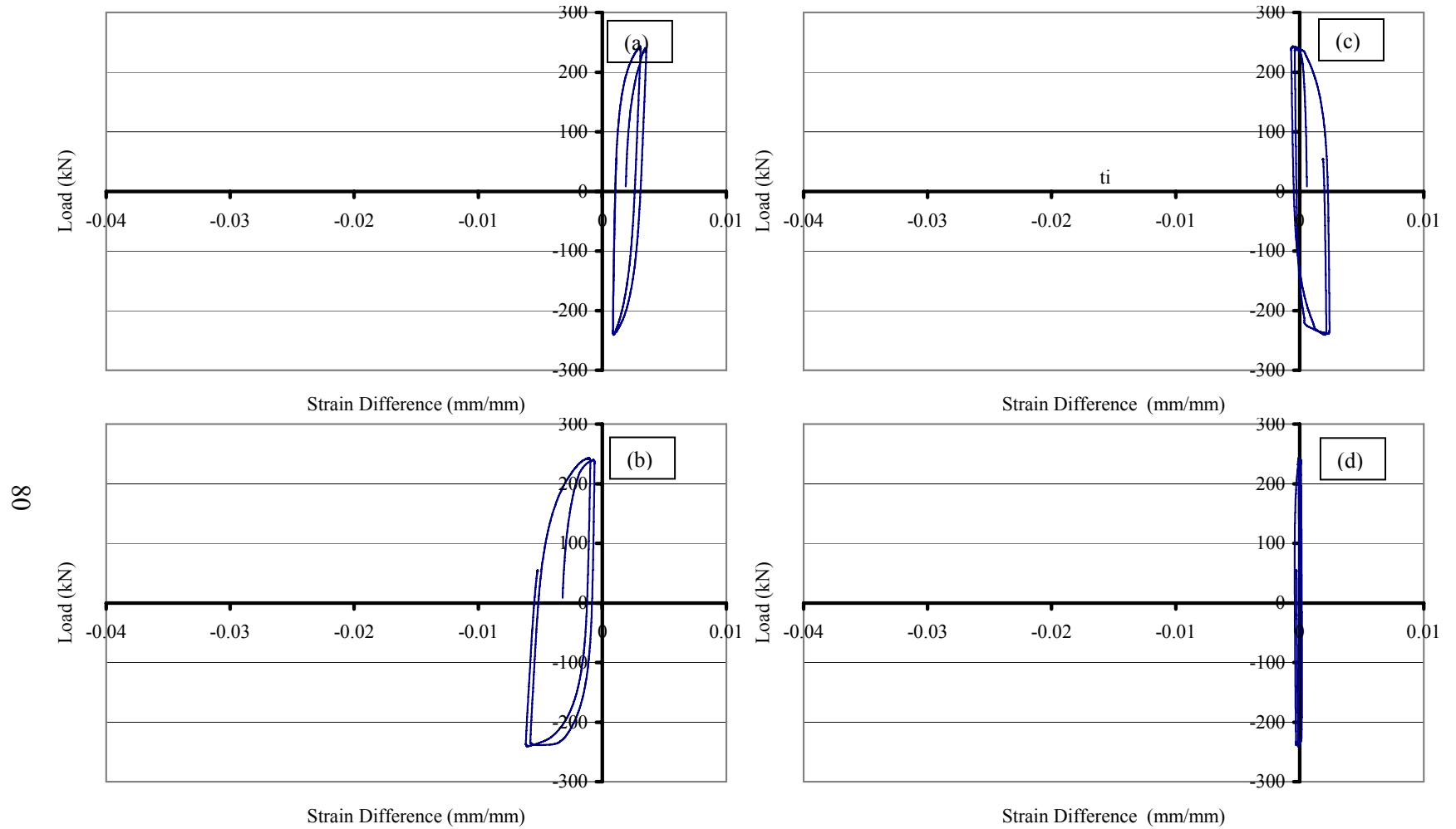
Figure 4.18 – Strain difference in flanges for DM assemblage test – step 9: (a) top flange-152 mm; (b) bottom flange-152 mm; (c) top flange-457 mm; and (d) bottom flange-457 mm

80
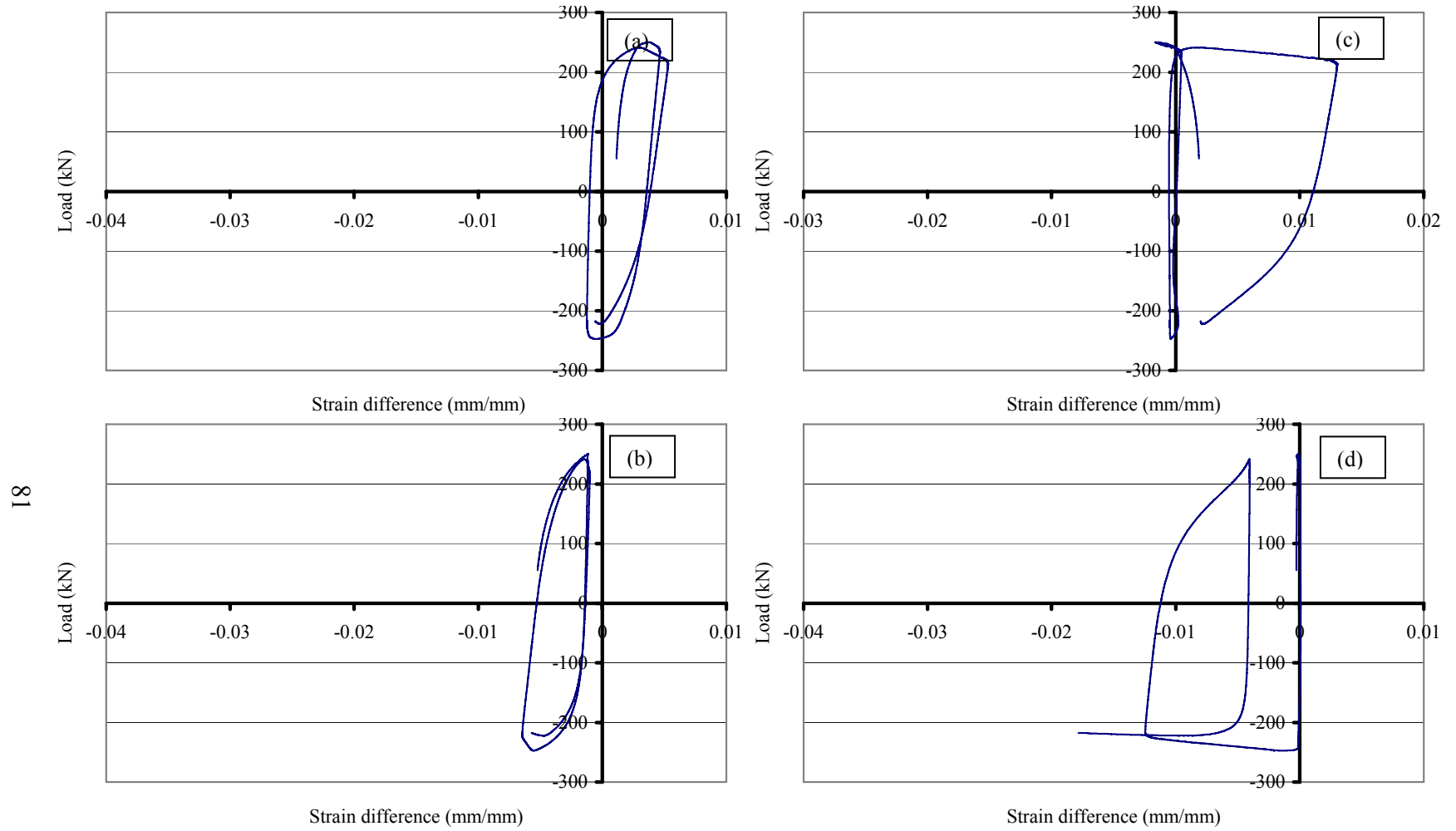
Figure 4.19 – Strain difference in flanges for DM assemblage test – step 10: (a) top flange-152 mm; (b) bottom flange-152 mm; (c) top flange-457 mm; and (d) bottom flange-457 mm

81

Figure 4.20 – DM assemblage showing buckling in the bottom flange at completion of testing
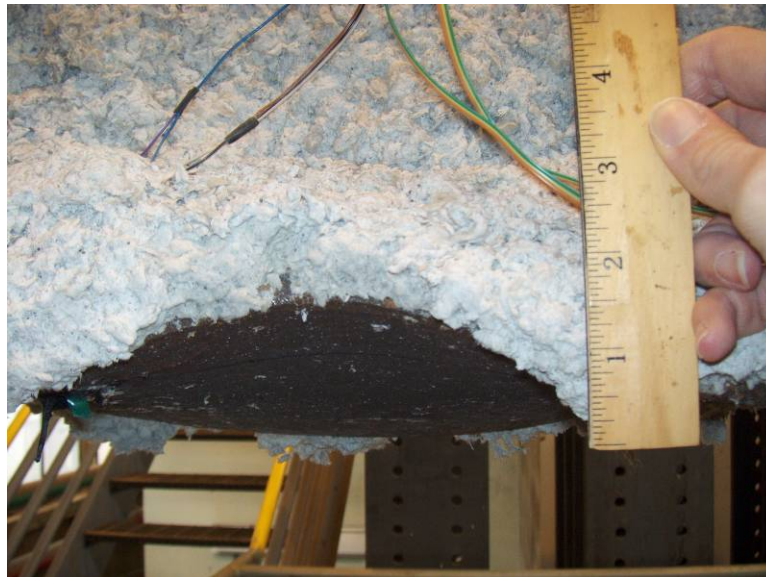
Figure 4.21 – Close-up of buckle in bottom flange of DM at completion of testing
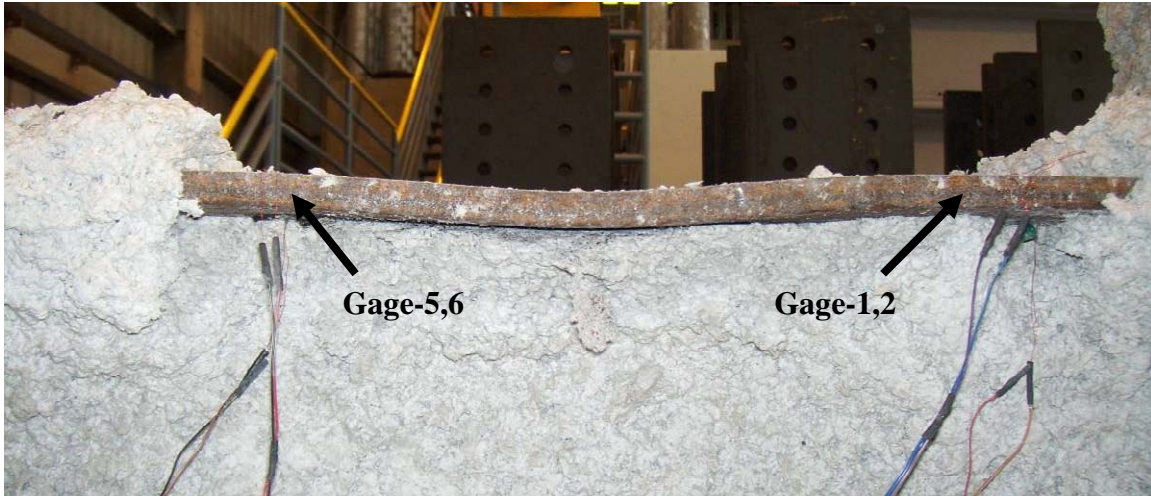
Figure 4.22 – DM top flange buckling at completion of testing
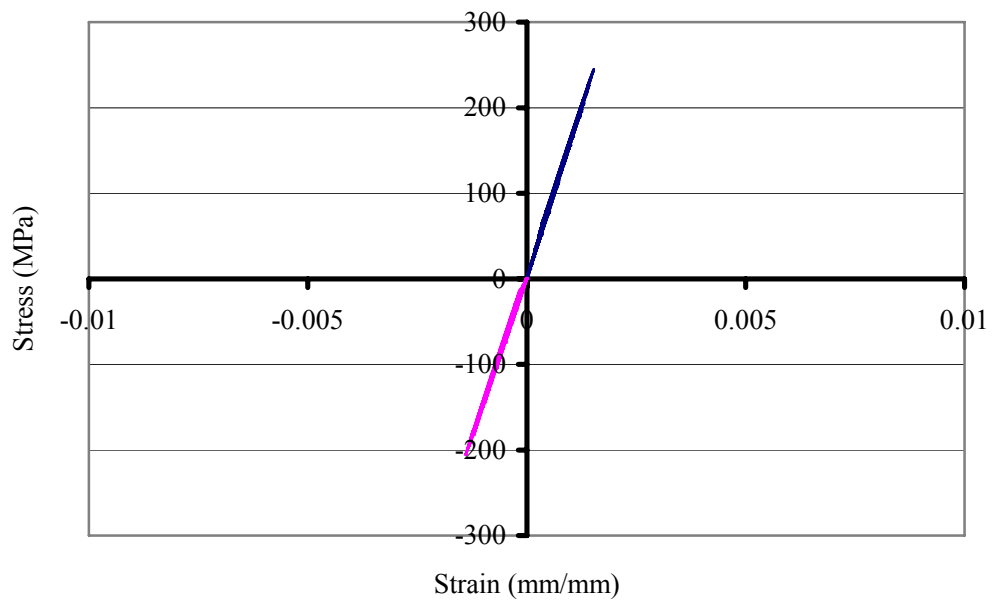
Figure 4.23 – Principle stresses versus principle strains in the panel zone
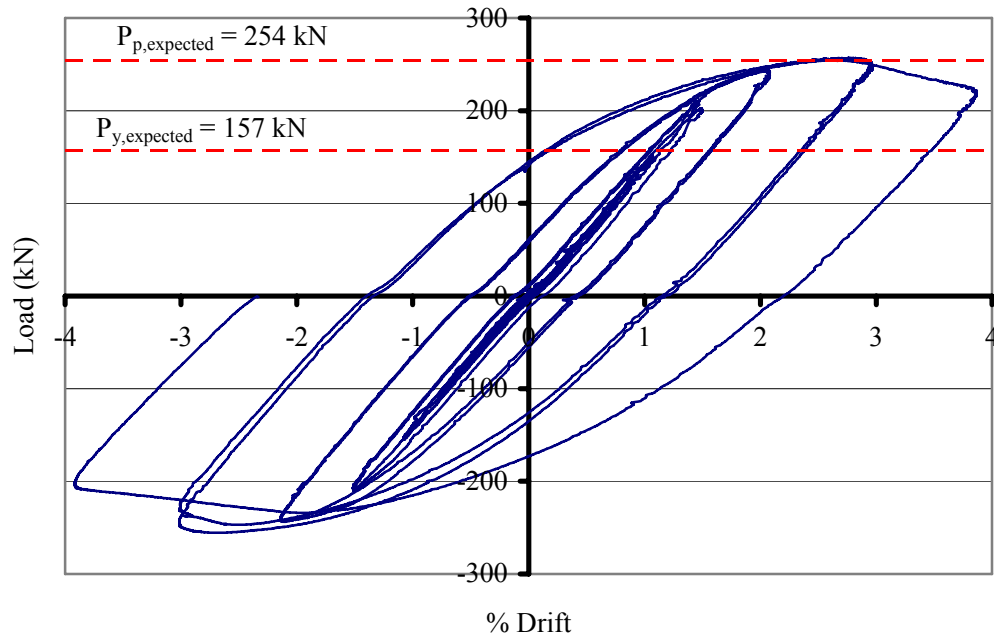
Figure 4.24 – Load vs. percent drift for WM assemblage test
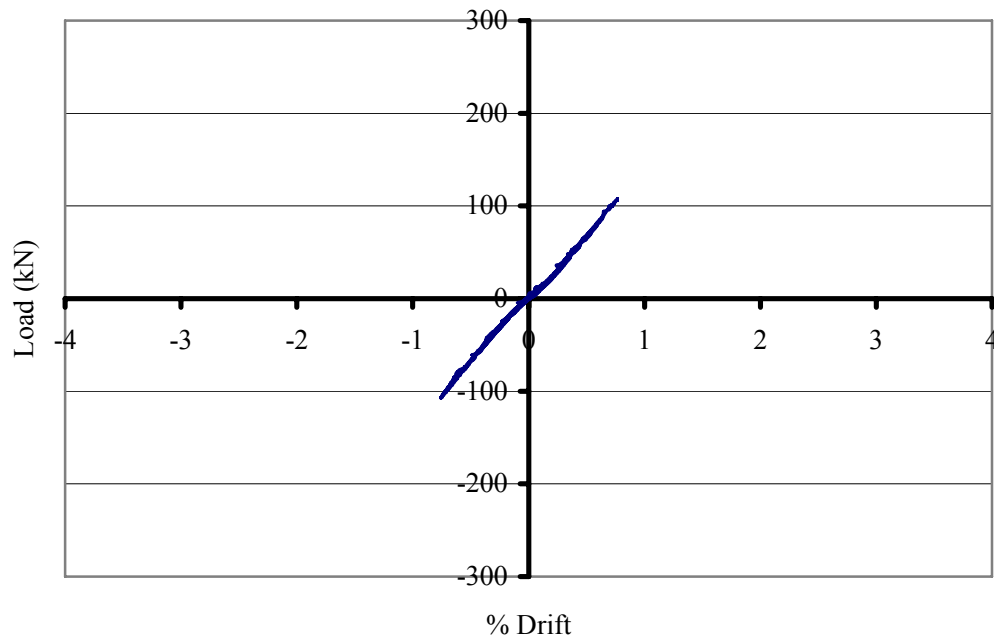
Figure 4.25 – Load vs. percent drift for WM assemblage test – steps 1 through 6
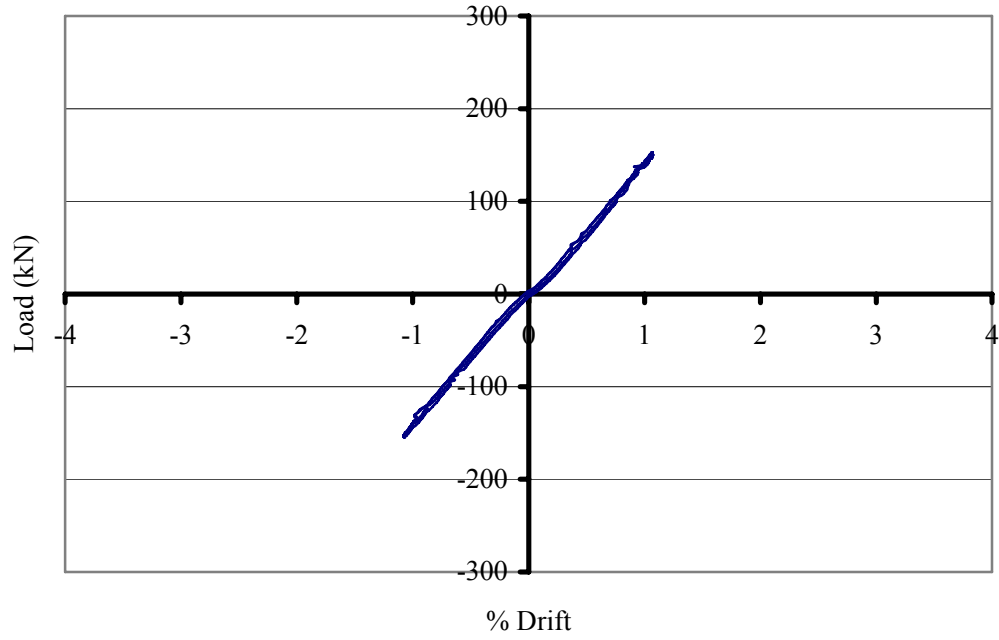
Figure 4.26 – Load vs. percent drift for WM assemblage test – step 7
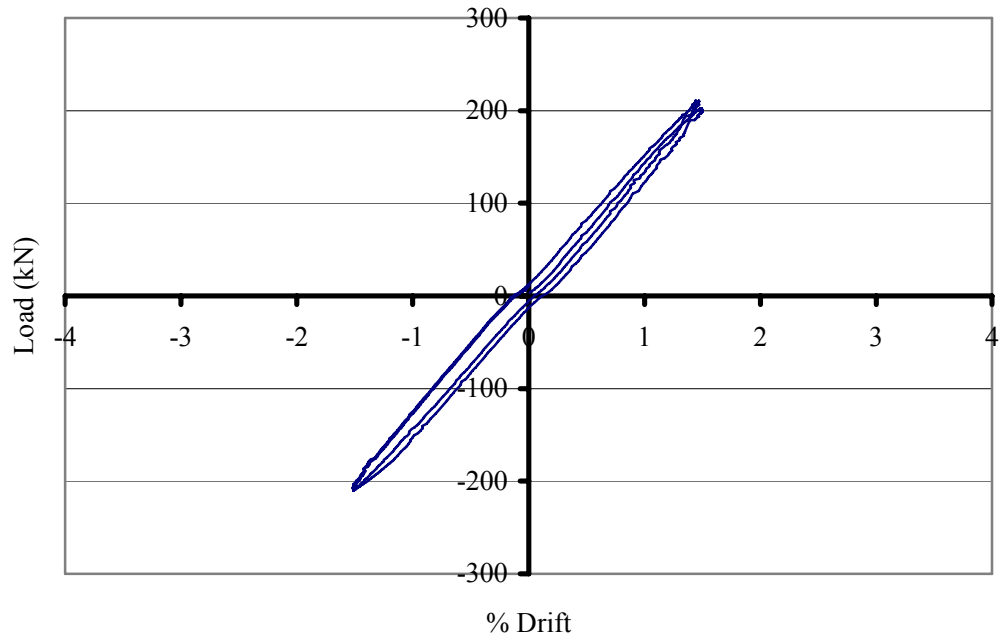
Figure 4.27 – Load vs. percent drift for WM assemblage test – step 8
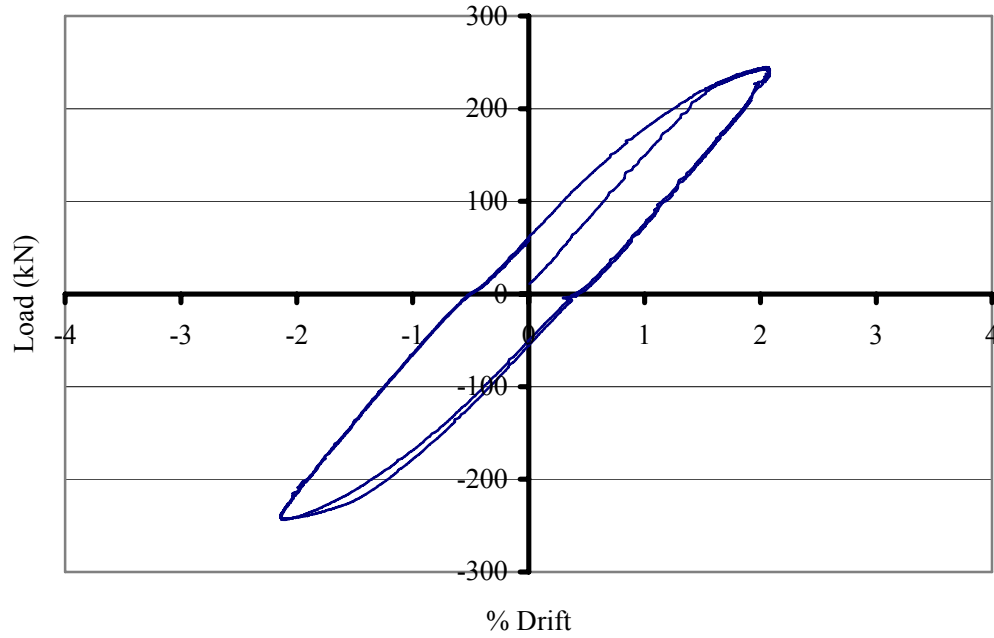
Figure 4.28 – Load vs. percent drift for WM assemblage test – step 9
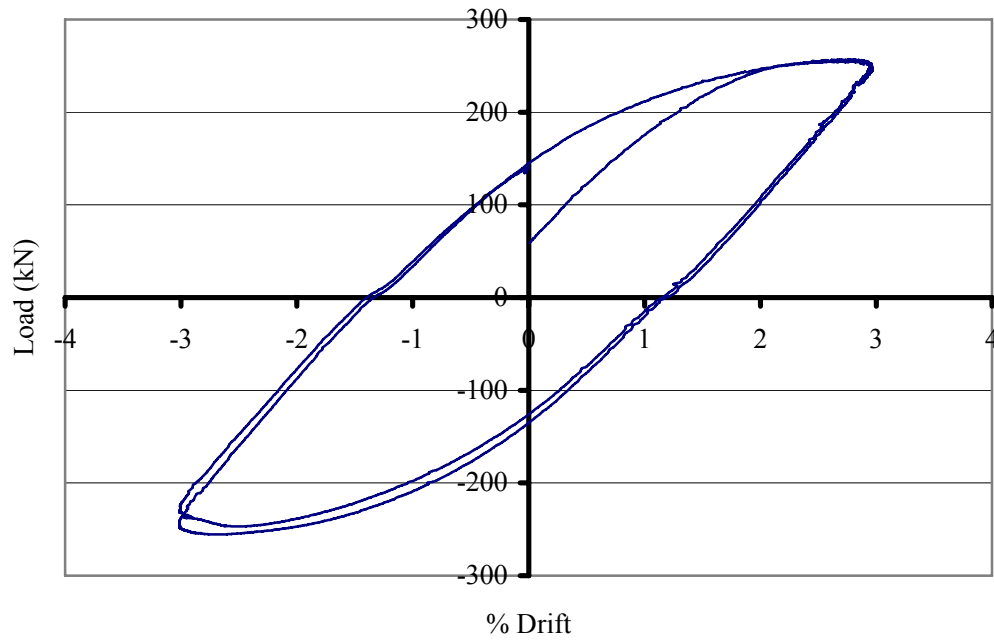
Figure 4.29 – Load vs. percent drift for WM assemblage test – step 10
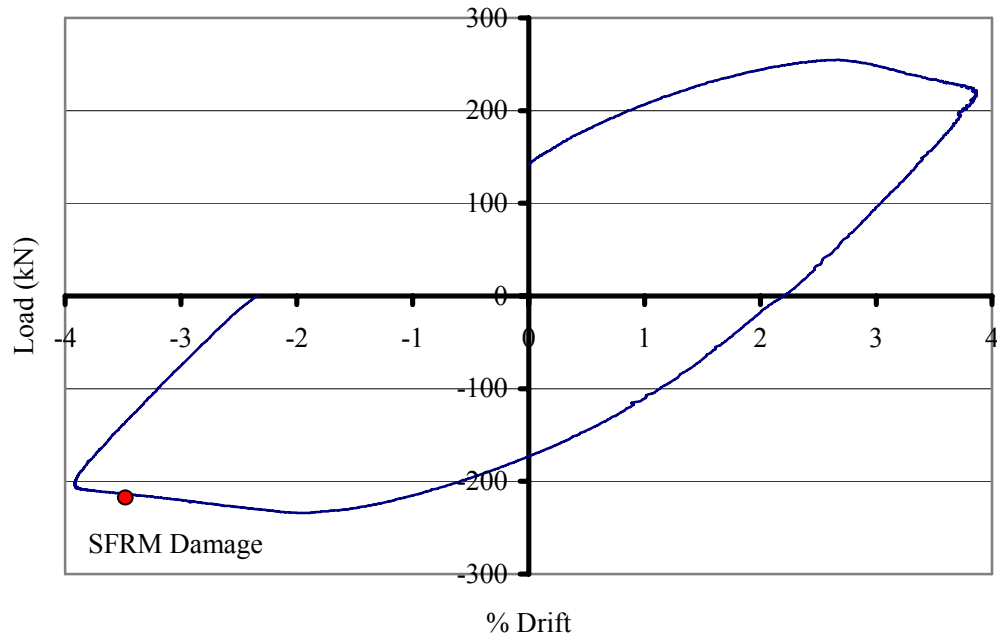
Figure 4.30 – Load vs. percent drift for WM assemblage test – step 11

Figure 4.31 – Damage to SFRM during step 11 of WM assemblage test
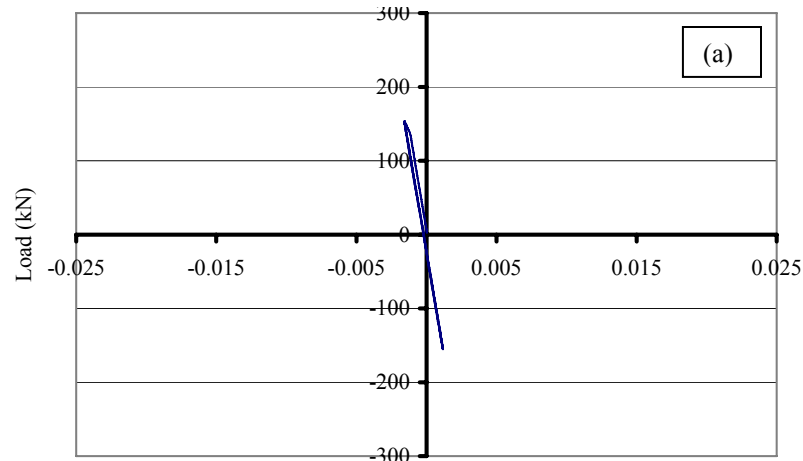
Figure 4.32 – WM assemblage test strain data – steps 1 through 6: (a) Gage-1; (b) Gage-2; (d) Gage-4; [continued]
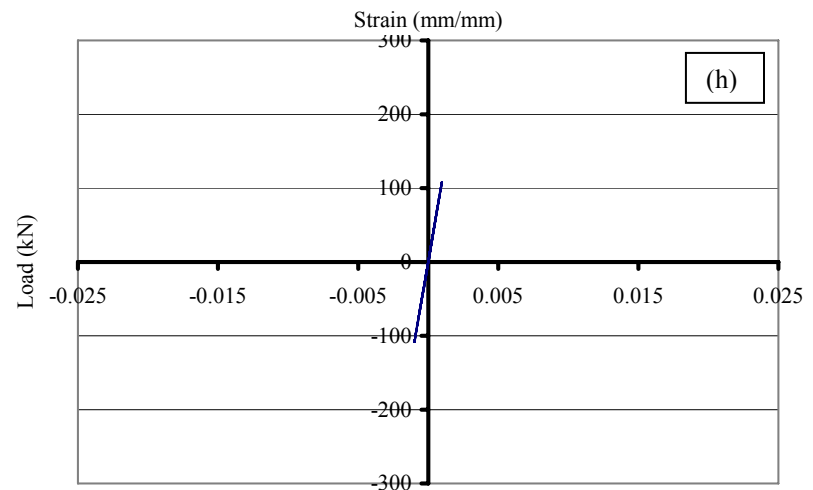
Figure 4.32 – [continued] WM assemblage test strain data – steps 1 through 6: (e) Gage-5; (f) Gage-6; (g) Gage-7; and (h) Gage-8

68

Gage-3 strain data not available

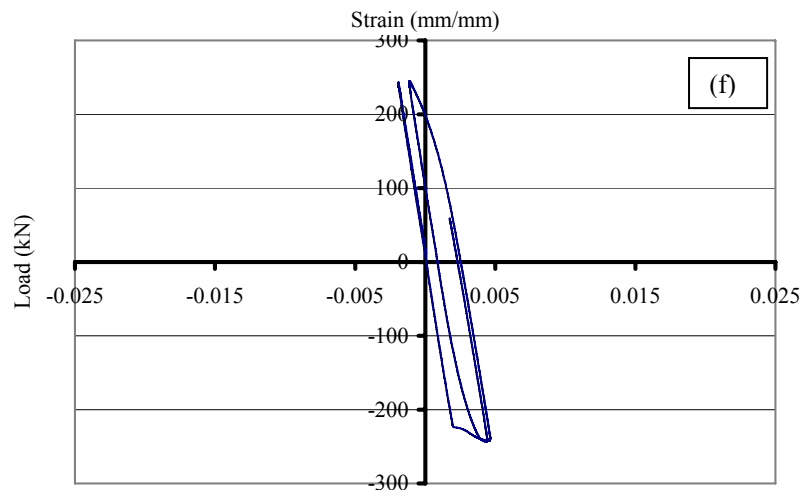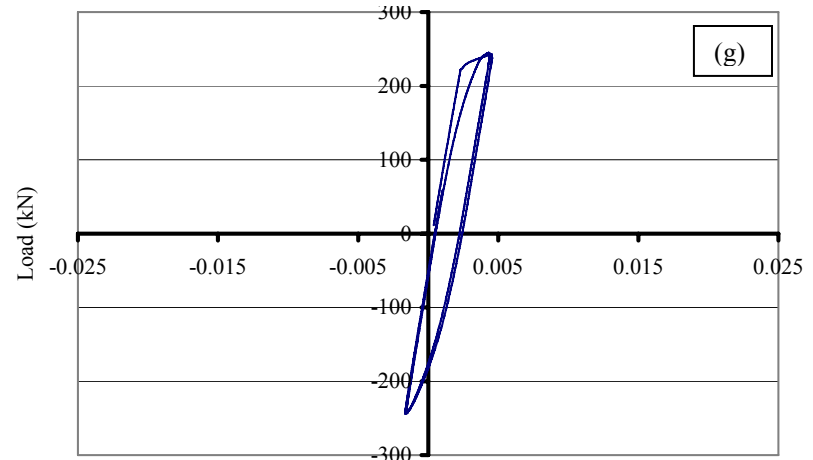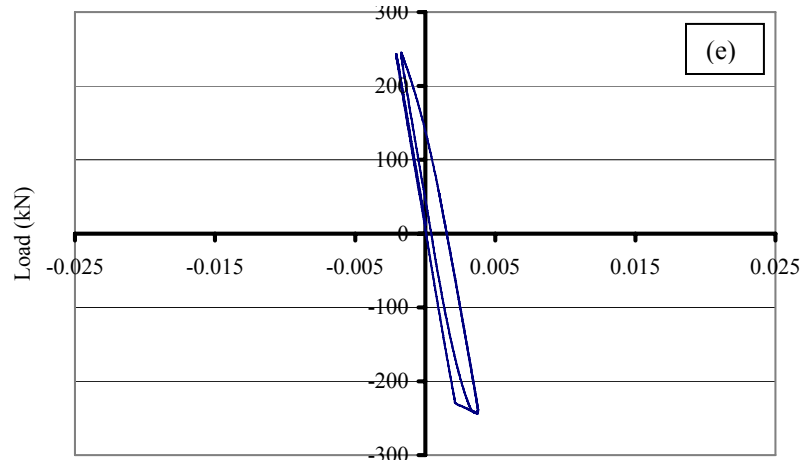Figure 4.33 – WM assemblage test strain data – step 7: (a) Gage-1; (b) Gage-2; (d) Gage-4; [continued]

Figure 4.33 – [continued] WM assemblage test strain data – step 7: (e) Gage-5; (f) Gage-6; (g) Gage-7; and (h) Gage-8

91
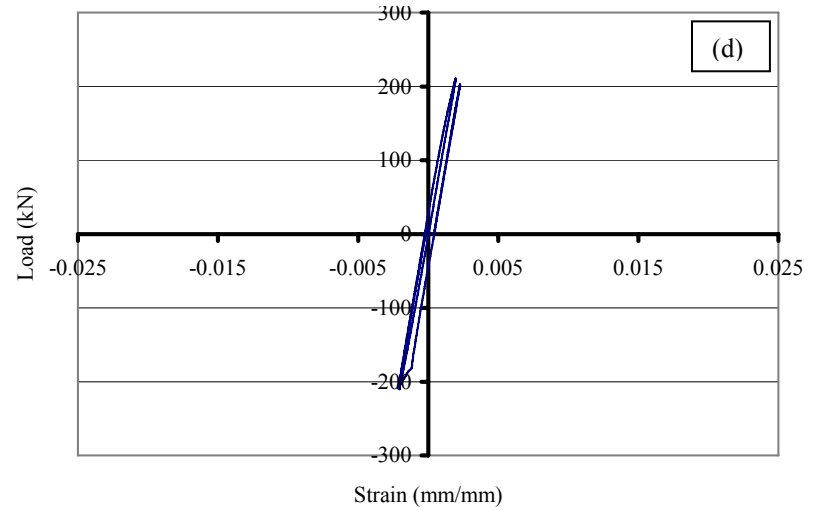
Figure 4.34 – WM assemblage test strain data – step 8: (a) Gage-1; (b) Gage-2; (d) Gage-4; [continued]
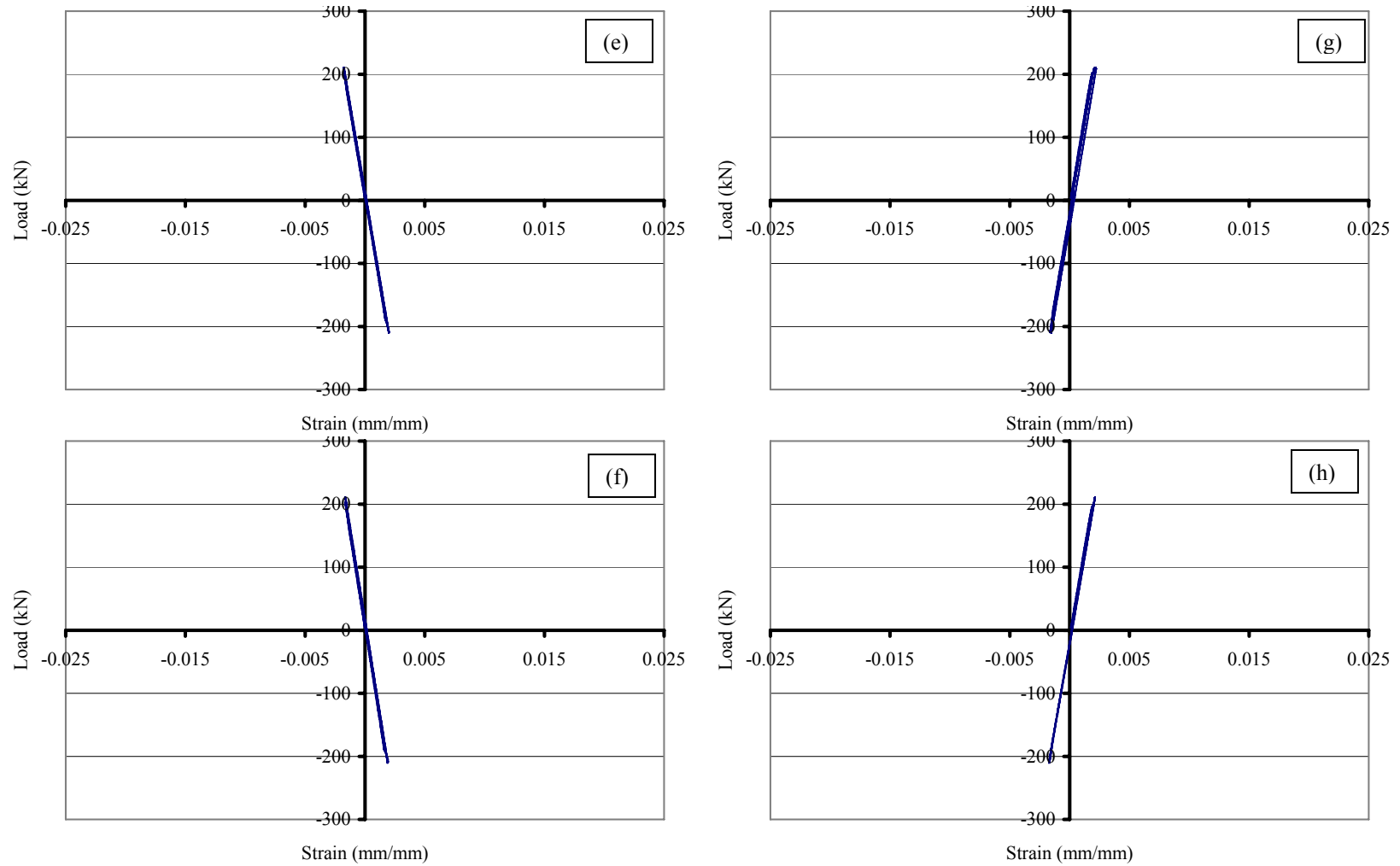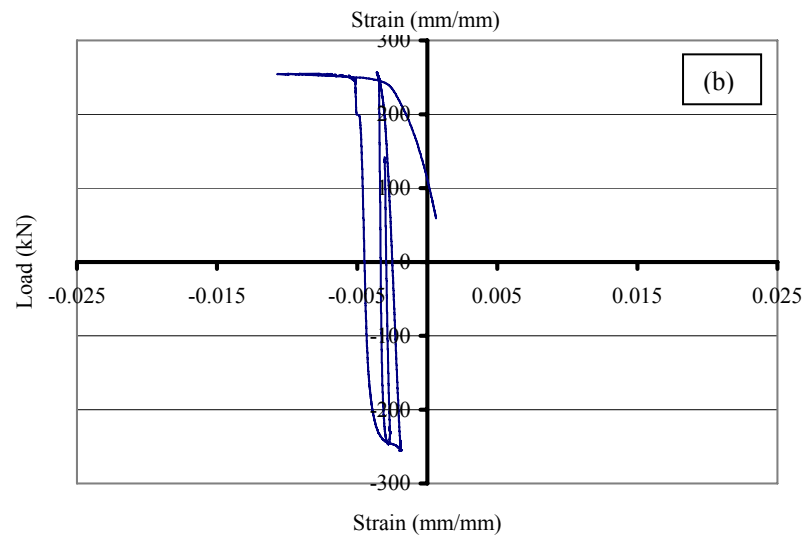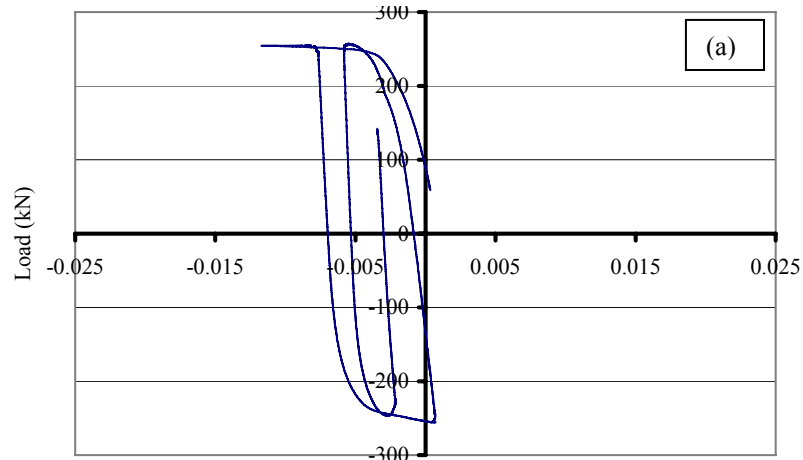
Figure 4.34 – [continued] WM assemblage test strain data – step 8: (e) Gage-5; (f) Gage-6; (g) Gage-7; and (h) Gage-8
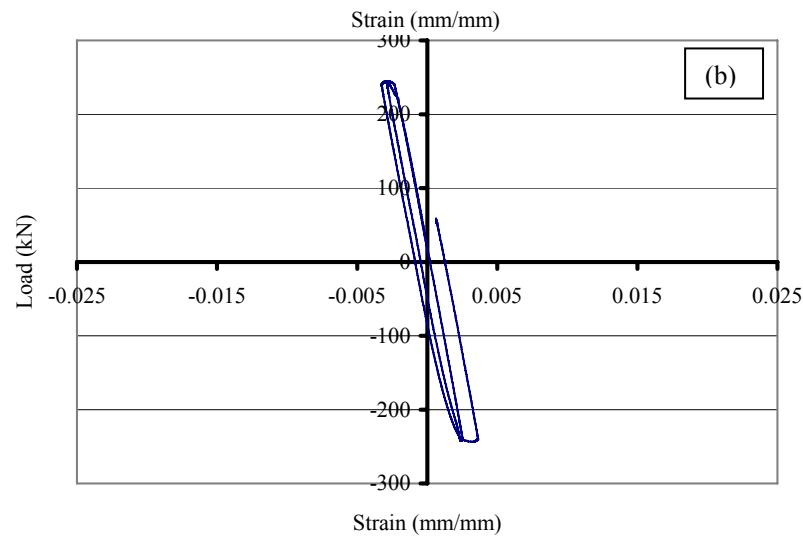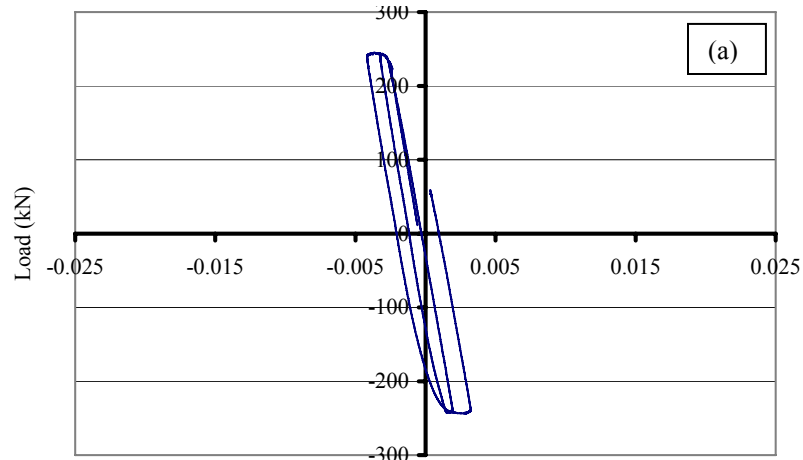
Gage-3 strain data not available
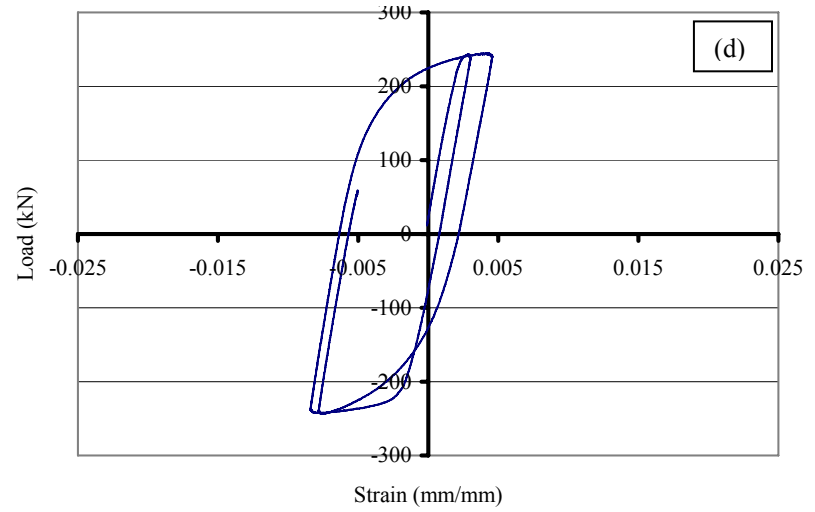
Figure 4.35 – WM assemblage test strain data – step 9: (a) Gage-1; (b) Gage-2; (d) Gage-4; [continued]
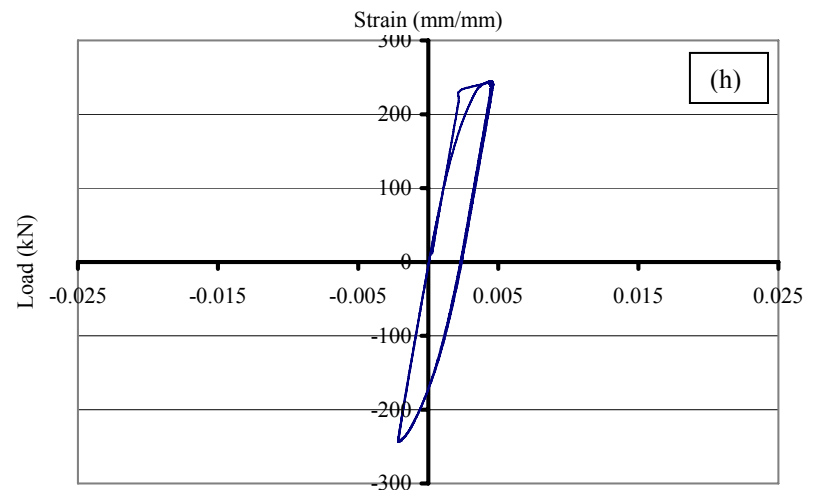
Figure 4.35 – [continued] WM assemblage test strain data – step 9: (e) Gage-5; (f) Gage-6; (g) Gage-7; and (h) Gage-8
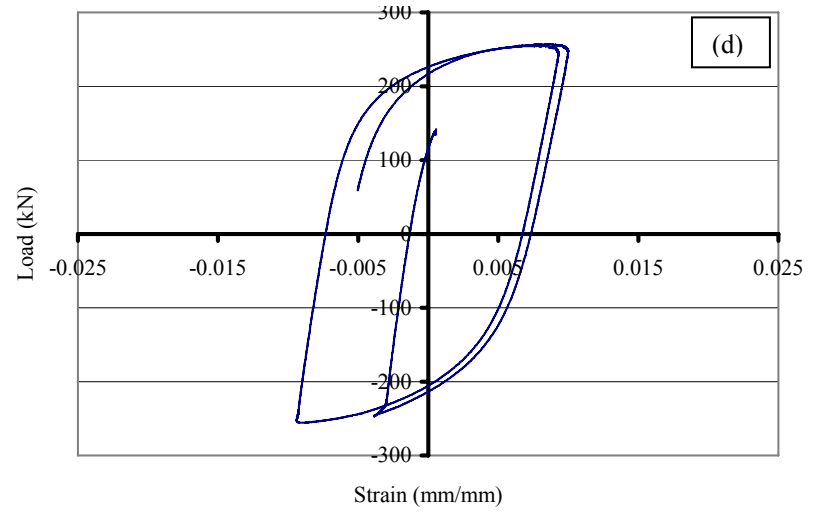
Gage-3 strain data not available

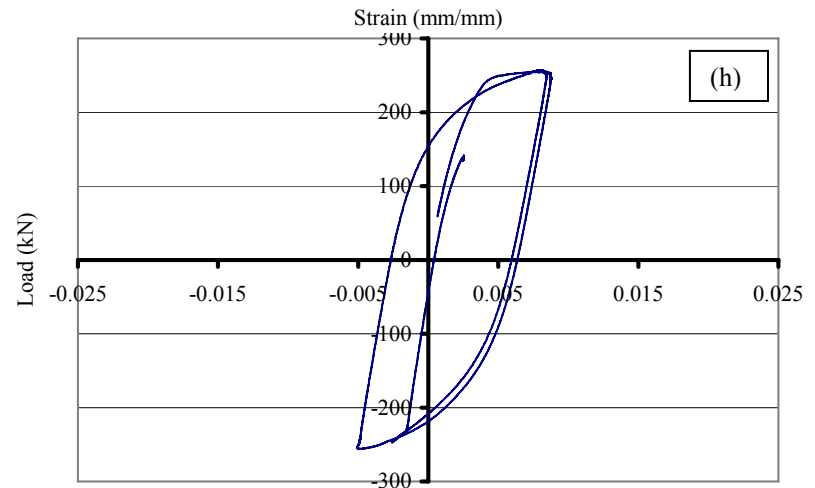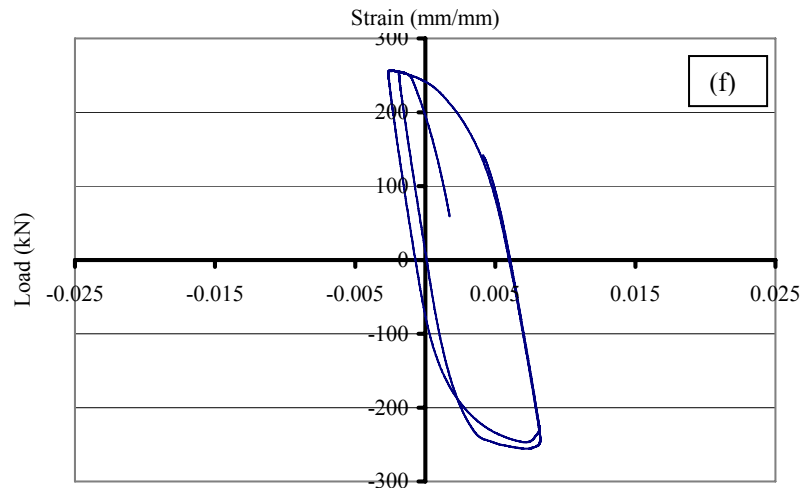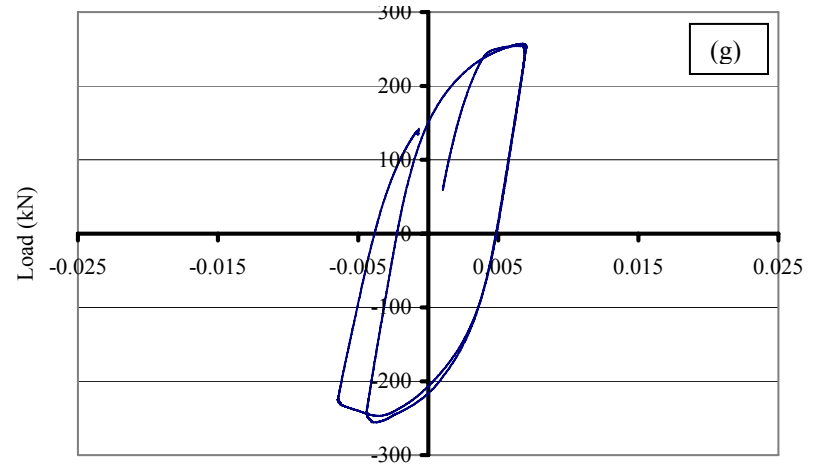Figure 4.36 – WM assemblage test strain data – step 10: (a) Gage-1; (b) Gage-2; (d) Gage-4; [continued]

Figure 4.36 – [continued] WM assemblage test strain data – step 10: (e) Gage-5; (f) Gage-6; (g) Gage-7; and (h) Gage-8

Figure 4.37 – WM assemblage test strain data – step 11: (a) Gage-1; (b) Gage-2; (d) Gage-4; [continued]
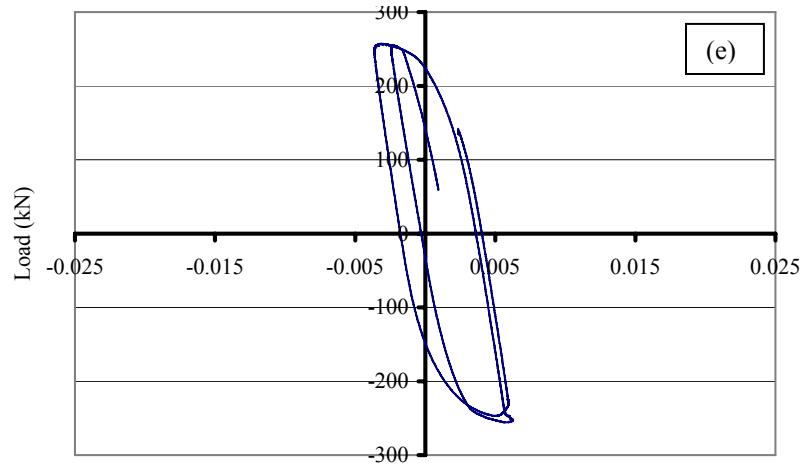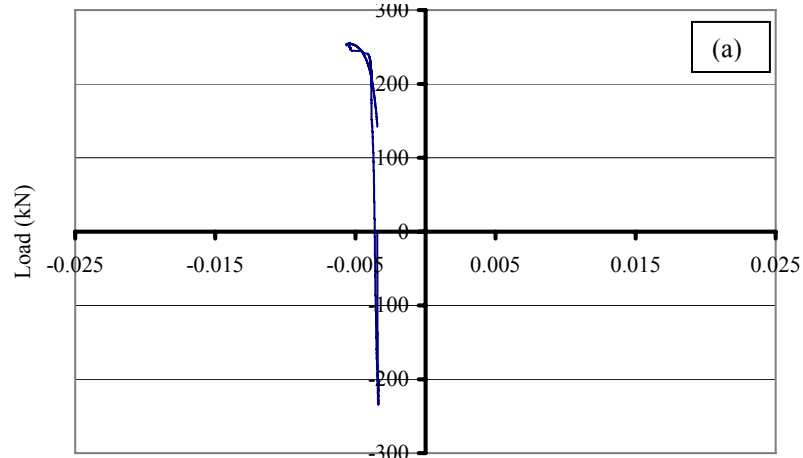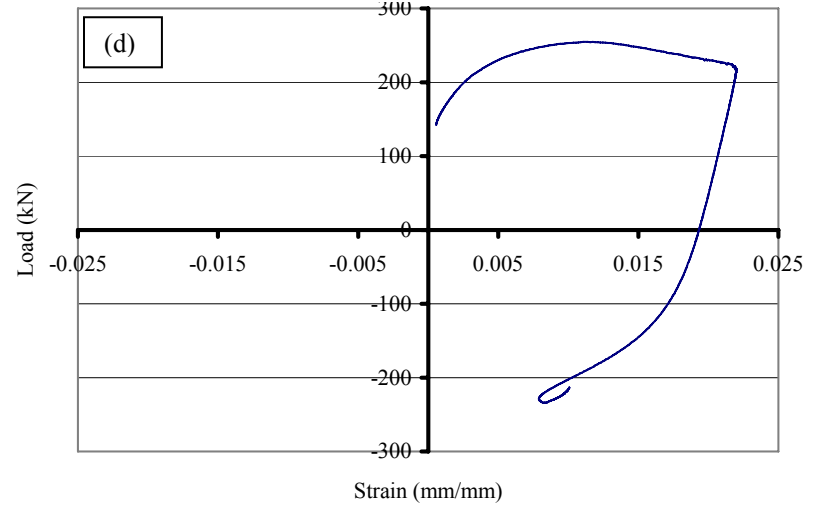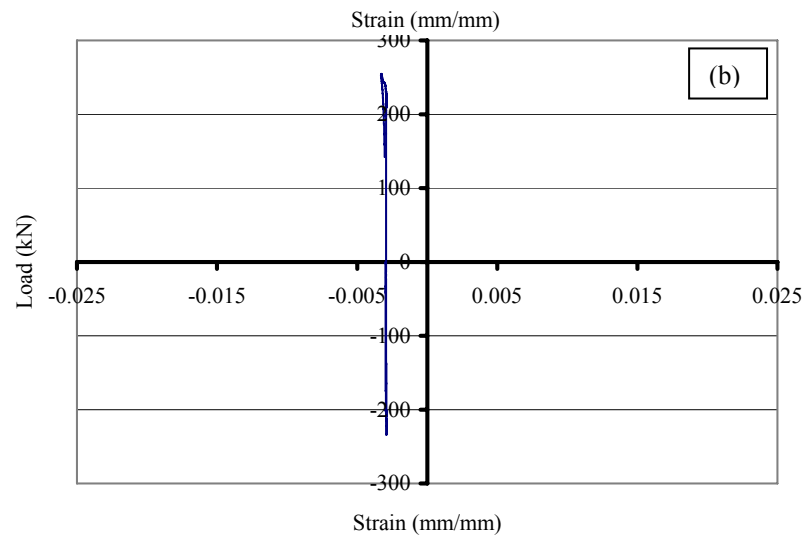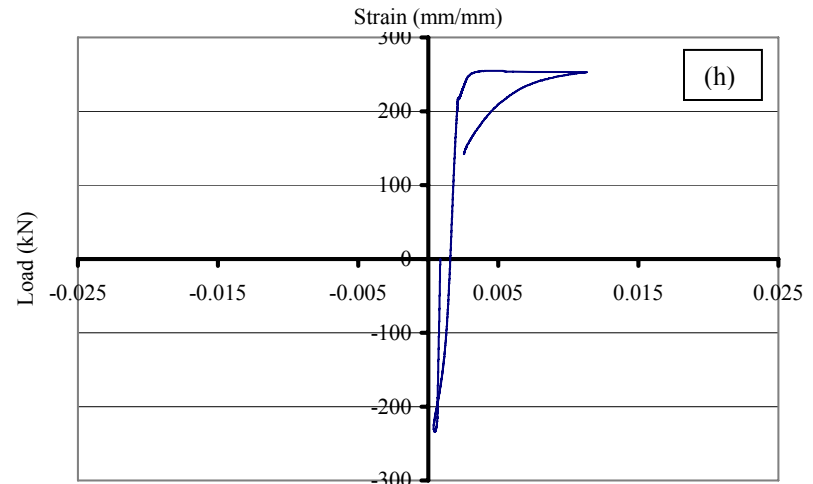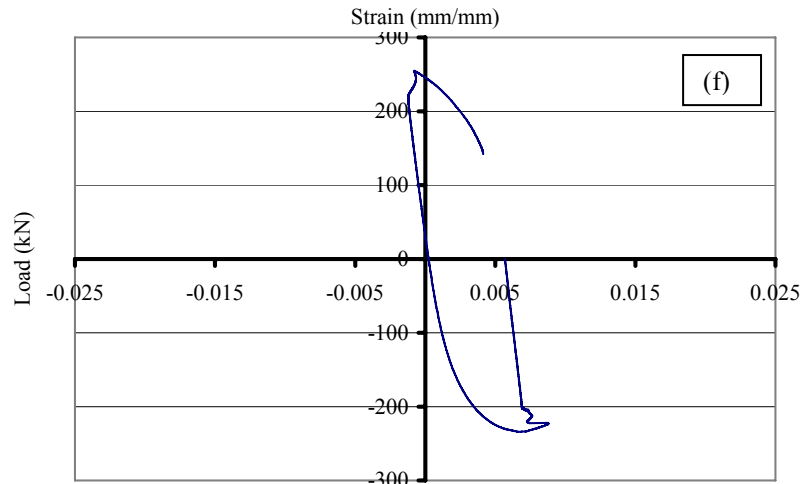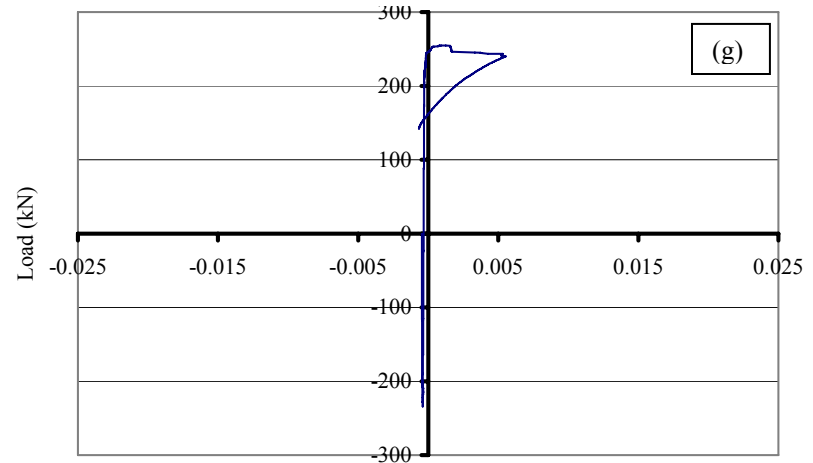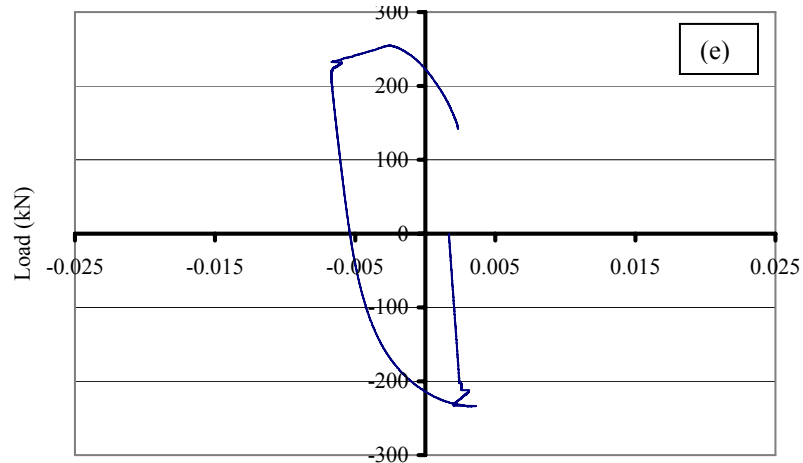
Figure 4.37 – [continued] WM assemblage test strain data – step 11: (e) Gage-5; (f) Gage-6; (g) Gage-7; and (h) Gage-8

66

(a)

Load (kN)

300

200

100

0

-100

-200

-300

-0.02　-0.015　-0.01　-0.005　0.005　0.01　0.015　0.02

Strain difference (mm/mm)

(c)

Load (kN)

300

200

100

0

-100

-200

-300

-0.02　-0.015　-0.01　-0.005　0.005　0.01　0.015　0.02

Strain difference (mm/mm)

Strain difference in bottom flange-152 mm not available

(d)

Load (kN)

300

200

100

0

-100

-200

-300

-0.02　-0.015　-0.01　-0.005　0.005　0.01　0.015　0.02
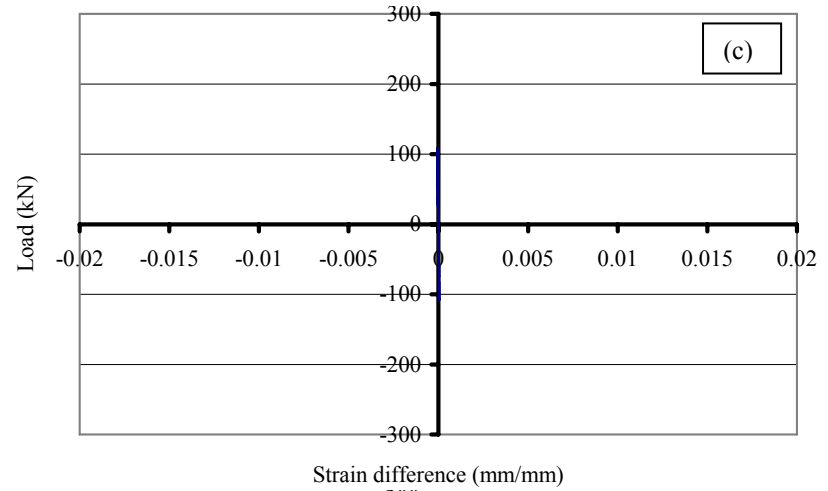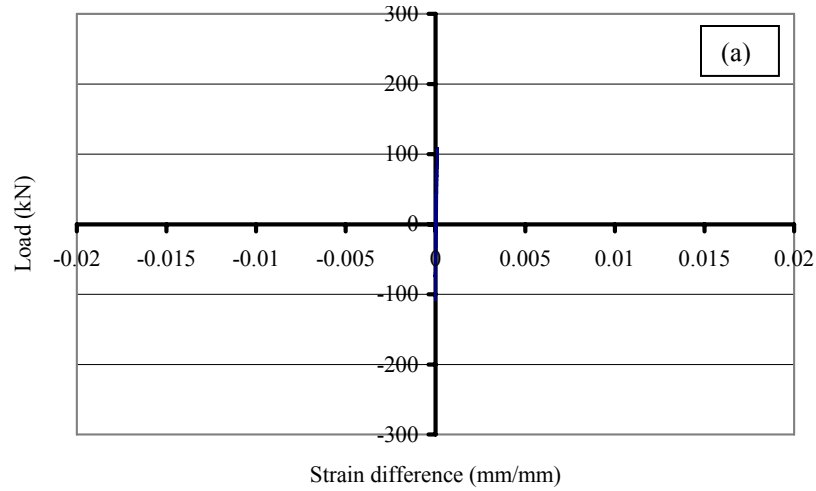
Strain difference (mm/mm)
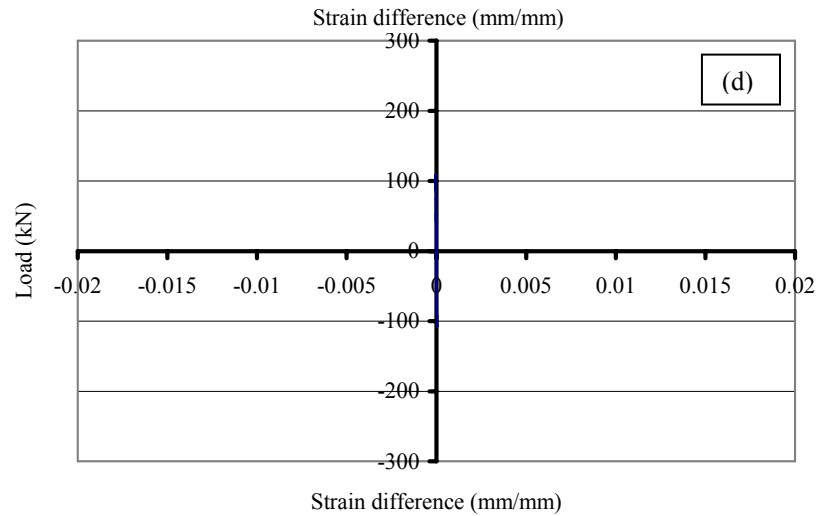
Figure 4.38 – Strain difference in flanges for WM assemblage test – steps 1 through 6: (a) top flange-152 mm; (c) top flange-457 mm; and (d) bottom flange-457mm
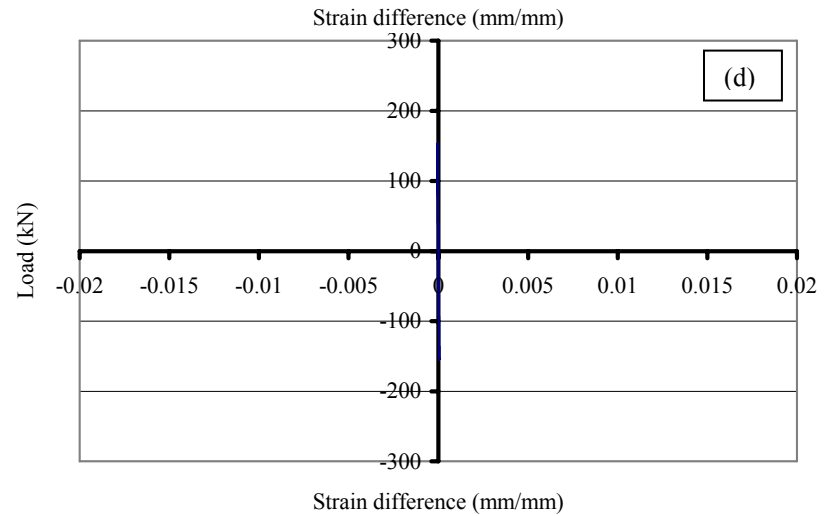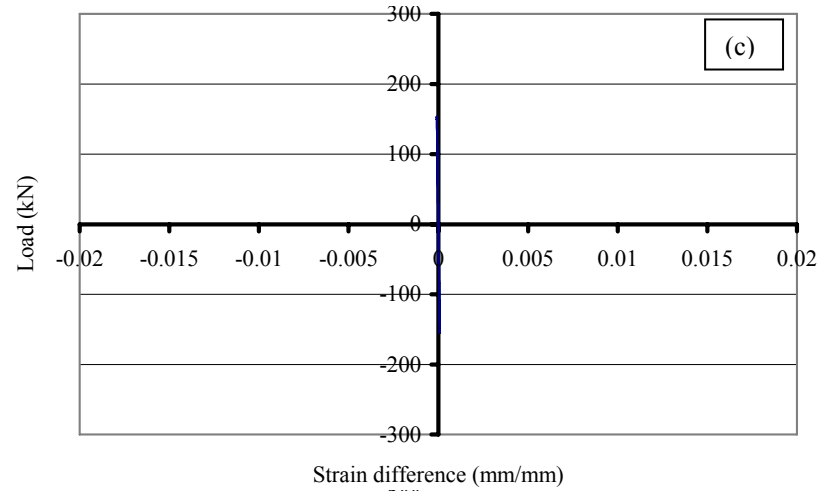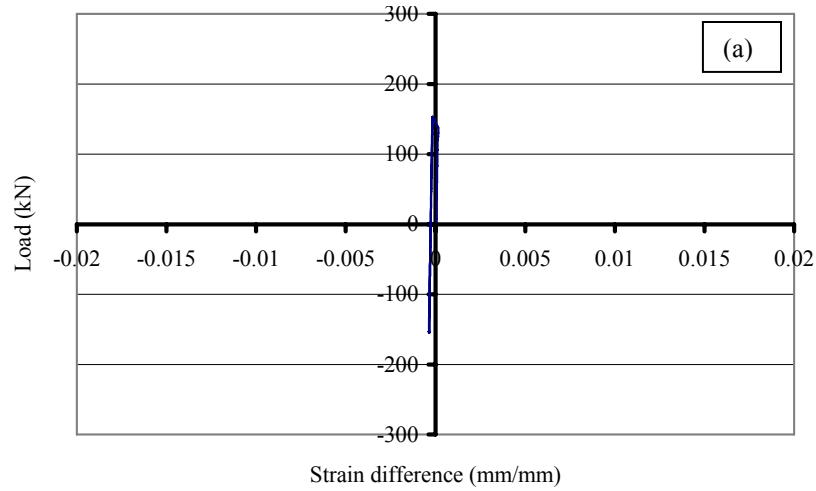
Strain difference in bottom flange-152 mm not available

Figure 4.39 – Strain difference in flanges for WM assemblage test – step 7: (a) top flange-152 mm; (c) top flange-457 mm; and (d) bottom flange-457 mm
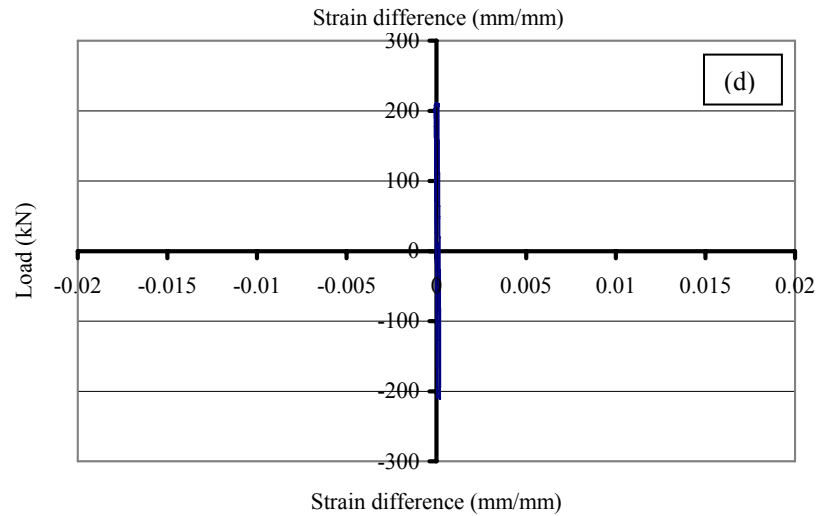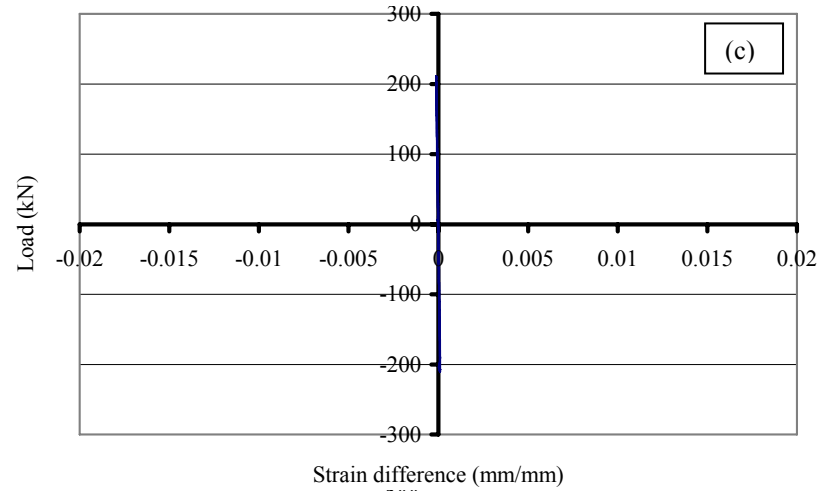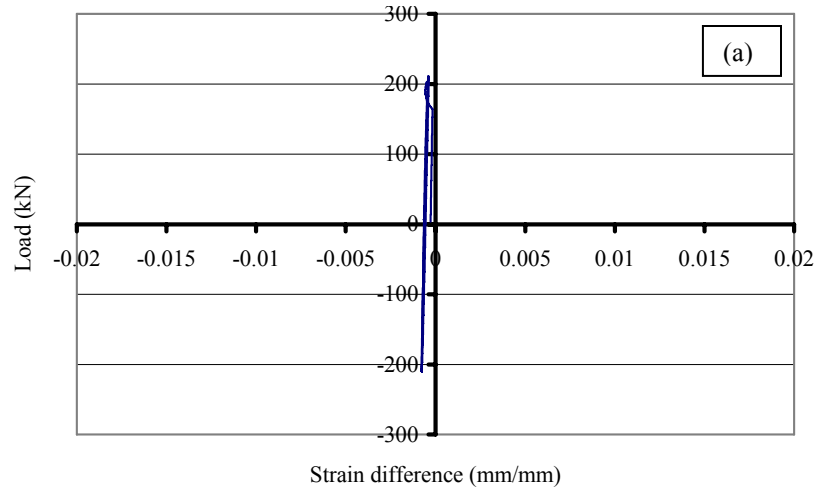
Strain difference in bottom flange-152 mm
not available

Figure 4.40 – Strain difference in flanges for WM assemblage test – step 8: (a) top flange-152 mm; (c) top flange-457 mm; and (d) bottom flange-457 mm
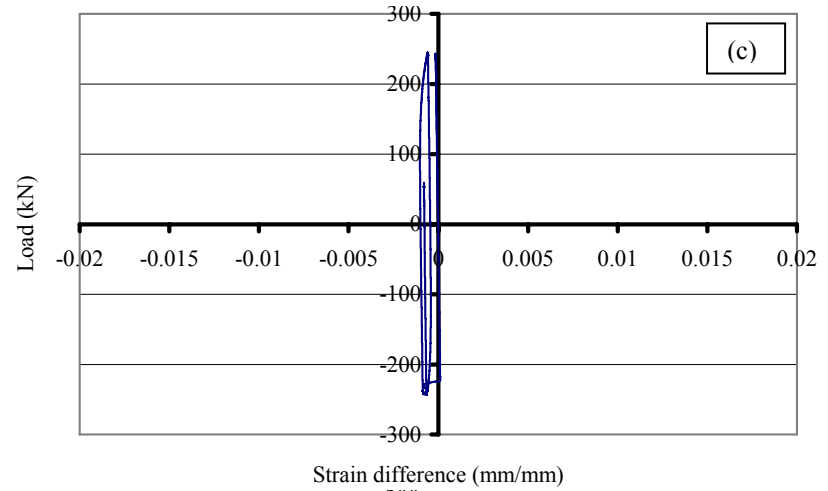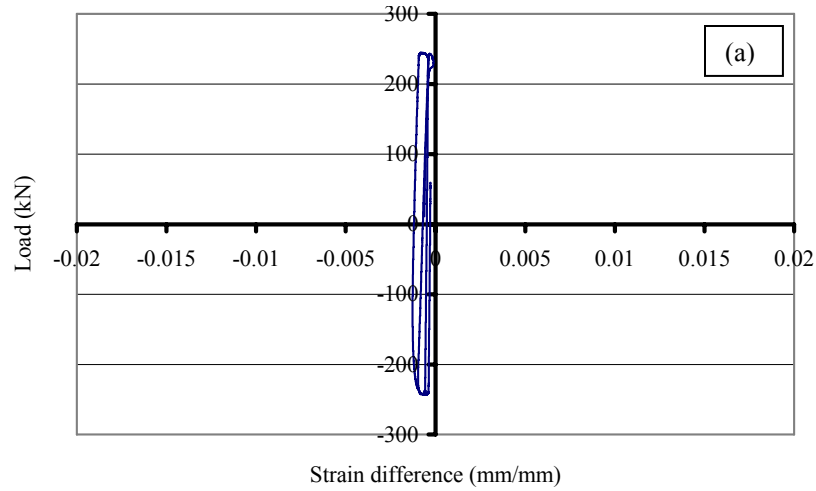
Strain difference in bottom flange-152 mm not available
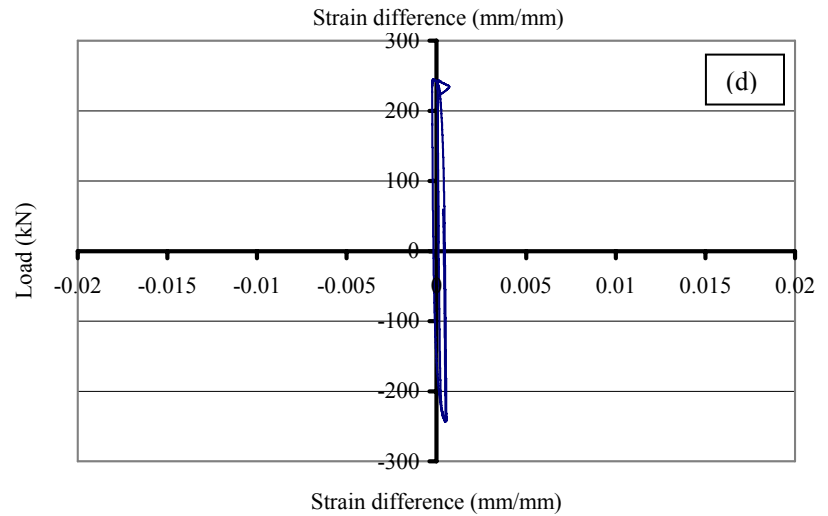
Figure 4.41 – Strain difference in flanges for WM assemblage test – step 9: (a) top flange-152 mm; (c) top flange-457 mm; and (d) bottom flange-457 mm
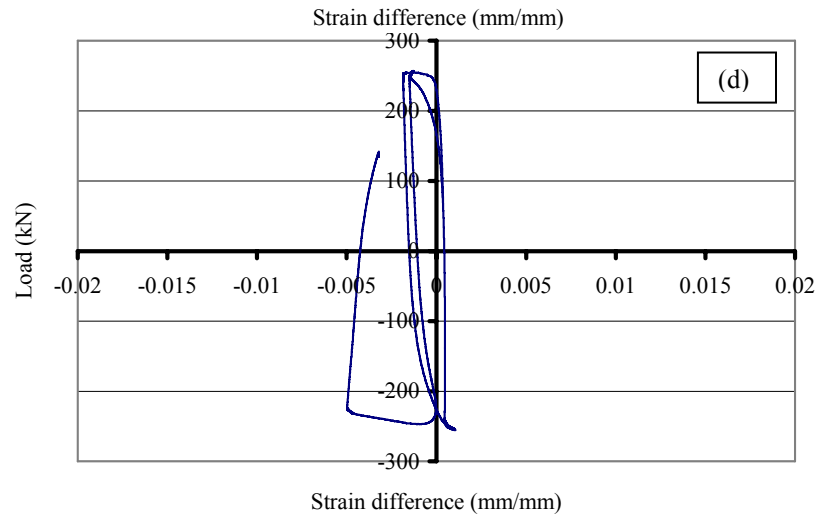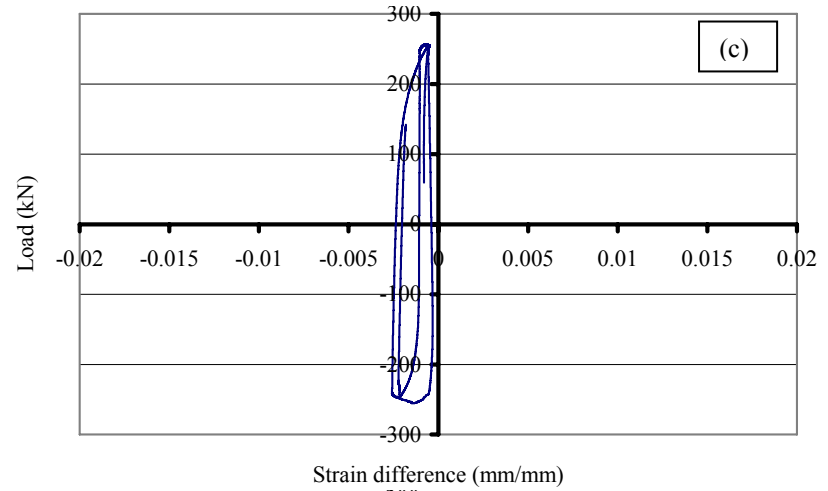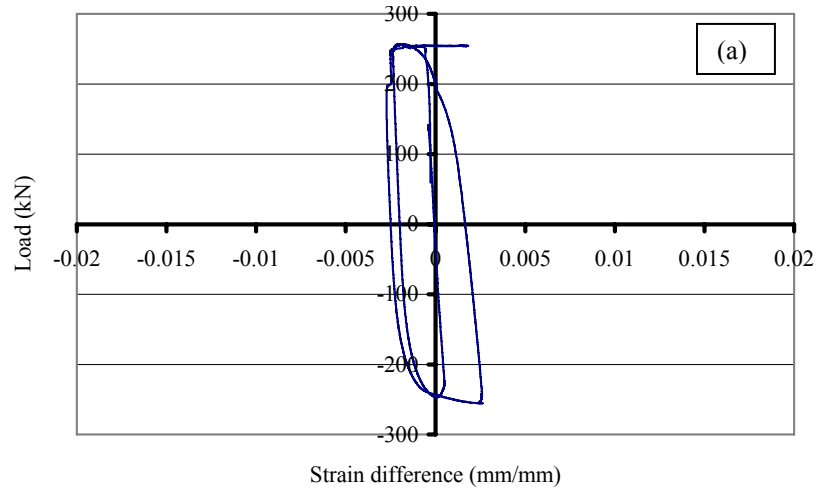
Strain difference in bottom flange-152 mm not available

Figure 4.42 – Strain difference in flanges for WM assemblage test – step 10: (a) top flange-152 mm; (c) top flange-457 mm; and (d) bottom flange-457 mm

Strain difference in bottom flange-152 mm not available
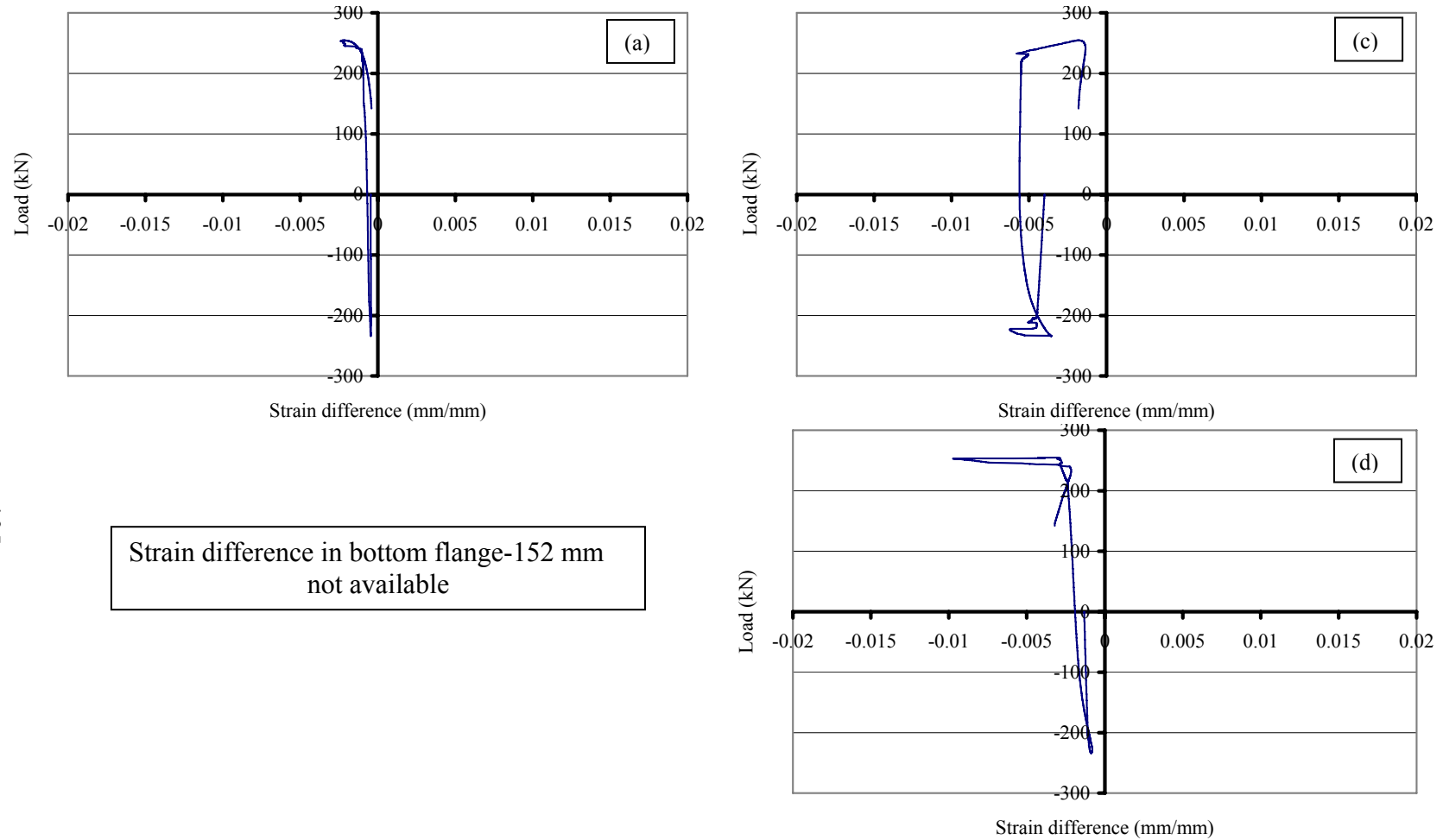
Figure 4.43 – Strain difference in flanges for WM assemblage test – step 11: (a) top flange-152 mm; (c) top flange-457 mm; and (d) bottom flange-457 mm
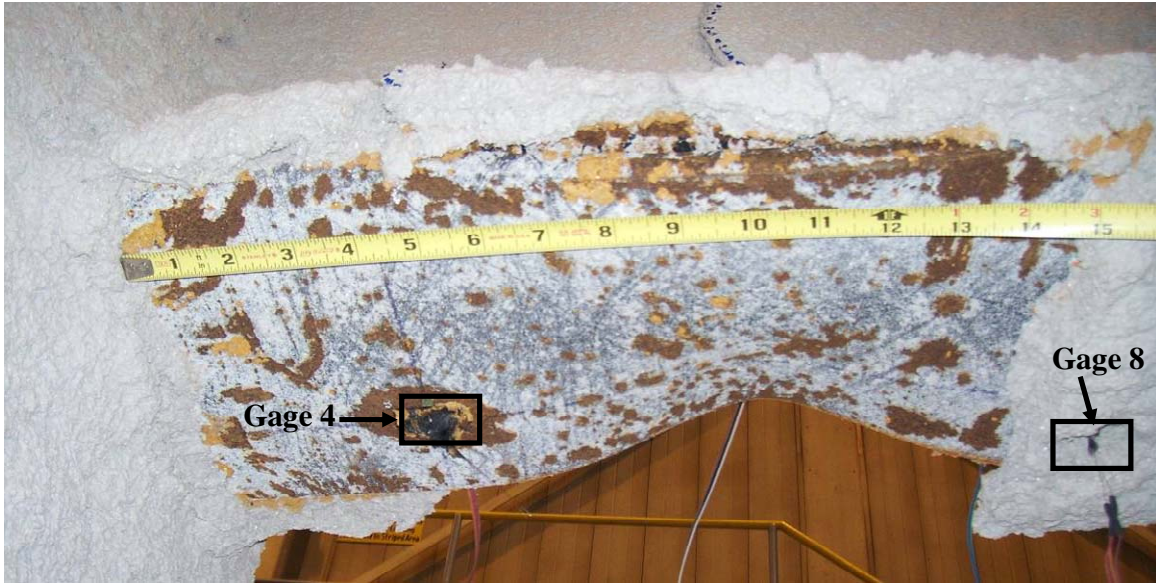
Figure 4.44 – Location of strain gages with respect to proximity to local flange buckling at completion of WM assemblage test

Figure 4.45 – Close-up of local buckling in bottom flange at completion of WM assemblage test

Figure 4.46 – Top flange of WM assemblage with gage locations at completion of test
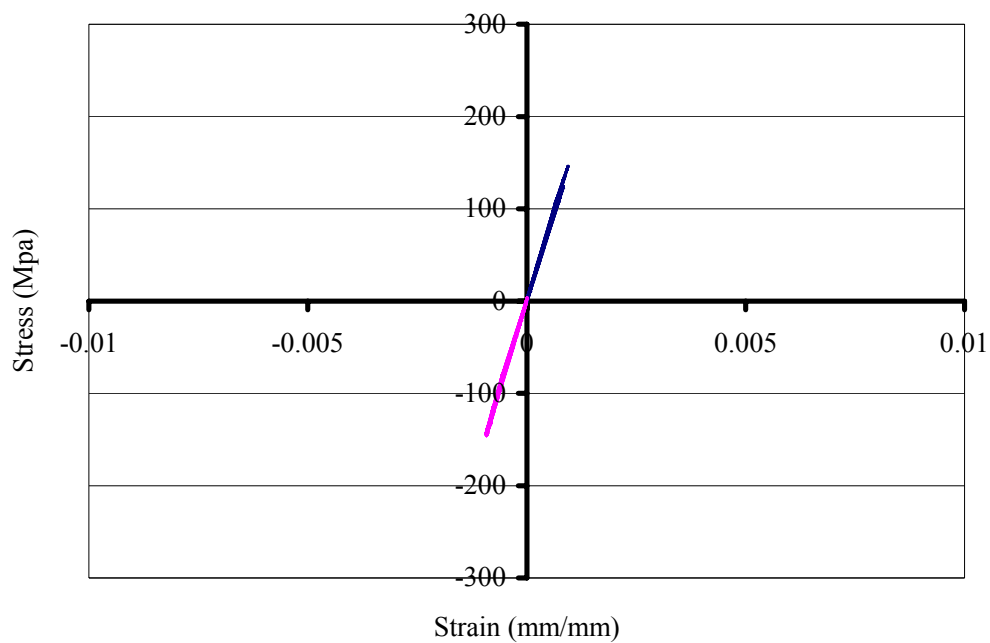
Figure 4.47 – Principle stresses vs. principle strains in panel zone for WM assemblage test

Figure 4.48 – Longitudinal splitting on top flange SFRM of DM assemblage during step 10

Figure 4.49 – Transverse crack in top flange of DM assemblage during post-testing inspection
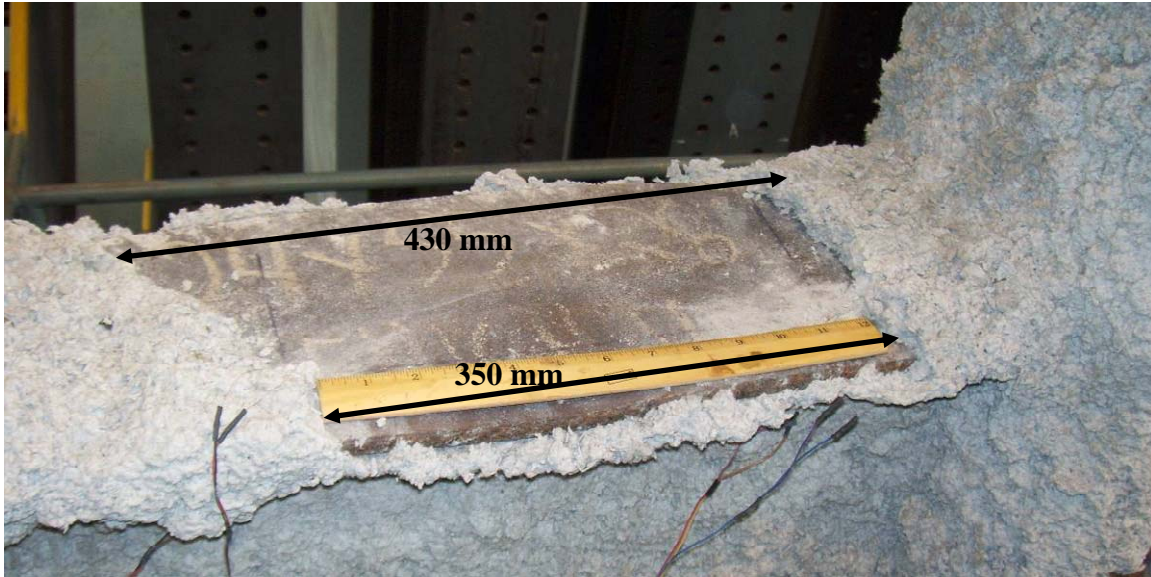
Figure 4.50 – Top flange of DM assemblage after loose SFRM was removed during post-testing inspection

Figure 4.51 – Top flange of DM assemblage after loose SFRM was removed from underside of flange post-testing inspection

Figure 4.52 – Close-up view of longitudinal splitting in bottom flange SFRM of DM
assemblage during step 10

Figure 4.53 – First damaged portion of SFRM on bottom flange of DM assemblage during step 10
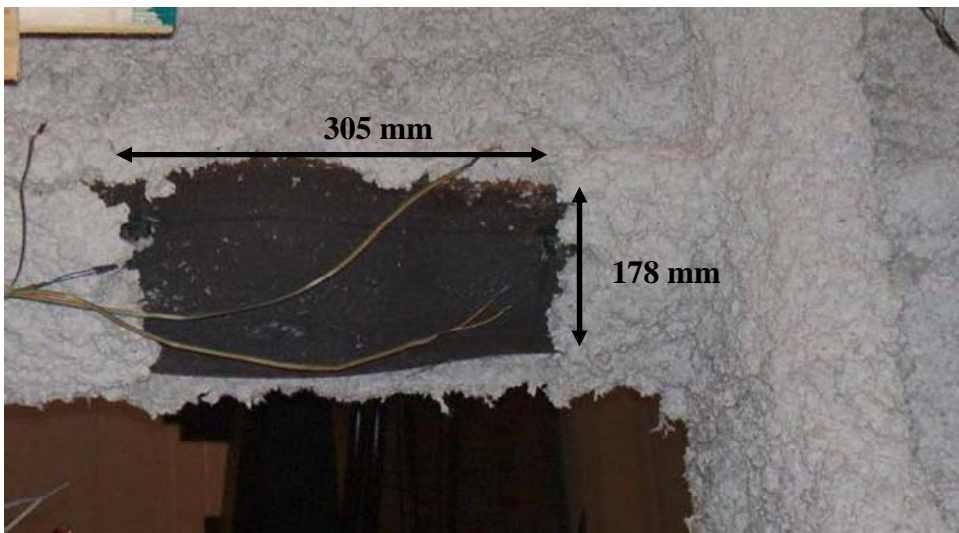
Figure 4.54 – Details of first damaged portion of SFRM on bottom flange of DM assemblage during step 10
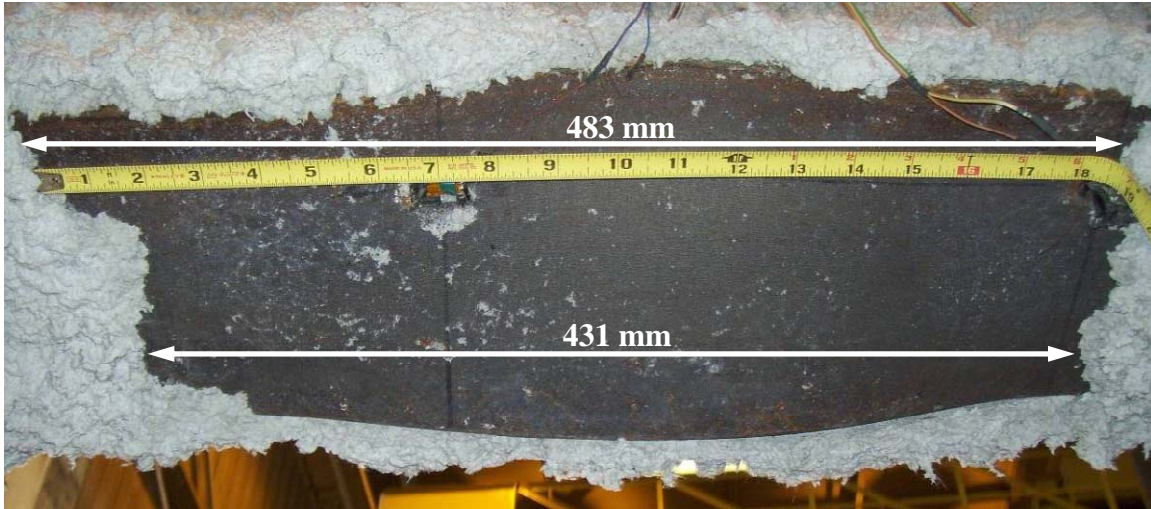
Figure 4.55 – Final section of SFRM on bottom flange of DM assemblage during post-testing inspection
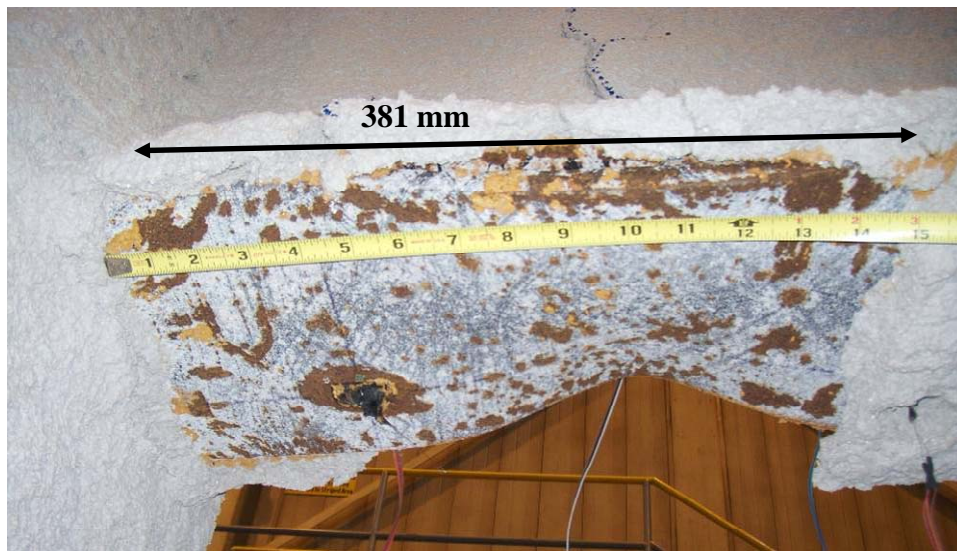
Figure 4.56 – Damage to SFRM on bottom flange of WM assemblage test during step 11

Figure 4.57 – Extensive cracking of SFRM on top flange of WM assemblage during post-testing inspection
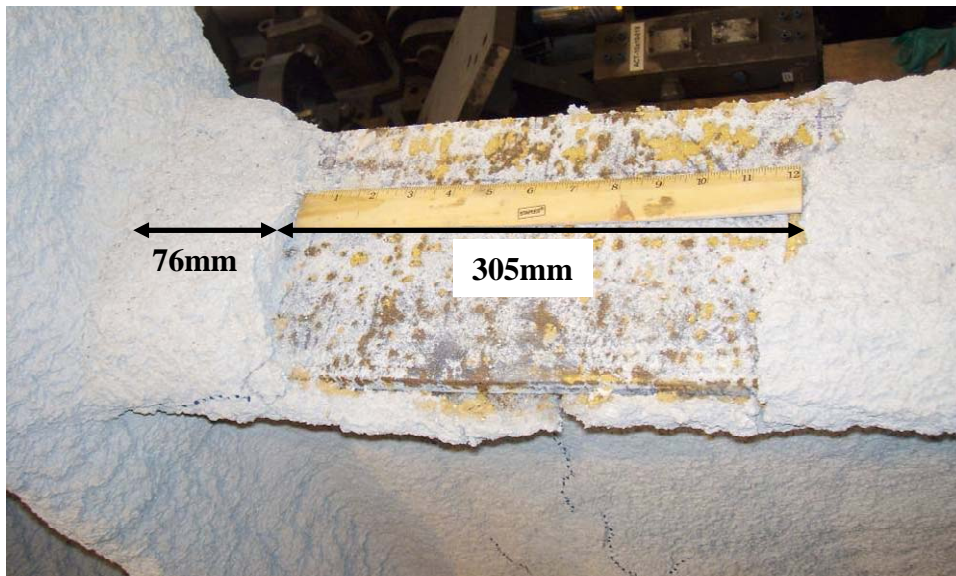
Figure 4.58 – Damage to SFRM on top of top flange of WM assemblage during post-testing inspection

Figure 4.59 – Extensive cracking in SFRM of WM assemblage throughout web during post-testing inspection

Figure 4.60 – Damage to SFRM on bottom of top flange, progressing into web of WM assemblage during post-testing inspection

Figure 4.61 – Damage to SFRM on top of bottom flange, progressing into web of WM assemblage during post-testing inspection
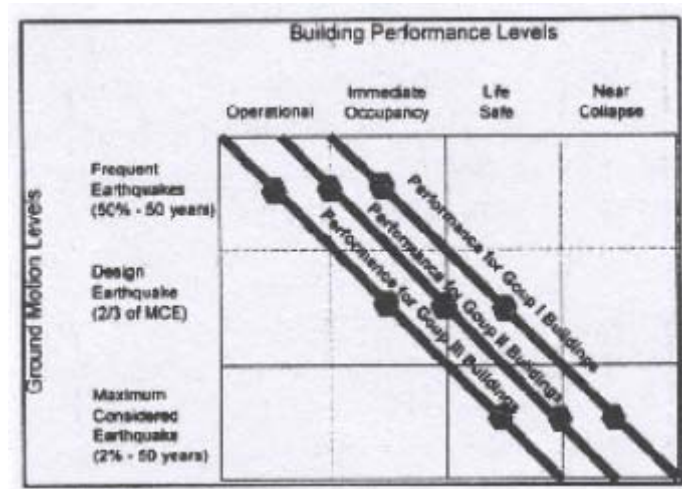
Figure 4.62 – Expected building performance during earthquakes (FEMA 450, 2003)

CHAPTER 5
CONCLUSIONS

5.1 INTRODUCTION

The work presented in this report is part of a broader research program to evaluate the post-earthquake efficacy of sprayed fire resistive material (SFRM) in steel moment frame building structures.

This report focuses on large-scale beam-column assemblage tests to examine the bond of SFRM to steel in the 3-D configuration of the beam-column connection region. Beam-column assemblages with SFRM applied are subject to quasi-static cyclic loading at the beam tip to cause large deformations in the beam. Damage to the SFRM at locations where there are large deformations in the steel is then investigated.

5.2 CONCLUSIONS

Damage occurred to the SFRM in the beam column assemblage specimens at story drift levels of 1% to 3.9%. The degree of damage to the SFRM depends upon the earthquake intensity. Damage to the SFRM begins with debonding of the SFRM from the steel as the steel yields. This occurs at drifts as low as 1%; the steel moment frame considered in this research is expected to develop 3% story drift under the action of a design earthquake and have a life safety performance level (BSSC, 2003). However, even though the SFRM is debonded from the yielded portions of the connection at this drift level, the three dimensional geometry of the SFRM in the beam-column connection prevents the SFRM from falling off the connection region.

Under a design earthquake causing story drifts of 3% to 4%, anticipated inelastic buckling (in the beam flanges in this study) creates tears in the SFRM at the locations of the buckling. The tears separate the SFRM in to sections that can then fall away from the connection, exposing the steel at those locations. The steel moment frame considered in this research is in the latter stages of the life safety performance level when this damage occurs.

For the strong-column, weak beam assemblages treated in this research, damage to the SFRM was concentrated in the beam flanges where inelastic damage to the underlying steel occurred. For the wet-mix SFRM, damage extended in to the beam web.

REFERENCES

Applied Technology Council. (2007). *Interim Testing Protocols for Determining the Seismic Performance Characteristics of Structural and Nonstructural Components (FEMA 461)*. Washington, DC: Federal Emergency Management Agency, 113 pp.

Braxtan, N.L. and Pessiki, P. (2010). *Bond Performance of Sprayed Fire Resistive Material (SFRM) on Steel Plates Subjected to Tensile Loading*. ATLSS Report No 10-01. Bethlehem, PA: Center for Advanced Technology of Large Structural Systems, Lehigh University, 58 pp.

Bruneau, M., Uang, C.M., & Whittaker, A. (1998). *Ductile Design of Steel Structures*. New York: McGraw Hill, 485 pp.

Buchanan, A.H. (2002). *Structural Design for Fire Safety*. New York: John Wiley & Sons Ltd., 421 pp.

Building Seismic Safety Council. (2003). *NEHRP Recommended Provisions for Seismic Regulations for New Buildings and Other Structures (FEMA 450)*. Washington, DC: Federal Emergency Management Agency, 752 pp.

Garlock, M.E.M. (2002). Design, Analysis, and Experimental Behavior of Seismic Resistant Post-tensioned Steel Moment Resisting Frames. Doctoral dissertation, Lehigh University, Bethlehem, PA, 786 pp.
International Building Code. (2003). Falls Church, VA: International Code Council, 658 pp.

Manual of Steel Construction, 13th Edition. (2005). Chicago: American Institute of Steel Construction.

Ricles, J.M., Sause, R., Garlock, M.M., & Zhao, C. (2001, February). Posttensioned Seismic-Resistant Connections for Steel Frames. *Journal of Structural Engineering*, pp. 113-121.

Ruddy, J.L., Marlo, J. P., Ioannides, S.A., & Alfawakhiri, F. (2003). *Steel Design Guide 19: Fire Resistance of Structural Steel Framing*. Chicago: American Institute of Steel Construction, 123 pp.

SAC Joint Venture. (2000). *Recommended Seismic Design Criteria for new Steel Moment-Frame Buildings* (FEMA-350). Washington, DC: Federal Emergency Management Agency, 224 pp.

Seismic Provisions of Structural Steel Buildings. (2005). Chicago: American Institute of Steel Construction, 309 pp.

Society of Fire Protection Engineers. (1988). *SFPE Handbook of Fire Protection Engineering, First Edition*. Quincy, MA: National Fire Protection Agency and Bethesda, MD: Society of Fire Protection Engineers.

Society of Fire Protection Engineers. (2007). *SFPE Standard on Calculating Fire Exposures to Structures*. Bethesda, MD: Society of Fire Protection Engineers,   28 pp. *Specification for Structural Steel Buildings*. (2005). Chicago: American Institute of Steel Construction.

Standard Test Method for Cohesion/Adhesion of Sprayed Fire-Resistive Material (SFRM) Applied to Structural Members. (2000). ASTM Designation E736-00. West Conshohocken, PA: ASTM International.

Standard Test Method for Fire Tests of Building Construction and Materials. (1999). ASTM Designation E119. West Conshohocken, PA: ASTM International.

Standard Test Method for Thickness and Density of Sprayed Fire-Resistive Material (SFRM) Applied to Structural Members. (2000). ASTM Designation E605-93. West Conshohocken, PA: ASTM International.

Underwriters Laboratories. (2008). *Fire Resistance Ratings – ANSI/UL 263*. Northbrook, IL: Underwriters Laboratories Inc.

Wang, Y.C. (2002). *Steel and Composite Structures: Behavior and Design for Fire Safety*. New York: Spon Press, 332 pp.

Youssef, N.F.G., Bonowitz, D., & Gross, J.L. (1995). *A Survey of Steel Moment-Resisting Frame Buildings Affected by the 1994 Northridge Earthquake*. Gaithersburg, MD: National Institute of Standards and Technology, pp. 594-607.

APPENDIX

A.1 Results of Ultrasonic Testing of Moment Connection

CTL — CERTIFIED TESTING LABORATORIES, INC.

REPORT OF ULTRASONIC INSPECTION

Client: Lehigh University   Date: 7/24/2008

Project: Fireproof Insulation 117 ATLSS Drive Building H,
Job #541587 Purchase Order #74050 - Bethlehem, PA   Report No: UT-1

Location:
Length: Various
Ultrasonic Unit: EPOCH LT
Serial No.: 070149904

Test Method Standard: Longitudinal and shear wave
Thickness: Various
Location: ATLSS Lab 117 ATLSS Drive - Bethlehem, PA

Acceptance Standard: AWS D1.1

Shift Time: Regular: Overtime:

Weld Identification:	Accept	Reject	Procedure Legend no.	Indication Number	Transducer Angle	From Face	Leg *	Indications Level	Reference Level	Attenuation Factor	Indication Rating	Length	Angular Dist. (sound path)	Depth from "A" surface	From X	From Y
Column 1	X		1		70°	A	1 and 2									
Column 2	X		1		70°	A	1 and 2									

Decibels: A | B | C | D
Discontinuity — *Distance

WELD LOCATION AND IDENTIFICATION SKETCH

Beam to column welds

Couplant: Ultragel II
Frequency: 2.25 MHZ
Calibration Blocks: DSC
Surface Condition: As welded
X - Y MARKERS

(Indicate X-Y Markings)   *Use Leg I, II, or III

Technician: CTL / S. Dunn Level III A.S.N.T. 3479   Interpreter: Level:

REMARKS:

Ultrasonic testing is subjective and subject to inherent limitations of methodology. Certified Testing Laboratories, Inc. is not liable for any misinterpretation of results or conditions or any claims or losses attributable to performance of a test. These services are rendered without and warranty. Certified Testing Laboratories Inc. liability is limited to the amount actually paid for the service at issue. Client is responsible for the permanent identification of welds and materials for location. This report is not to be construed as a guarantee or warranty of the materials or welds tested.

Comments: Full penetration welds of column to beam for fireproofing evaluation

Report to: 2 - above (Attn: John Hoffner)

Respectfully submitted,
CERTIFIED TESTING LABORATORIES, INC.

ROBERT W. RUHF
CWI 01101261
QC1 EXP. 10/01/10

Robert W. Ruhf,
Vice President
CWI #01101261

754 East Fairview Street • Bethlehem, PA 18018 • (610) 865-2674 • Fax (610) 974-9215